

Oxygen measurement in the Labrador Sea: Profiling oxygen floats as a new observation method

Dissertation
zur Erlangung des Doktorgrades
der Mathematisch-Naturwissenschaftlichen Fakultät
der Christian-Albrechts-Universität zu Kiel

vorgelegt von
Christoph Kihm

Kiel
Februar 2010

Referent: Prof. Dr. Arne Körtzinger

Korreferent: Prof. Dr. Andreas Oschlies

Tag der mündlichen Prüfung: 31.03.2010

Zum Druck genehmigt:

gez.

This work is based on the following prepared manuscripts:

1. **Manuscript:** Kihm, C. and A. Körtzinger, Air-sea gas transfer coefficient for oxygen derived from float data, *submitted to Journal of Geophysical Research Oceans*.

Contribution: Christoph Kihm performed the calculation, evaluated the data and wrote the paper. Arne Körtzinger gave advise and helpfull input to the manuscript and reviewed the manuscript.

2. **Manuscript:** Kihm, C. and A. Körtzinger, Particulate organic carbon flux deduced from profiling oxygen float data in the Labrador Sea, *prepared to be submitted to Journal of Marine Systems*.

Contribution: Christoph Kihm performed the calculation, evaluated the data and wrote the paper. Arne Körtzinger gave advise and helpfull input to the manuscript and reviewed the manuscript.

Contents

Contents	5
Zusammenfassung	7
Summary	9
1 Introduction	11
1.1 Regional Oceanography and Bathymetry	12
1.2 North Atlantic Oscillation (NAO)	14
1.3 Dissolved Oxygen (O_2)	16
1.3.1 Apparent Oxygen Utilization	17
1.3.2 Oxygen Utilization Rate	19
1.4 Biological Pump	20
1.5 Air-Sea Gas Transfer	22
1.6 Motivation	24
2 Profiling Floats	25
2.1 Measuring Principle of the Oxygen Optode	28
2.2 Calibration of Oxygen Data	30
3 Variability on Seasonal to Interannual Time Scales	35
3.1 Study Region	36
3.2 Mixed Layer Structure and Depth	37
3.3 Labrador Sea Salinity and Temperature Cycle	43
3.4 Oxygen Cycle	46
4 Air-Sea Gas Transfer of Oxygen	55
4.1 Introduction	57

4.2	Methods	57
4.2.1	Oxygen floats	57
4.2.2	Mixed Layer Depth	58
4.2.3	Wind Data	58
4.2.4	Calibration of oxygen data	59
4.2.5	Estimation of gas transfer coefficient	60
4.2.6	Wind distribution	61
4.3	Results and Discussion	62
5	Particulate Organic Carbon Flux	71
5.1	Introduction	73
5.2	Methods	74
5.2.1	Oxygen floats	74
5.2.2	Calibration of oxygen data	74
5.2.3	Oxygen Utilization Rate	75
5.2.4	Estimation of particulate organic carbon flux	76
5.3	Results and Discussion	77
6	Conclusions and Outlook	84
6.1	Conclusions	84
6.2	Outlook	86
	Danksagung	89
	Bibliography	91

Zusammenfassung

Die Zielsetzung dieser Arbeit war es, den Jahresgang von Sauerstoff (O_2) in der zentralen Labradorsee mit Hilfe von Daten zu untersuchen, die von autonom profilierenden Tiefendriftern (Floats) über den Zeitraum September 2003 bis August 2006 gewonnen wurden. Die Labradorsee ist eine von wenigen Regionen, in denen Tiefenkonvektion stattfindet, die bis zu 2000 m und tiefer reichen kann. Die jahreszeitlichen und zwischenjährlichen Schwankungen in Temperatur, Salzgehalt und Sauerstoff werden von physikalischen und biologischen Faktoren bestimmt. Die in der Literatur dokumentierte Aufteilung des jährlichen Süßwasserpulses zwischen März und September in zwei Pulse sowie ein leichter Anstieg von 0.3°C bis 0.8°C der Oberflächentemperatur wurden bestätigt. Diese Ergebnisse stimmen mit früheren Arbeiten gut überein. Der O_2 -Jahresgang in der Deckschicht ist von hoher Dynamik geprägt und variiert zwischen erheblicher winterlicher Untersättigung und kräftiger frühlommerlicher Übersättigung. Das publizierte klimatologische Bild wurde weitgehend bestätigt, wobei der glättende Effekt der Klimatologie offenkundig ist.

Die Deckschichttiefe wurde mit Hilfe eines O_2 -Differenzkriteriums von $5 \mu\text{mol L}^{-1}$ bestimmt, was ein angemessener Schwellenwert für diese Region zu sein scheint. Durch Konvektion bedingte Vertiefung der Deckschicht ist mit einer Zunahme des O_2 -Inventars von jährlich 8.3 bis $15.1 \text{ mol } O_2 \text{ m}^{-2}$ verbunden. Hierbei korreliert die Inventarzunahme in etwa mit der maximalen winterlichen Konvektionstiefe und erreicht somit im Winter 2003/2004 den größten Wert von $15.1 \text{ mol } O_2 \text{ m}^{-2}$. Es gibt Anzeichen dafür, dass die tiefe Ventilation in der Labradorsees von der Nordatlantischen Oszillation (NAO-Index) beeinflusst wird. So wurde eine Korrelation zwischen dem NAO-Index und der winterlichen Zunahme des tiefen O_2 -Inventars (710-1350 m) mit einer Zeitverschiebung von einem Jahr gefunden. Ferner wurde ein Anstieg des O_2 -Konzentrationsmaximums im Sommer um $17.4 \mu\text{mol L}^{-1}$ beobachtet, welcher auf erhöhte oder schneller akkumulierende Primärproduktion hinweist.

Die gewonnenen Sauerstoffdaten wurden außerdem genutzt, um den Gasaustauschkoeffizienten von Sauerstoff als Funktion der Windgeschwindigkeit zu bestimmen. Im Allgemeinen zeigten unsere Ergebnisse eine gute Übereinstimmung mit prominenten Parameterisierungen. Dabei liegen sie jedoch am oberen Ende der Windgeschwindigkeitsabhängigkeit. Die Daten konnten mit einer kubischen oder sogar biquadratischen Funktion am besten repräsentiert werden, was auf den überproportionalen Einfluss hoher Windgeschwindigkeiten zurückzuführen ist.

Im letzten Teil der Arbeit wurde der Vertikalfluss von partikulärem organischen Kohlenstoff (POC) durch vertikale Integration der Kohlenstoffremíneralisationsraten bestimmt. Letztere konnten aus den beobachteten sommerlichen Sauerstoffzehrungsraten im Mesopelagial der zentralen Labradorsee und angrenzenden Kontinentalhangregion gewonnen werden. Er gibt Hinweise auf eine raschere Remíneralisation des organischen Materials in der Kontinentalhangregion. Es wurde der "b"-Parameter der prominenten Martin-Funktion für den vertikalen POC-Fluss ermittelt. Dieser stimmt für die zentrale Labradorsee hervorragend mit dem in der jüngeren Literatur angegebenen Wert für das North Atlantic Bloom Experiment im subpolaren Nordatlantik überein.

Summary

The aim of this study was to analyze the annual cycle of dissolved oxygen (O_2) in the central Labrador Sea on the basis of oxygen data observed by autonomous profiling floats during the period September 2003 and August 2006. The Labrador Sea is one of just a few regions where open-ocean deep winter convection occurs reaching depths of 2000 m and more. The seasonal and interannual cycles of temperature, salinity, and oxygen are affected by physical and biological factors. The published separation of the seasonal freshwater pulse between March and September into two freshening periods as well as a slight increase of maximum sea surface temperature by 0.3°C to 0.8°C was confirmed. The seasonal oxygen cycle of the mixed layer is highly dynamic varying from moderate undersaturation during late winter to marked supersaturation in spring and early summer. The published climatological picture for oxygen was largely confirmed whereby the smoothing effect of the climatology becomes obvious.

The mixed layer depth was determined using an O_2 difference criterion of $5 \mu\text{mol L}^{-1}$ which seems to be a reasonable threshold for this region. Convective deepening of the mixed layer is associated with a strong increase of the upper ocean O_2 inventory which was estimated at 8.3 to $15.1 \text{ mol } O_2 \text{ m}^{-2}$. This inventory increase is correlated with the maximum depth of the winter mixed layer. Hence the increase found during winter 2003/2004 was largest at $15.1 \text{ mol } O_2 \text{ m}^{-2}$. There is indication that the North Atlantic Oscillation (NAO index) affects the deep ventilation in the Labrador Sea as a correlation was found between the NAO index and the winter increase of the deep O_2 inventory (710-1350 m) with a time lag of 1 year. Also, an increase of the maximum summer oxygen concentration by $17.4 \mu\text{mol L}^{-1}$ in surface waters was observed which is indicative of a stronger or more rapid primary production.

The oxygen dataset was also used to estimate the air-sea gas transfer coefficient of oxygen as a function of wind speed. The results in general agree well with prominent published parameterizations. They fall, however, on the high end of the wind speed

dependence. Best fits were found using cubic or even biquadratic functions which points at the strong importance of very high wind speed for air-sea gas exchange. Finally, the vertical flux of particulate organic matter (POC) was estimated by vertical integration of carbon remineralization rates. The latter were derived during the summer/fall period for the central Labrador Sea and the adjacent slope region from oxygen utilization rates in the mesopelagial. The data are indicative of more rapid remineralization in the slope region. The "b" parameter of the famous Martin curve for the vertical POC flux was estimated. The value for the central Labrador Sea agrees very well with more recently published values for the North Atlantic Bloom Experiment in the subpolar North Atlantic.

Chapter 1

Introduction

The world ocean plays an important role in shaping our climate and weather patterns and together with the atmosphere it forms a closely linked dynamic duo. Energy from the sun, marine and land plant distributions and greenhouse gases, like carbon dioxide (CO_2) or methane (CH_4) in the atmosphere can affect temperature and circulation patterns of this ocean-atmosphere duo. The ocean can act as conveyor or buffer for atmospheric fluctuations, e.g. in oxygen concentration (O_2), on timescales from days up to centuries. Changing the concentration of greenhouse gases in the atmosphere affects the climate.

In the last few decades the oceans have considerably warmed [e.g., *Levitus et al.*, 2005; *Barnett et al.*, 2005] and until the end of this century the oceans will continue to become warmer. The consequences of this heat uptake on ocean circulation, ocean biogeochemistry and biology are not yet predictable. It is important to understand the role of the ocean in the global carbon cycle and its response to a changing environment. This requires global observations in time and space. Traditional ship-based ocean sampling methods rarely achieve measurements on the spatial and temporal time scales required to answer questions regarding various phenomena, such as the uptake of anthropogenic CO_2 [*Sabine et al.*, 2004], ventilation of the thermocline in different regions [e.g., *Sarmiento et al.*, 2004], export and transport of nutrients in the euphotic zone [e.g., *Jenkins et al.*, 2003], rate and spatial distribution of ocean deoxygenation [*Stramma et al.*, 2008] and mechanisms controlling the oceans biological (carbon) pump [e.g., *Ducklow et al.*, 2001].

Ocean deoxygenation can be expected as one consequence of the global warming [*Bopp et al.*, 2002; *Keeling et al.*, 2010]. Oxygen is produced in the photic surface layer by

biological production (photosynthesis), however, it is removed from sub-surface waters by respiration of sinking organic matter.

Near surface waters are usually well equilibrated with the atmosphere by air-sea gas exchange and the sub-surface removal is balanced by the transport of oxygen-rich surface waters into the deep sea. Decreasing concentrations of dissolved oxygen in surface waters thus results in a decrease of the ventilation of sub surface waters.

Satellite ocean color measurements have helped to overcome the locally restricted ship-based sampling on spatial and temporal scales, but the observable biogeochemical variables, of the upper ocean, or, in other words the upper part of the euphotic zone, depends on cloud-free periods. Time series programs (e.g., Hawaii Ocean Timeseries [HOT], Bermuda Atlantic Timeseries Study [BATS] or the European Station for Time Series in the Ocean [ESTOC]) have helped in our understanding of local temporal variability of biogeochemical processes [Bates *et al.*, 2007; Dore *et al.*, 2009; Santana-Casiano *et al.*, 2007].

Observation of biogeochemistry at reasonable spatial and temporal scales requires development of new observation platforms. Within the past five years the development of chemical and biological sensors (e.g., oxygen optodes, nitrate and chlorophyll sensors) has made rapid progress, and is still going on.

1.1 Regional Oceanography and Bathymetry

The Labrador Sea is an arm of the North Atlantic Ocean and located in the northwest Atlantic Ocean, separating southwest Greenland and Labrador/Canada (Fig. 1.1). It is one of the important sites that contributes to deep water formation, e.g. Labrador Sea Water, North Atlantic Deep Water, and is part of the Atlantic meridional overturning circulation (MOC) and for this reason plays an important role in the thermohaline circulation (THC), often called "conveyor belt". This circulation transports warm, shallow, saline water poleward, heating the atmosphere. The combination of buoyancy loss, through cooling, evaporation and sea-ice formation produces cold and salty water masses that sink. This high latitude cooling and the low latitude heating drive the movement of the deep water in southward flow. Deep convection, i.e. the process of vertical mixing between upper and intermediate or deeper layers, is an important component of the thermohaline circulation of the world ocean which is strongly influenced by the seasonal cycle of temperature as well as salinity [Lab Sea Group, 1998]. During winter a harsh

climate remains over the Labrador Sea with westerly and northerly winds bringing cold air from Canada and the Arctic with an average wind speed of about 6 m s^{-1} [Lilly *et al.*, 1999]. In the central Labrador Sea the mean wind typically blows in NW-SE direction, in response of the topography of Greenland, with higher average wind speeds in wintertime of up to 18 m s^{-1} in some individual monthly averages.

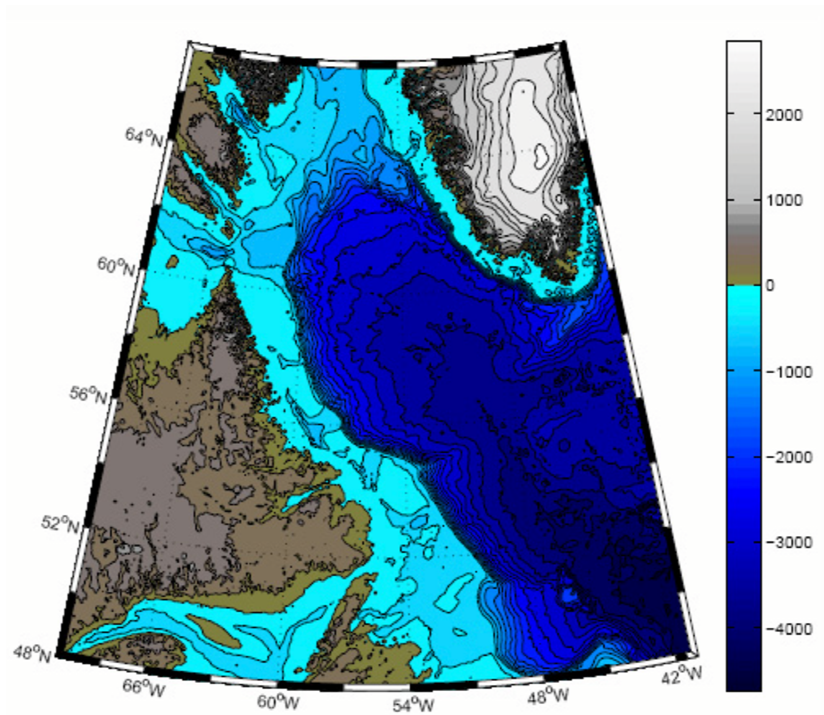


Figure 1.1: Bathymetry of the Labrador Sea [Schmidt, 2008]. The contour interval is 100 dbar. The used bathymetry is assembled by Smith and Sandwell [1997].

The large-scale regional ocean circulation is dominated by a cyclonic circulation, the western extremity of the cyclonic subpolar gyre of the North Atlantic. The convection depth variation is influenced by the stratification buildup of the late summer in the Labrador Sea and by the varying atmospheric forcing. The region of open ocean convection varies but has been observed roughly between 55°N - 60°N (e.g., [Lab Sea Group, 1998; Pickart *et al.*, 2002; Körtzinger *et al.*, 2004]). Open-ocean convection in the subpolar North Atlantic Ocean affects not only the meridional overturning circulation and the oceanic heat flux, it drives moreover the atmospheric carbon which sinks to depth with the the surface water as a distinct water mass.

1.2 North Atlantic Oscillation (NAO)

Strong variations in the Labrador Sea water formation were shown by *Dickson et al.* [2002]. The interannual and seasonal variability varies from local sources and sinks, e.g. Hudson Bay outflow, freshwater export, heat flux, rain and East Greenland Arctic freshwater export. Labrador Sea Water variations (convection) have been related to changes in the North Atlantic Oscillation (NAO) index [*Hurrell et al.*, 2003](Fig. 1.2).

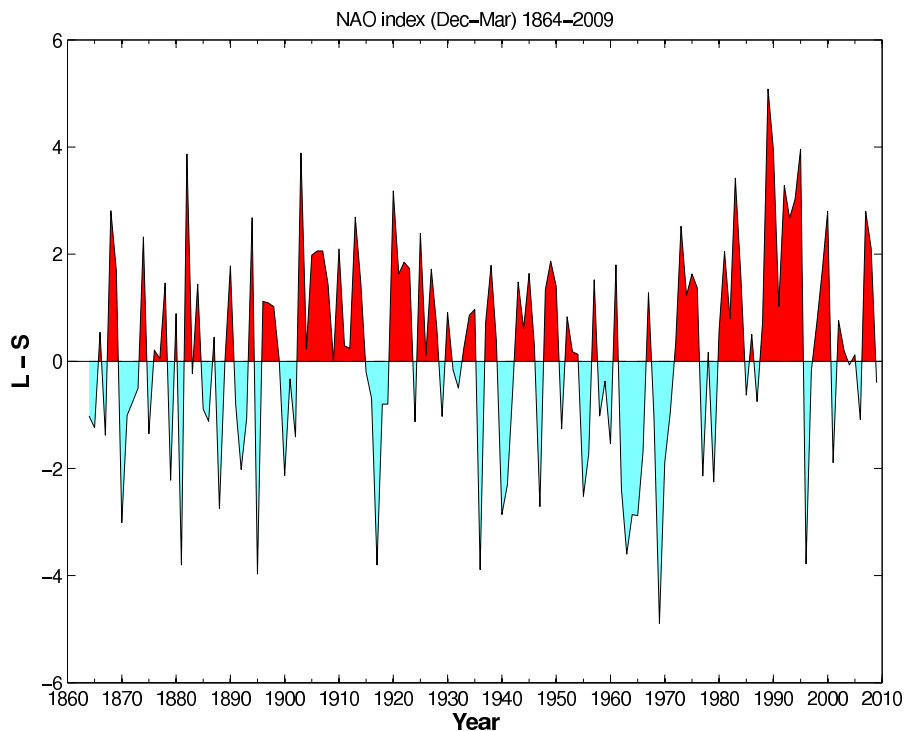


Figure 1.2: Winter (December to March) index of the NAO based on the difference of normalized sea level pressure (SLP) between Lisbon (Portugal) and Stykkisholmur (Iceland) since 1864. The SLP anomalies at each station were normalized by division of each seasonal mean pressure by the long term mean (1864-1983) standard deviation. Positive (negative) NAO index values indicate stronger (weaker) than average westerlies over the middle latitudes NAO. Index Data provided by the Climate Analysis Section, NCAR, Boulder, USA, Hurrell (1995). Data source: <http://www.cgd.ucar.edu/cas/jhurrell/indices.html>.

The NAO is a climate phenomenon in the North Atlantic ocean of fluctuations in the difference of the location and intensities of the subtropical high in atmospheric pressure near the Azores and the subpolar low near Iceland. A positive NAO index phase shows a stronger than normal subtropical high pressure and a deeper than normal icelandic low

pressure resulting in more and stronger westerly winds in the Atlantic Ocean and strong heat loss associated with dry winters in Canada and mild and wet winter conditions in the eastern United States and enhanced air-sea fluxes of heat. A positive NAO index is often linked to the onset of deep convection in the Labrador Sea [Dickson *et al.*, 1996] and the Labrador Sea water tends to be colder, fresher, denser and thicker [Johnson *et al.*, 2005]. The negative NAO index phase shows a weak subtropical high and a weak Icelandic low resulting in weaker westerly winds associated with milder winter in Greenland and cold air and hence snowy winter in eastern United States.

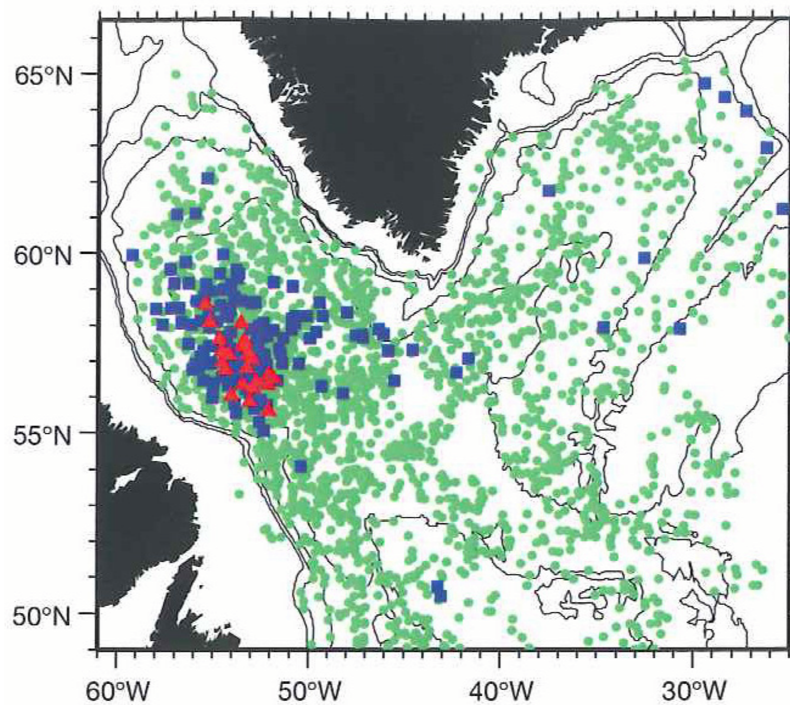


Figure 1.3: Mixed layer depth (MLD), computed from float temperature profiles, in winters 1996-97 and 1997-98. MLD ≤ 400 m are marked with green circles, $400 \text{ m} < \text{MLD} \leq 800 \text{ m}$ with blue squares, and MLD $> 800 \text{ m}$ with red triangles. The deepest mixed layer are located in the western basin of the Labrador Sea [Lavender *et al.*, 2002].

Since the mid-90s open ocean convection in the Labrador Sea has been comparatively shallow [Yashayaev *et al.*, 2007; Lazier *et al.*, 2002; Pickart *et al.*, 2002] with the exception of the winters of 1995-1996 with maximum depth of about 2300 m [Avsic *et al.*, 2006] and the winters of 1999-2000 with an approximate maximal depth of 2000 m. During the winter 2007-2008 floats recorded a maximal mixed layer depth in the

Labrador Sea of approximately 1800 m [Våge *et al.*, 2009]. The recorded periods of deep convection were characterized by high positive NAO index. Figure 1.3 shows mixed layer depths in winters 1996-97 and 1997-98. The deepest mixed layers were located in the western basin of the Labrador Sea [Lavender *et al.*, 2002].

1.3 Dissolved Oxygen (O_2)

The most commonly discussed effect of climate change is the trend in globally averaged temperature. Rising global average temperatures in the atmosphere and in the ocean, melting of snow and ice and the global average sea level rise are unequivocally reported by the IPCC's Fourth Assessment Report [IPCC, 2007]. A consequence of global warming that is recently receiving attention is a decrease in the dissolved O_2 content of the oceans, called deoxygenation, due to the fact that O_2 is less soluble in warmer water. Global warming may increase the stratification in the upper ocean resulting in reduced O_2 supply to the deeper ocean. Oxygen is fundamental for all aerobic life on earth, and plays a direct role in the biogeochemical cycling of carbon, nitrogen and other biogeochemical cycles. If the O_2 concentration drops below a certain threshold value, changes in the biogeochemical cycle occur and new conditions emerge such as hypoxic conditions, at approximately $60 \mu\text{mol kg}^{-1}$ [Gray *et al.*, 2002]. At O_2 concentration below $\sim 5 \mu\text{mol kg}^{-1}$, nitrate eventually becomes important in respiration replacing O_2 as terminal electron acceptor. These environments are termed suboxic and at O_2 concentrations close to zero is commonly termed as anoxic zone. Several models predict a decline of O_2 over the next century (e.g., by $\sim 30 \mu\text{mol kg}^{-1}$) in the deep North Atlantic Ocean, associated with reduced deep water formation [Plattner *et al.*, 2001; Fröhlicher *et al.*, 2009].

Oxygen is an important chemical tracer, because measured changes in O_2 concentration, combined with changes in nutrients, can be useful for detecting changes in biogeochemistry. The distribution of oxygen can also be used to estimate the rate of produced, redistributed and decomposed organic matter due to the fact that O_2 is directly linked to carbon by photosynthesis and respiration. The variation of O_2 concentration on annual to interannual time scales is controlled by air-sea gas exchange, circulation and biology. The seasonal anomaly of air-sea oxygen fluxes in the Northern and Southern hemispheres is shown in figure 1.4.

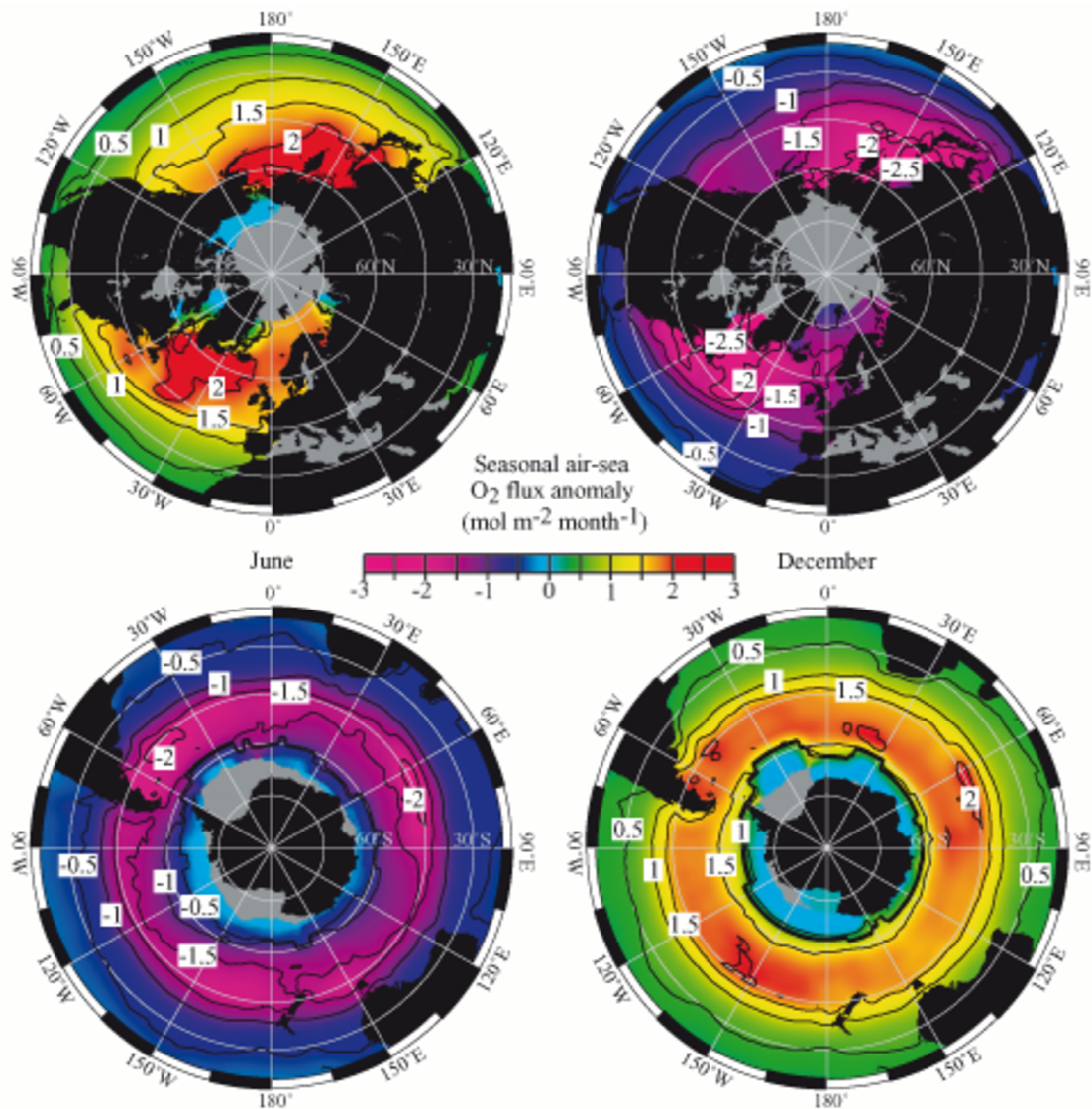


Figure 1.4: Seasonal anomaly of air-sea oxygen fluxes in the northern (top) and southern hemispheres (bottom) during June (left) and December (right). Positive fluxes indicates sea-to-air fluxes, negative fluxes indicates air-to-sea fluxes. During summer the Labrador Sea is a region of strong outgassing however, during winter time there is substantial oxygen uptake. For the northern and southern hemisphere, largest fluxes are observed between 30° and 60° latitude *Garcia et. al* [2001].

1.3.1 Apparent Oxygen Utilization

Oceanic surface waters are rich in nutrients, which are consumed by phytoplankton. If phytoplankton biomass was not reconverted into dissolved nutrients, the entire water

column would be depleted in nutrients and growth would stop. The reverse reaction, i.e. conversion of biomass to dissolved nutrients, is called remineralization and is initiated by organic respiration. Production via photosynthesis by autotrophic organisms (e.g. phytoplankton), can only occur in surface waters, where light is available. The depth of the euphotic zone can be affected by seasonal turbidity. In contrast, the remineralization by heterotrophic organisms can occur over the entire water column as well as in the underlying sediments. It follows that deep seawater contains nutrients from different sources. First, it may contain nutrients that were present in the water when it sank from the surface (preformed nutrients) on top of which nutrients accumulate that are derived from the in situ remineralization of organic matter (oxidative nutrients). To study the impact of aerobic remineralization on the water column distribution of oxygen we have to estimate its remineralization component, i.e the change in O_2 that occurred since a water parcel was last in contact with the atmosphere:

$$\Delta[O_2]_{remin.} = [O_2]_{obs.} - [O_2]_{preformed} \quad (1.1)$$

The exchange of O_2 across the air-sea interface is fast, relative to perturbations of this balance, so that it is difficult to maintain large under- or supersaturation for a certain time period. Oxygen is generally close to its saturation concentration, i.e. $[O_2]_{preformed} \simeq [O_2]_{sat}$. The saturation concentration can be calculated as a function of in situ temperature and salinity, and one atmosphere of total pressure using the solubility function of *Garcia and Gordon* [1992] based on the values of *Benson and Krause* [1984]. Thus we can estimate the remineralized component of oxygen which is commonly expressed as apparent oxygen utilization (*AOU*):

$$AOU = O_{2,sat.} - O_{2,obs.} \quad (1.2)$$

where $AOU = -\Delta[O_2]_{remin.}$. *AOU* is hence defined as the difference between the saturation oxygen concentration, $O_{2,sat}$ and the observed oxygen concentration $O_{2,obs}$ [*Ito et al.*, 2004]. However, where deep waters are formed (high latitudes, e.g. Labrador Sea) significant surface disequilibrium have been observed. Note that *AOU* does not include the effect of remineralization that is due to denitrification, the only known mechanism consuming N_2O in the ocean. Denitrification only occurs in suboxic environments such as the oxygen minimum zones (OMZ).

1.3.2 Oxygen Utilization Rate

If the observed distribution of dissolved oxygen in the deep ocean below the euphotic zone is in stationary or steady state, then it can be assumed that the *in situ* consumption of oxygen is balanced by ventilation, physical transport of oxygen from regions of higher dissolved oxygen and biological production. The oxygen utilization rate (*OUR*) decreases quasi-exponentially with increasing depth [Jenkins, 1998], as would be expected from the attenuation of the available carbon flux with depth. *OUR* is the time rate of change in *AOU* or O₂ associated with the remineralization of organic matter, or in other words the rate at which O₂ is consumed by the oxidation of organic matter and is defined as:

$$OUR = \frac{dAOU}{dt} \quad \text{or} \quad \frac{d[O_2]}{dt} \quad (1.3)$$

For the North Atlantic ocean several authors [e.g., Jenkins, 1987; Sarmiento *et al.*, 1990] estimated thermocline *OUR* by dividing the *AOU* by the e.g., tritium/³He or ²²⁸Ra age. A summary of *OUR* estimates from the thermocline of the North Atlantic ocean using a variety of techniques is shown in figure. 1.5.

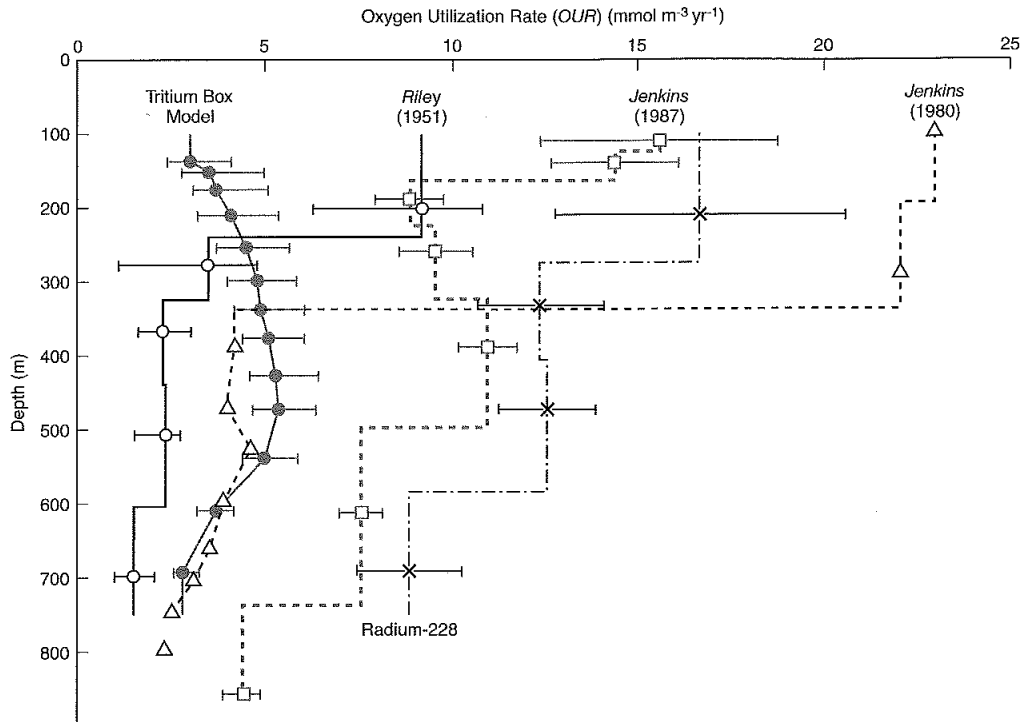


Figure 1.5: Compilation of *OUR* estimates for the North Atlantic using a variety of techniques [Sarmiento *et al.*, 1990].

1.4 Biological Pump

The interaction of biological processes, physical processes and gravity are the most important procedures to pump organic carbon into the interior ocean, particularly the amount of phytoplankton can significantly affect the greenhouse gas CO₂. Phytoplankton produces organic matter by the photosynthetic uptake of CO₂ and a major part of the produced biomass is consumed on the spot. Some fraction, however, finds its way to the deep ocean through the aggregation and settling of particles or through advection in the course of global circulation patterns. Most of the organic carbon which sinks to the deep ocean is finally remineralized by bacteria, into inorganic forms. The combined action of these processes is commonly called the biological pump [Volk and Hoffert, 1985].

The biological pump, consisting of primary producers, consumers and the bacteria, plays an important role in the global carbon cycle (Fig. 1.6). The elemental composition of phytoplankton is C:N:P = 106:16:1, referred to as the Redfield ratio [Redfield *et al.*, 1963], 106 units of carbon are delivered to the deep ocean for one unit of phosphorus or for 16 units of nitrogen. This carbon sequestered by the biological pump carbon from the atmosphere is stored for period of decades to centuries, depending on the depth of remineralization. A very small fraction escapes from the ocean through sedimental burial.

There are three different mechanisms by which the nutrients are returned to the surface, upwelling of nutrient-rich deep water (e.g., along the western coasts of continents), vertical (eddy) diffusion across the thermocline or on seasonal scale wind-driven deep mixing, which erodes the thermocline and entrains the sub-surface water into the surface. In some regions nutrients such as nitrate, phosphate and silicate are not limiting for phytoplankton growth, e.g. Southern Ocean, the equatorial Pacific and the subarctic North Pacific Ocean. These are the so called "high-nutrient, low-chlorophyll" (HNLC) waters. In this waters the biological pump is inefficient because the phytoplankton is limited by other factors and cannot fully utilized the nutrients in the surface waters (such as the micor-nutrient).

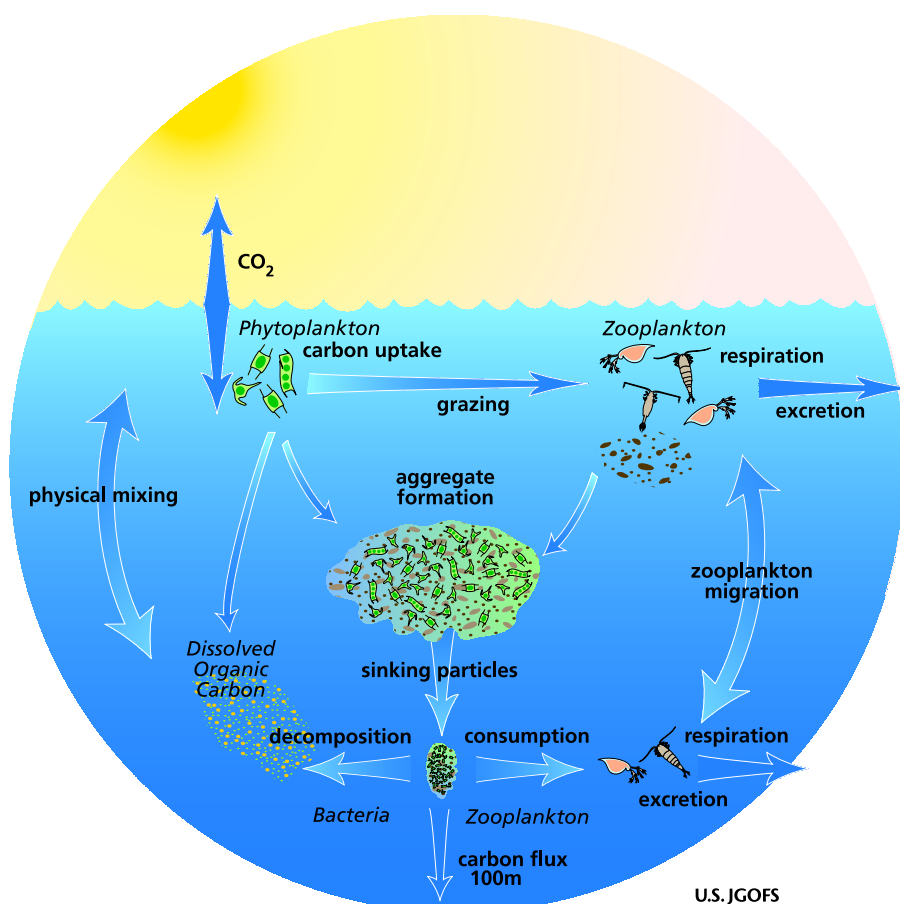


Figure 1.6: Schematic diagram of the components of the biological pump, which transforms Dissolved Inorganic Carbon (DIC) into organic biomass and pumps it in dissolved or particulate form into the deeper ocean. CO_2 is fixed by phytoplankton (photosynthesis), in the euphotic zone, thereby forming Particulate Organic Carbon (POC) and also releasing some fraction as Dissolved Organic Matter (DOM) which is consumed by zooplankton. The major part of Particulate Organic Matter (POM) is consumed by bacteria and respired, the remaining part of DOM is advected and mixed into the deeper ocean where other bacteria decompose and respire it, thus returning organic carbon into the enormous deep ocean reservoir of (DIC). Thermohaline circulation returns deep-ocean DIC to the atmosphere on millennial time scales. Copyright United States Joint Global Ocean Flux Study (http://www1.whoi.edu/general_info/gallery_modeling/slide4.html).

Light and nutrients are the primary factors regulating the phytoplankton growth. Light decreases dramatically with depth and the euphotic zone depths vary from only a few centimeters in highly turbid eutrophic lakes, to around 200 m in the open oligotrophic ocean.

1.5 Air-Sea Gas Transfer

The subpolar north Atlantic Ocean is a prominent CO₂ sink [Watson *et al.*, 2009]. The uptake of atmospheric CO₂ is variable in time and space, decreasing pH of the surface waters (ocean acidification) and increasing the CO₂ concentration (ocean carbonation) [Riebesell *et al.*, 2009]. Therefore, these changes are expected to change the marine biota, their structure and functionality, and the cycling of carbon. Estimates of the magnitude causes of temporal variations have come from atmospheric observations in inverse models and from ocean carbon models. There are different processes that affect the concentration of gases in the water column: vertical mixing, photochemistry, air-sea exchange and biological production and consumption. Air-sea gas exchange is being investigated since ~50 years because of its importance in biogeochemical cycling of climate, weather and health-related gaseous compounds [Wanninkhof *et al.*, 2009]. Air-sea gas exchange is additionally important in suppressing the anthropogenic greenhouse effect by absorption of atmospheric CO₂ by the oceans and it furthermore indirectly affects the radiative balance due to the sea-to-air flux of dimethylsulfide (DMS), which provides as cloud condensation nuclei [Simó, 2001].

Our understanding of exchange processes at the molecular level has improved the understanding of how environmental factors control the rate of exchange at the air-sea interface. To better quantify the air-sea gas transfer and the gas flux a lot of effort in improving and validating of techniques and theories has been realized. In 1998 the Ocean-Atmosphere Carbon Exchange Study (OACES) of the NOAA Office of Global Programs was started with the goal to improve the quantification of air-sea CO₂ fluxes and gas transfer velocity. For quantification of the gas exchange of oxygen at the air-sea interface, it takes advantage of oxygen disequilibria that arise from biological consumption or production or utilize excesses of ¹⁴C in the atmosphere. This ¹⁴C, resulting from nuclear bomb test in the early 1960s, invaded the ocean and can also be used for determination of gas exchange over the ocean [Sweeney *et. al.*, 2007].

The measurement of gas transfer velocities and fluxes can be generally separated into three categories:

- **direct flux measuring techniques:** measurement of flux F in the air above the sea, the difference of the gas concentration (thermodynamically driven potential) at the sea water surface and the well-mixed bulk fluid below is used to determine the air-sea gas exchange velocity k , e.g., direct flux measuring [McGillis *et al.*,

2001], covariance (or eddy correlation) technique [Fairall *et al.*, 2000].

- **bulk concentration techniques:** measurement of the partial pressure of the gas in air and the change of the partial pressure of the gas in water as a function of time. Assuming the water volume and surface area are known, flux F is equal to the change in water multiplied by the ratio of the volume to the surface area and the air-sea gas exchange velocity k , which is parameterized based on wind speed.
- **Proxy techniques:** measurement of the air-sea flux of a nongaseous tracer, as a surrogate for a gas using the principle that all air-sea transfer is controlled by the hydrodynamics at the surface.

The most commonly used relationship is that of *Wanninkhof* [1992], which relates the air-sea gas transfer-coefficient to wind speed. Using this relationship to calculate air-sea fluxes on a regional or global scale, it is important to use consistent wind. The estimates of the global wind speed can differ by more than 1 m s^{-1} [Boutin *et al.*, 2002; Naegler *et al.*, 2006]. The National Center for Environmental Prediction (NCEP) yields a global average wind of 6.6 m s^{-1} compared with a global average wind of 7.9 m s^{-1} [Naegler *et al.*, 2006] estimated by the Quick Scatterometer (QuikSCAT) satellite, resulting in biases in global flux estimations. Spatial distributions of winds are not consistent among different wind speed climatologies either. Due to the fact that most wind speed dependent parametrizations of the transfer coefficient are non-linear, the use of time averaged winds will lead to an underestimation, which has to be corrected for by an enhancement factor [Wanninkhof *et al.*, 2002]. Globally, the enhancement factor is 1.14 ± 0.07 for the quadratic dependence and 1.45 ± 0.23 for the cubic dependence. The flux across the air-sea interface is not controlled by the wind itself, the wind rather affects the turbulence. Several mechanisms can affect turbulence at the air-sea interface, e.g. friction velocity, waves, bubbles, rain, chemical enhancement and surface films.

1.6 Motivation

A decrease of O_2 concentration in the thermocline has been observed in several repeated hydrographic sections of the world oceans [Keeling *et al.*, 2010]. The reported decrease of O_2 concentration range from 0.1 to 6 $\mu\text{mol kg}^{-1}$ [IPCC, 2007]. A critical point is the spatial and temporal undersampling of the ocean. The successful implementation of oxygen optodes on profiling floats has principally modified this situation. Oxygen profiling floats are a good method to determine seasonal to decadal time scales variations in O_2 concentrations on a global scale. There are a lot of scientific reasons for using oxygen optodes on profiling floats as proposed by Gruber *et al.* [2009]:

- Determine transport and air-sea gas exchange of O_2 .
- Determine seasonal to interannual changes in the net community and export production.
- Detect, survey and document the ocean's deoxygenation (suboxic-, anoxic regions and oxygen minimum zones (OMZ)).
- Prediction and assessment of anoxic and hypoxic events.
- Improve atmospheric O_2 / N_2 constraint on the oceanic uptake of anthropogenic CO_2 .
- Aid interpretation of variations in ocean circulation and mixing.
- Provide constraints for ocean biogeochemistry models.
- Aid in interpretation of sparse data from repeat hydrographic surveys.

In chapter 4 and 5 we discuss the first two points. We estimate air-sea gas transfer coefficients derived from oxygen float data using wind speed data acquired by scatterometry from the QuikSCAT satellite. Particulate organic carbon fluxes are calculated by vertical integration of carbon remineralization rates, obtained by converting oxygen utilization rates by using a Redfield stoichiometric ratio of $-O_2:C_{org}$ of 1.34 ± 0.06 [Körtzinger *et al.*, 2001].

Chapter 2

Profiling Floats

Observing the physical and biological processes in the world ocean on a broad scale requires high-endurance and relatively low-cost sensors. Since 2003, more than 3000 profiling floats (e.g., Apex, Provor, Nemo) were deployed in the world ocean (Fig. 2.1) which was the explicit goal of the Argo array of profiling floats [Roemmich *et al.*, 2004; 2009]. The development is still going on and new types of autonomous platforms, gliders, were developed. More than 100 seagliders [Rudnick *et al.*, 2004] are operating additionally to the large number of profiling floats the oceans.

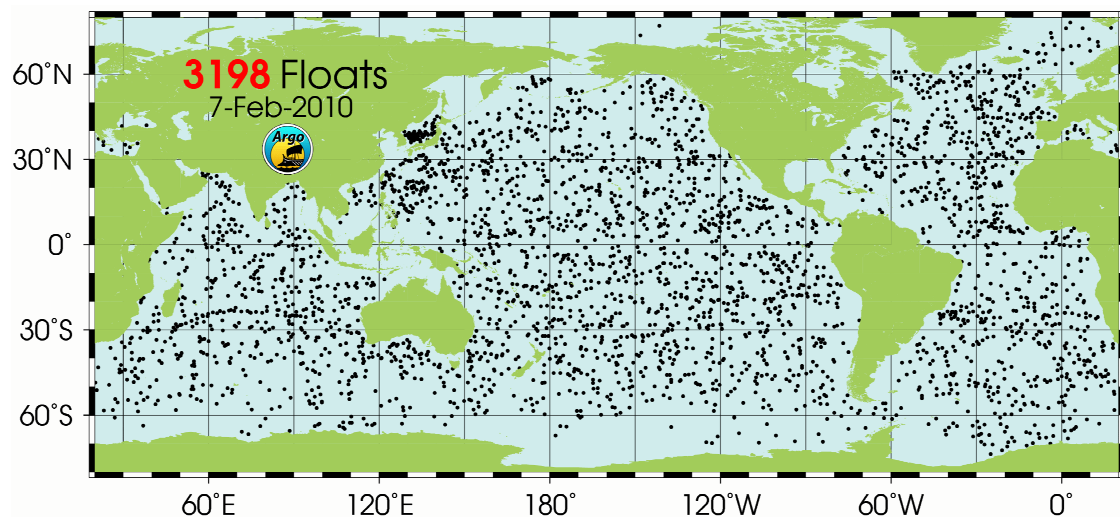


Figure 2.1: Argo float observatory on February 7, 2010. Shown are the latest positions of the floats that have delivered data within the last 30 days (<http://www.argo.uscd.edu>).

Profiling floats and seagliders are autonomous underway vehicles that profile vertically by changing their buoyancy. Seagliders transit additionally horizontally by gliding on their wings during descent and ascent. Both change their density by pumping oil stored in an internal reservoir into an external reservoir (bladder) to increase the volume, at conservation of mass, to ascent or by deflating the bladder to descend (Fig. 2.2, left). Floats descend from the surface to a programmed parking depth (here 800 dbar) where they remain for a certain time (here about 6 days), drifting with the current, before diving to their profile depth (here 2000 dbar). During the ascent from the profile depth to the surface, temperature and conductivity (salinity), measured by a SBE-41 CTD sensor (Sea-Bird Electronics Inc., Bellevue/WA, USA), are recorded at predefined depth levels. The average ascent speed is 0.08 m s^{-1} for an Apex float and $0.09\text{-}0.1 \text{ m s}^{-1}$ for a Provor float (User Manuals: MARTEC Provor CTS3, 2006; Apex-SBE Profiler). At the end of each cycle the float remains for about 6-12 hours at the surface, where it is localized by, and transmit the data to, the Argos satellite system or more recently the Iridium system (Fig. 2.2, right). This measurement cycle is repeated at programmed time intervals of several days (here 7 days).

A small number of floats and seagliders are additionally equipped with chemical and biological sensors, e.g. oxygen optode sensors, bio-optics, chlorophyll fluorometers, pCO_2 sensors, nitrate sensors or particle backscatter sensors [Johnson *et al.*, 2009](Fig. 2.3). In the following sections we focus on Apex floats equipped additionally with oxygen optode sensors, mounted on the upper endcap of the float.

The number of deployed floats with oxygen sensors is growing continuously. More than 200 floats, about 60% of which are currently active, have been deployed whereas the number of collected oxygen data by profiling floats is twice as large as from ship measurements [Johnson *et al.*, 2009]. Oxygen sensors have been deployed on seagliders also with excellent results. Long-term stability is one advantage of the oxygen optode sensors [Tengberg *et al.*, 2003; Körtzinger *et al.*, 2005]. They spend only a short time at the surface and during most of the time they stay in cold and dark environments and consequently biofouling is not a problem in contrast to optodes fixed at moorings in the upper ocean [Tengberg *et al.*, 2006].

Since the sensor responds to the oxygen partial pressure, it is also capable of measuring in air. At the surface, oxygen measurements are performed half-hourly. These measure-

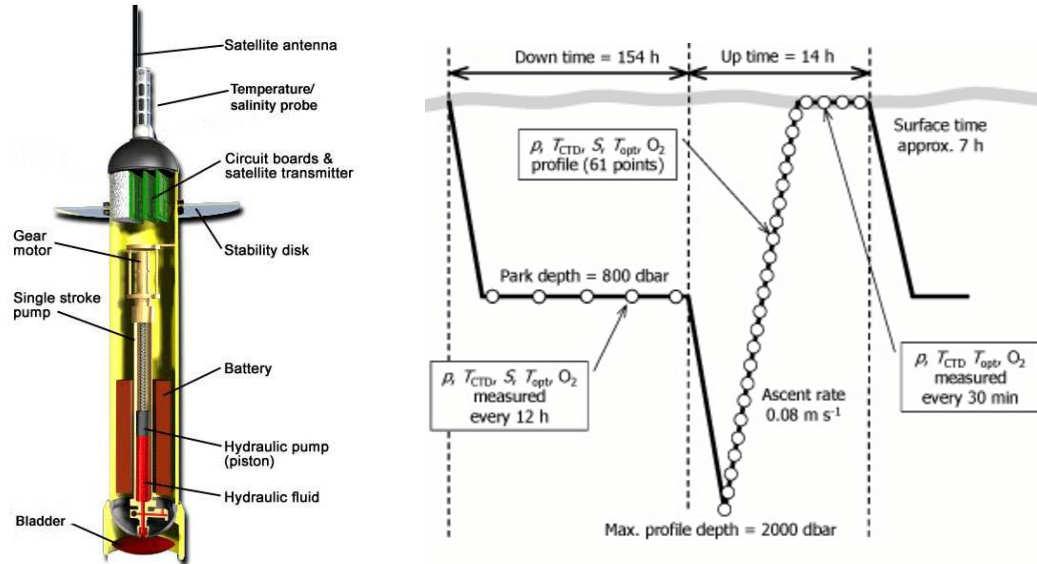


Figure 2.2: Cross section of an APEX float (APEX, Webb Research Inc., Falmouth, USA) (<http://www.argo.ucsd.edu/pictures.html>) (left) and measurement cycle of an APEX float with oxygen optode sensor (right) [Körtzinger *et al.*, 2005].

ments can in principle be used for drift control of the sensor, the barometric pressure can be provided from other sources (e.g., NCAR reanalysis). The sensor reading should equal of the oxygen concentration of freshwater in equilibrium with air (at ambient atmospheric temperature and pressure, 100 % humidity and an oxygen volume mixing ratio of 0.2095). Note, the air around the sensor may not to be at 100 % humidity in reality, however. The oxygen measurements in air at the surface can be compared with calculated equilibrium concentrations using ambient barometric pressure. Therefore, it is a useful method in long-term drift check [Körtzinger *et al.*, 2005].

To use the oxygen data from profiling floats as climate-research-quality data it is important that the oxygen measurements are made at high precision and accuracy. These are requirements for the oxygen optode sensors in order to observe seasonal variation in the upper thermocline, which varies by 10 to 20 $\mu\text{mol kg}^{-1}$ (e.g., [Riser *et al.*, 2004; Najjar *et al.*, 1997]). Further, is the observation of the long-term trend of deoxygenation of the world oceans an important research topic.

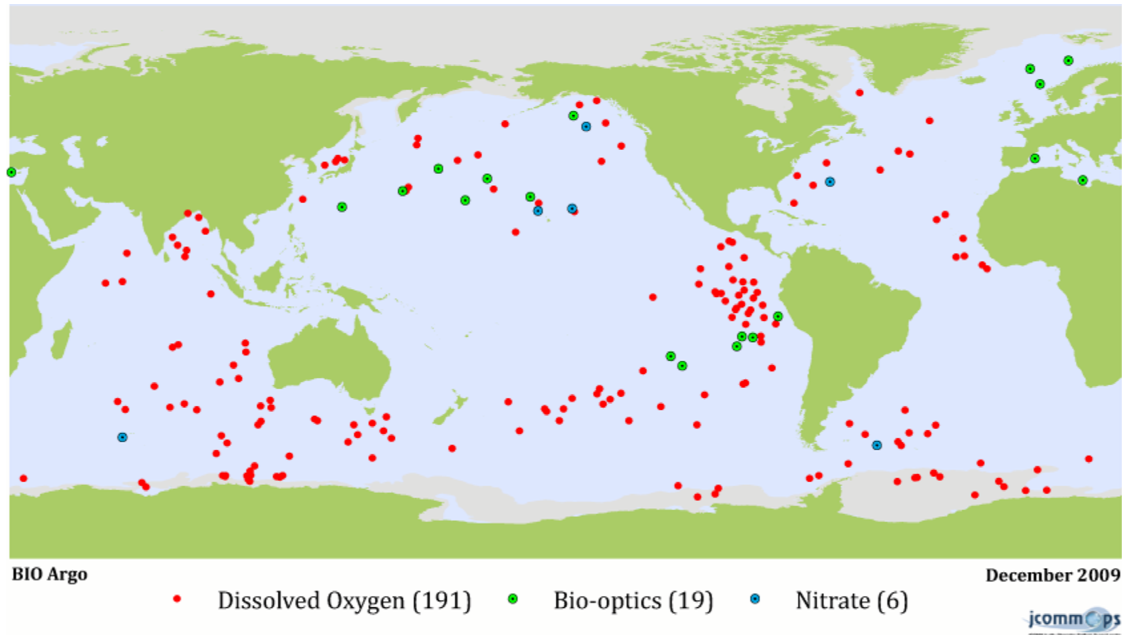


Figure 2.3: All active Argo floats equipped with an oxygen sensor (191, red circles), bio-optical sensors (19, green circles) and nitrate sensors (6, blue circles). Map was downloaded from the Argo Information Center (jcommops) at <http://wo.jcommops.org/cgi-bin/WebObjects/Argo.woa/wa/maps>.

For accuracy a threshold of $5 \mu\text{mol kg}^{-1}$ with a target of $1 \mu\text{mol kg}^{-1}$ is called for. For precision a threshold of $2 \mu\text{mol kg}^{-1}$ with a target of $0.5 \mu\text{mol kg}^{-1}$ has been proposed by *Johnson et al.* [2009].

2.1 Measuring Principle of the Oxygen Optode

The theory of operation of the oxygen optode is based on a principle called dynamic luminescence quenching. This phenomenon is the ability of a substance (here oxygen) to influence the fluorescence of a luminophore. Fluorescence is the emission of a photon, by a molecule that has absorbed light of a certain energy and emits a photon with lower energy, that is longer wavelength (fluorescence). Luminophores can be divided into organic and inorganic substances with the subcategories of fluorophores and phosphores. The difference between luminophores belonging to these two subcategories is derived from the nature of the excited state responsible for the emission of photons. The luminophore, will after absorbing light of a certain energy, enter an excited state. The

collision between the luminophore in its excited state and the quencher (oxygen) results in radiationless deactivation so that no photon is emitted. After collision, energy transfer takes place from the excited luminophore to oxygen which consequently is transferred from its ground state to its excited state. The nonemitting of a photon is called dynamic quenching (Fig 2.5).

The luminophore used in the oxygen optode, is platinum porphyrin (indicator, sensing layer) and is embedded in a polymer layer, and thus is immobilized in the sensing foil mounted on a sapphire optical window. On the outside, the sensing foil is covered by a black gas-permeable coating, to avoid influence from surrounding fluorescent material and to shade it from incoming light in the photic zone (optical isolation, silicon layer)(Fig. 2.4).

The luminophore is excited by a blue-green light (505 nm) from the inside and produces a red fluorescence that is measured by a photodiode through the same window. The gas permeable foil equilibrates with the surrounding seawater. If oxygen is present, the red light will be quenched. The intensity, and lifetime of the returned red light therefore depends on the oxygen concentration in the ambient seawater.

The presence of oxygen will influence the lifetime of the returned red light with respect to the excitation with the blue-green light. This delay is called the luminescence decay time, or lifetime and it will decrease with increasing oxygen concentration. Lifetime-based optode measuring are considered a long-term stable (i.e. drift free) and fast response application (e.g., [Klimant *et al.*, 1997]).

A relationship exists between the oxygen concentration and the luminescence decay time which is described by the Stern-Volmer (e.g., [Demas *et al.*, 1999]) equation:

$$O_2 = \frac{1}{K_{SV}} \left\{ \frac{\tau_0}{\tau} - 1 \right\} \quad (2.1)$$

where O_2 is the oxygen concentration, K_{SV} is the Stern-Volmer constant (the quenching efficiency), τ_0 is the decay time in the absence of O_2 and τ is the decay time in presence of oxygen (for detailed information see Aanderaa Instruments manual). Measurement of the luminescence decay time has some advantages compared to the conventional intensity measurement:

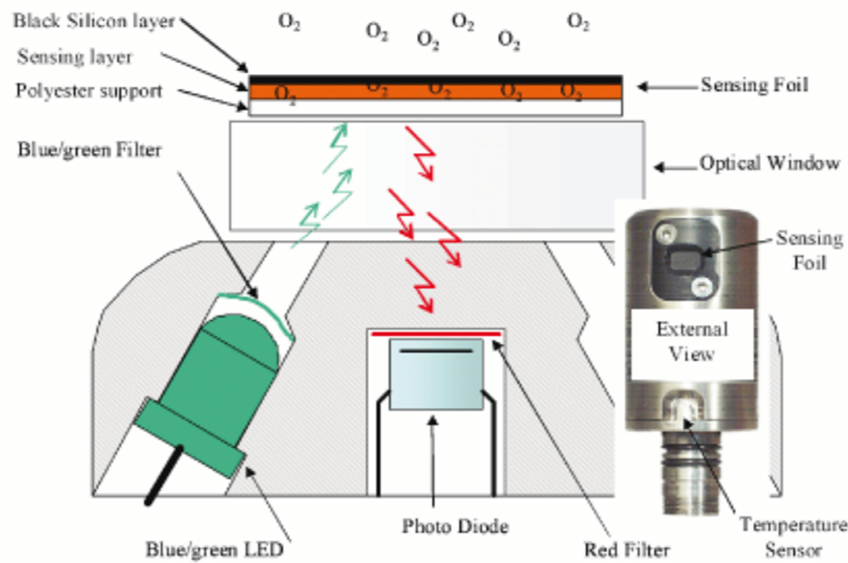


Figure 2.4: Diagram of the optical design and front view of the optode-based oxygen sensor [Tengberg *et al.*, 2006].

- The decay time does not depend on fluctuations in the intensity of the light source and the sensitivity of the detector.
- The decay time is not influenced by variations in the optical properties of the sample including turbidity and coloration.

The oxygen sensor returns oxygen concentration in μM . The sensor is capable of measuring oxygen concentrations in a range of 0-500 μM , that is the full oceanic concentration range, with a resolution of $< 1 \mu\text{M}$ and a nominal accuracy of $< 8 \mu\text{M}$ (or 5 % whichever is greater)[Tengberg *et al.*, 2006].

2.2 Calibration of Oxygen Data

The oxygen raw data have to be corrected for salinity and pressure. The salinity correction is due to the fact that the foil senses the partial pressure of oxygen in the surrounding sea water, but does not sense the salinity, hence the optode measures as if it was deployed in fresh water. The calculated oxygen concentration has to be corrected to the actual salinity, due to the fact that the partial pressure of any gas is salinity

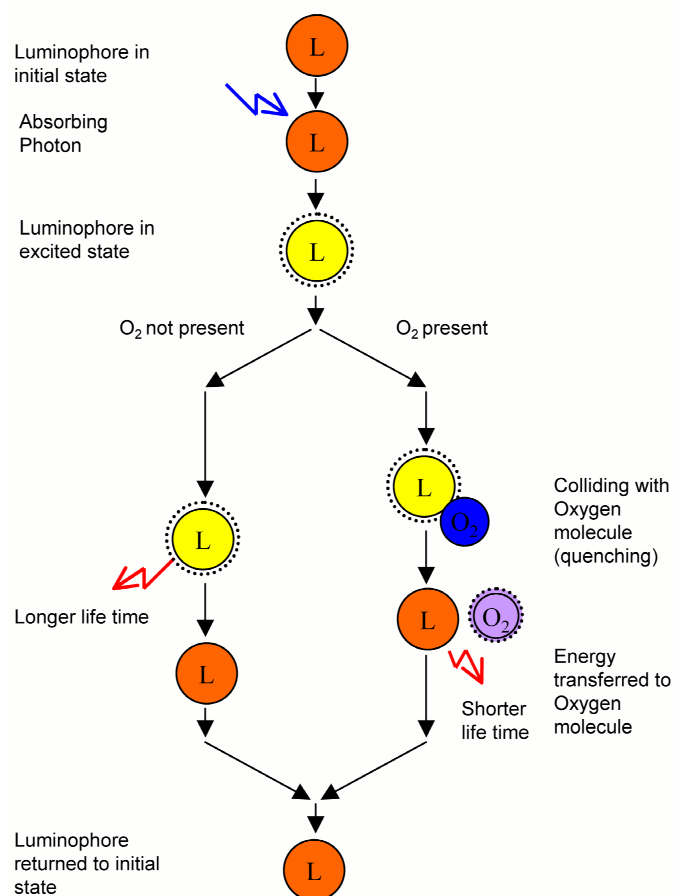


Figure 2.5: Principle of dynamic quenching of luminescence by molecular oxygen [Tengberg et al., 2003; Aanderaa manual].

dependent. If the salinity variation in the study region is small (less than ± 1 psu), the oxygen concentration can be corrected by setting the internal salinity to the average salinity of the study region before deployment. If the salinity varies significantly and in-situ salinity is available, a more accurate correction may be applied by a post correction of the data.

The response of the sensing foil decreases with increasing ambient water pressure. This pressure effect is reported to be linear and fully reversible by using following equation [Tengberg *et al.*, 2006]:

$$O_{2c} = O_2 \cdot \left(1 + \frac{C_p \cdot p}{1000} \right) \quad (2.2)$$

where O_{2c} is the pressure compensated O_2 -concentration, p is depth in meters or pressure in dbar and C_p is the compensation coefficient in %. The compensation coefficient was determined by Tengberg *et al.*, [2006] to be 4% per 1000 dbar. In a recently published study of Uchida *et al.*, [2008], the pressure effect was determined to be smaller than this. They compared high-quality oxygen data obtained by eleven oxygen optodes in the North Pacific with discrete samples. Currently, the oxygen community uses the 3.2% per 1000 dbar pressure correction of Uchida *et al.* [2008] on the basis of these results.

Finally, the relative oxygen saturation in % can be calculated as a function of salinity and temperature:

$$O_{2,sat} = \frac{[O_2] \cdot 2.2414}{C^*} \quad (2.3)$$

where $O_{2,sat}$ is the relative O_2 -saturation in %, O_2 is the oxygen-concentration and C^* is the O_2 solubility at standard air mixture and pressure (1013 hPa) [Garcia and Gordon, 1992].

The standard method to determine dissolved oxygen concentration in seawater is a two-step chemical reaction. Dissolved oxygen is fixed by the addition of manganese(II) under basic conditions, resulting via oxydation of Mn(II) in a heteroganic reaction in a brown precipitation of manganese(III)hydroxide. Prior to analysis, the sample is acidified to pH 1.0-2.5. This causes the precipitated hydroxides to dissolve, liberating the Mn(III) ions. The Mn(III) ions oxidize previously added iodide ions to iodine. The iodine is then titrated with thiosulfate ($S_2O_3^{2-}$), where iodine is reduced to iodide and the thiosulfate is oxidized to tetrathionate ($S_4O_6^{2-}$). The thiosulfate must be standardized with a primary standard, typically potassium iodide (KIO_3). Standardization is based on the co-proportionation reaction of iodide with iodate, thereby forming iodine. The iodine

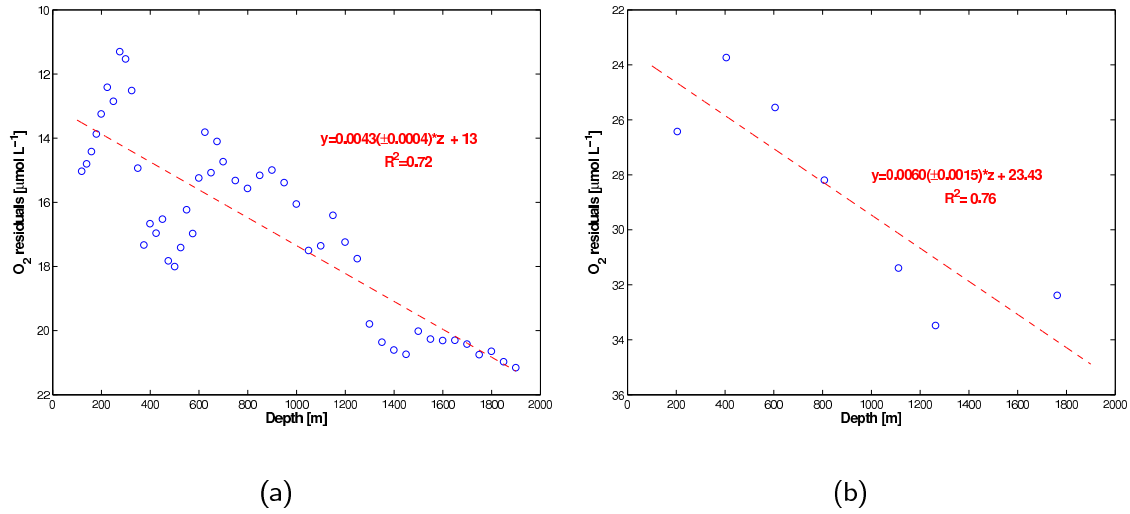


Figure 2.6: Residuals (Winkler - optode) vs. depth for float 4900607, a) and float 4900611, b). The linear regression of residuals vs. depth yields a depth-dependent correction function to post calibrate the oxygen data. After correction the residuals still show a depth dependence. The raw oxygen data were corrected for pressure by 3.2% per 1000 dbar as proposed by *Uchida et. al* [2008].

binds with excess iodide, and the complex is titrated with thiosulfate. The calculation of the oxygen concentration (mL L^{-1}) from this analysis follows in principle the procedure outlined by *Carpenter* [1965].

This method was originally developed by *Winkler* [1888] and modified by *Carpenter* [1965] as described by *Hansen et al.* [1999]. Winkler titration (accuracy $< 1.0 \mu\text{mol L}^{-1}$) has become the standard method and is always performed on collected water samples. The success of this method is critically dependent on the manner in which the sample is treated. At all phases, primarily if the water samples are collected, care must to be taken to ensure that oxygen is neither introduced to nor lost from the collected water samples. The Winkler titration is still used to check instrument calibration.

The raw oxygen data from the oxygen optodes of both floats were corrected for pressure and salinity using the floats pressure and salinity readings [*Aanderaa Manual*; *Tengberg et al.*, 2006] and using the 3.2% per 1000 dbar pressure correction of *Uchida et al.* [2008]. As shown by several other authors (e.g. [*Körtzinger et al.*, 2005; *Uchida et al.*, 2008]) the factory calibration of the oxygen optodes is generally inadequate. For post-calibration the float oxygen data were compared to oxygen concentrations measured on

discrete samples by Winkler titration (accuracy $< 1.0 \mu\text{mol L}^{-1}$). The float and Winkler reference data points were matched in depth-space.

For float 4900611, the first profile was compared with 7 discrete water samples measured by Winkler titration on R/V Charles Darwin cruise 162 taken 7 days before and in a distance of approx. 17 nm. The oxygen concentrations of float 4900611 were corrected with a linear depth-dependent function yielding corrections ranging from $23.7 \mu\text{mol L}^{-1}$ (shallow) to $32.5 \mu\text{mol L}^{-1}$ (deep) with a standard deviation of $\pm 1.8 \mu\text{mol L}^{-1}$ ($R^2=0.76$). For float 4900607, the first profile was compared with a Winkler-calibrated CTD oxygen profile taken during R/V Meteor cruise 59/3 taken 8 days before and in a distance of approx. 20 nm. Float 4900607 was also corrected with a linear depth-dependent function yielding corrections ranging from $11.3 \mu\text{mol L}^{-1}$ to $21.2 \mu\text{mol L}^{-1}$ with a standard deviation of $\pm 1.5 \mu\text{mol L}^{-1}$ ($R^2=0.72$). Matching floats and reference data points in density-space did not significantly improve the results nor the accuracy of the correction. The compared Winkler and float density (σ_θ) is within a mean density of $\pm 0.002 \text{ kg m}^{-3}$ with an standard deviation of $\pm 0.003 \text{ kg m}^{-3}$. Oxygen data shallower than 100 dbar were not included in the correction. The remaining residuals between calibrated oxygen float data did show, however, a clear depth-dependence (Fig. 2.6).

The observed depth-dependence of the O_2 residuals (Winkler - optode) disappears for both floats when a correction of 4.8% per 1000 dbar is applied. This point at the 3.2 % per 1000 dbar depth correction of *Uchida et. al* [2008] as well as the original factory correction of 4 % per 1000 dbar being too low.

Because of the importance of accurately describing the pressure effect, a thorough understanding the source of this disagreement should motivate future work.

Chapter 3

Variability on Seasonal to Interannual Time Scales

The Labrador Sea is the coldest and freshest basin of the subpolar North Atlantic Ocean. It also is a region of particular interest for several groups, because it is one of just a few regions where open-ocean deep convection occurs. In the process of open-ocean convection, surface water sinks as distinct water mass to depth, known as Labrador Sea Water (LSW). Intense air-sea interaction supports the generation of deep winter convection, by loss of heat, resulting in a loss of buoyancy. Labrador Sea Water is characterized as cold and fresh water mass, and can be traced at depths of 500 to 2000 m [Lavender *et al.*, 2000]. The net transfer of heat from the ocean to the atmosphere, is balanced by northward advection of heat through the meridional overturning circulation (MOC). Deep convection is a central component of the thermohaline circulation (THC). First results from hydrographic data have identified deep convection in the Labrador Sea [Clarke *et al.*, 1983] and have inferred a general cyclonic circulation [Lazier *et al.*, 1973]. The Labrador Sea is characterized by strong wind events, incursion of icebergs and sea ice, great contrast in buoyancy, high biological activity [Lab Sea Group, 1998] and as a seasonally varying sink and source of oxygen [Körtzinger *et al.*, 2004;2008] as well as a sink for atmospheric CO₂ [Körtzinger *et al.*, 2008; Watson *et al.*, 2009]. The amplitude of the seasonal and interannual cycles of temperature, salinity and O₂ are affected by physical and biological processes. Freshwater pulses can have a direct impact on the convective process, temperature, salinity and O₂ in the Labrador Sea. Therefore is

the spatial and temporal variation of interest and understanding the pathways of the freshwater cycle and seasonal to interannual time scales has received much more interest in the past time [Schmidt, 2008]. Freshwater input in the North Atlantic Ocean consists of precipitation, continental runoff, Greenland ice shield melt, icebergs and sea ice melt.

Since the mid 90's convection in the Labrador Sea has been reported to be relatively shallow [Yashayaev *et al.*, 2007; Lazier *et al.*, 2002; Pickart *et al.*, 2002], which has reduced the deep ventilation of the Atlantic Ocean.

3.1 Study Region

A suite of physical (temperature, salinity and pressure) and chemical parameters (O_2) were measured successfully with two autonomous profiling floats in the time period of September, 2003 to August, 2006 in the Labrador Sea (Fig. 3.1).

Each float (APEX, Webb Research Inc., Falmouth, USA) was equipped with an oxygen optode sensor (Model 3830, Aanderaa Data Instruments, Bergen, Norway) as well as the SBE-41 CTD sensor (Sea-Bird Electronics Inc., Bellevue/WA, USA) (See section 2). The float data used consist of the data sets of two floats, taken within the rectangular box which marks the approximate location of the area of deep winter convection (Fig. 3.1). Both floats drift at nominal depth of 800 db and the profiles are taken from 2000 db with a cycle time of 7 days. The first float, 4900607, was deployed on September 7, 2003 at 56.552°N and 52.695°W remaining 385 days (corresponds to 55 vertical profiles) in the central Labrador Sea, the later one, 4900611, was deployed on September 15, 2004 at 56.968°N and 50.963°W remaining 665 days (corresponds to 95 vertical profiles) in the central Labrador Sea.

After post-calibration to within $1.8 \mu\text{mol L}^{-1}$ and $1.5 \mu\text{mol L}^{-1}$ resp. of the Winkler-based oxygen reference, we obtained a high-quality oxygen time-series of the upper 2000 m (Fig. 3.8) of the central Labrador Sea as well as for temperature and salinity. Figure 3.2 shows the raw (a,b) and salinity and pressure corrected (c,d) oxygen profiles of both floats. Float 4900607 was the first prototype APEX profiling float with oxygen optode sensor ever deployed. The internal salinity setting of the oxygen optodes sensor was $S=0$ for float 4900607 and $S=35$ for float 4900611 (Fig. 3.2).

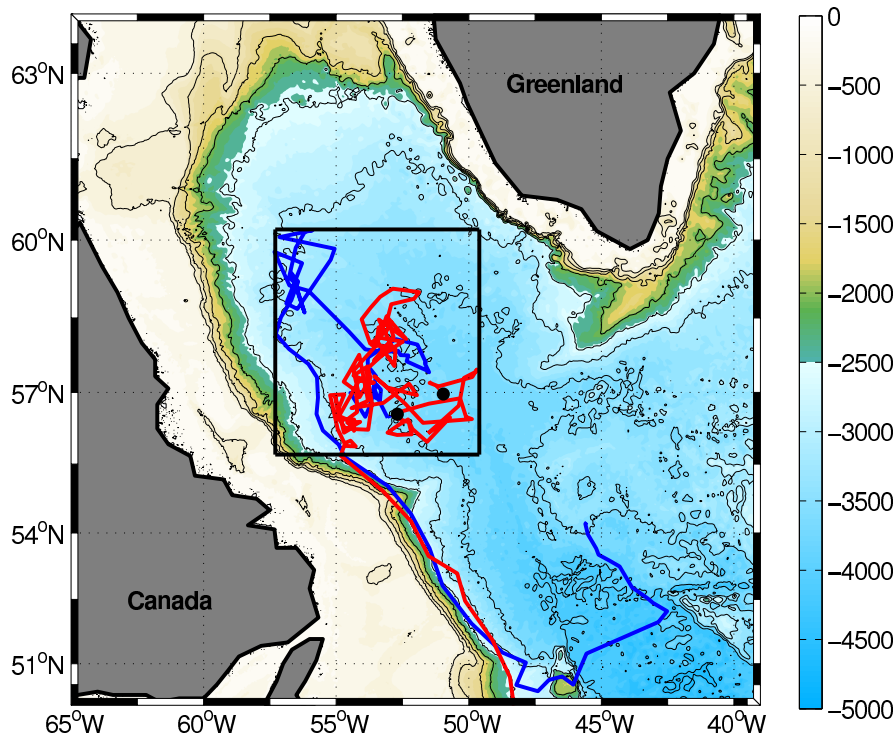


Figure 3.1: Trajectories of two APEX floats equipped with an Aanderaa oxygen optode (Model 3830, Aanderaa Data Instruments, Bergen, Norway) in the central Labrador Sea during the period September, 2003 to August, 2006. The red line shows the track of float 4900607 (September 14, 2003 to October 3, 2004) and the blue line that of float 4900611 (October 13, 2004 to August 9, 2006); the black dots denote the deployment positions. The rectangular box marks the approximate location of the area of deep winter convection. The drift depth of both floats was 800 dbar and the profiling depth was 2000 dbar. The bathymetry contour interval is 500 dbar.

3.2 Mixed Layer Structure and Depth

Seawater properties such as temperature, salinity and density vary with depth. Near the surface the variations of these properties are much smaller than deeper down. The reason for this vertical uniformity is turbulent mixing which is stronger near the surface. Therefore, the upper ocean is often referred as mixed layer. The oceanic mixed layer is considered as a quasi homogenous region of the upper ocean, within which temperature, salinity and density are approximately uniform [*de Boyer Montégut et al.*, 2004]. This definition based on profiles from in situ data that show approximately uniform regions

3 Variability on Seasonal to Interannual Time Scales

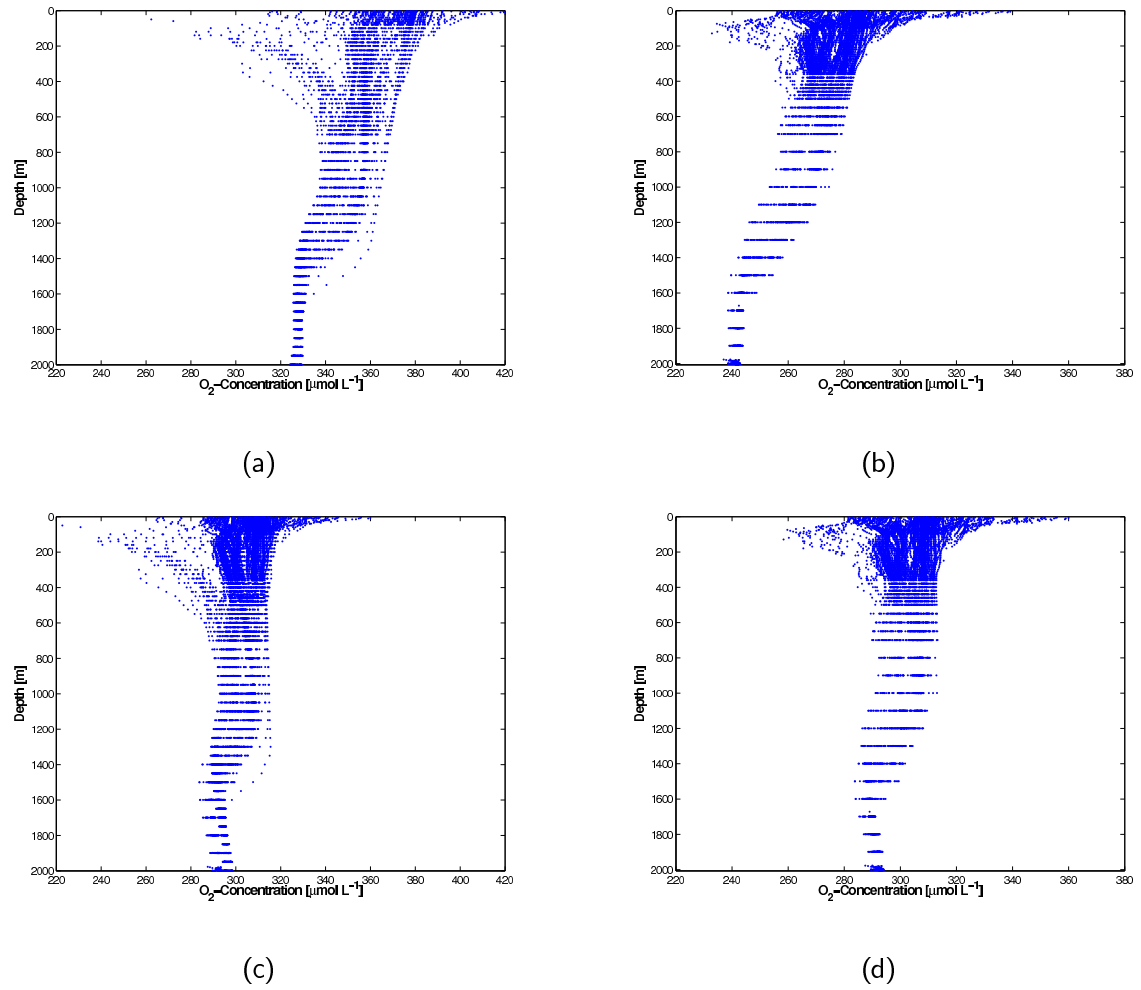


Figure 3.2: Raw oxygen float data of float 4900607 (a) and float 4900611 (b) and salinity and pressure corrected data (c,d), collected in the central Labrador Sea.

of temperature and salinity [e.g., *Pickard and Emery*, 1990].

The transfer of mass, momentum and energy across the mixed layer provides the source of almost all oceanic motion. The thickness of the mixed layer determines the heat content of the layer, which directly interacts with the atmosphere [*Kara et al.*, 2000]. A common difficulty is in determining the base of the mixed layer due to thermal and density stratification sensitivity of the depth of the turbulent mixing, thereby by the chosen criterion to define the mixed layer depth (MLD). The mixed layer depth is an important parameter for determining how the ocean and atmosphere interact. Temporal variability on seasonal (interseasonal) to interannual time scales of the MLD, are linked to many processes occurring in the mixed layer (e.g., surface forcing, lateral advection or waves). During the course of a year, the mixed layer typically undergoes a cycle of deepening, when the surface water becomes colder and denser, and shallowing when surface water becomes warmer and less dense. This cycle is more pronounced at higher latitudes, like the Labrador Sea. The spatial variability of the MLD can be less than a few tens of meters in the summer season, up to 2000 m and more during the winter season of the region of deep convection.

There exists a variety of criteria to determine the mixed layer depth. The most commonly used determination of the MLD is the use of the threshold method (so called Δ -criterion), based on which the MLD is the depth at which temperature or potential density changes by a given threshold value relative to the one at a near surface reference depth. Estimating the MLD by visual examination [*Sprintall and Roemmich*, 1999] or by using a vertical gradient criterion [*Lorbacher et al.*, 2006] are other ways to proceed. Like the Δ -criterion, the gradient criterion depends critically on the prescribed gradient threshold.

Estimating the MLD using classical methods, e.g. *Monterey and Levitus* [1997] for temperature ($\Delta T = 0.5^\circ\text{C}$) as well as for density ($\Delta \sigma = 0.125 \text{ kg m}^{-3}$) are not suitable in subpolar oceans. During the winter period the temperature and density stratification is weak and the use of the classical criterion lead to a gross overestimation of the maximum mixed layer depth (Fig. 3.3)

Another way in determining the wintertime MLD, especially in regions of weak winter-time stratification or where temperature and salinity data are very sparse, is the use of oxygen as proxy. For instance, *Reid*, [1982] used a 95% oxygen saturation limit from

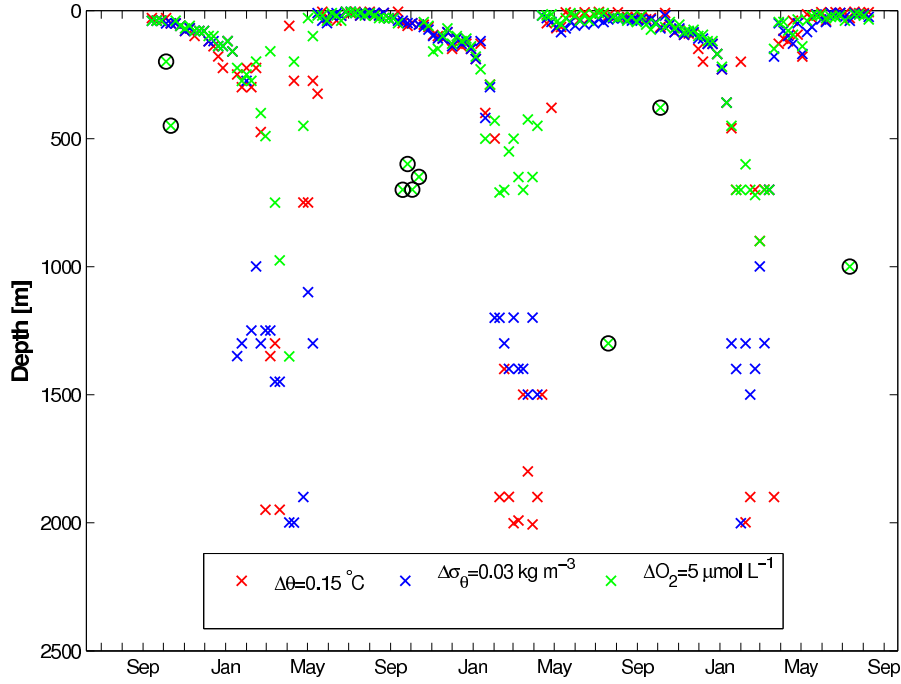


Figure 3.3: Estimation of mixed layer depth using different criteria. A modified classical criterion ($\Delta\theta = 0.15^\circ\text{C}$ (red) and $\Delta\sigma_\theta = 0.03 \text{ kg m}^{-3}$ (blue)) is used for comparison with the oxygen criterion of $\Delta\text{O}_2 = 5 \mu\text{mol L}^{-1}$. Ambiguous oxygen MLDs (black circles) were replaced by $\Delta\sigma_\theta$ determined MLDs.

CTD data to determine the global maximum annual MLD. This 95% oxygen saturation assumption of *Reid* [1982] corresponds roughly to the oxygen dissolved during ventilation at the surface at the time of deepest convective mixing during the year. Such a fixed oxygen saturation threshold is static, however, to take into account the regional dynamics of the surface oxygen reservoir.

The mixed layer depth in this study was determined by using a ΔO_2 -criterion. The depth at which the O_2 concentration differs from the surface O_2 concentration by $5 \mu\text{mol L}^{-1}$ was determined as lower bound of the MLD. We also applied a modified classical criterion ($\Delta\theta = 0.15^\circ\text{C}$ and $\Delta\sigma_\theta = 0.03 \text{ kg m}^{-3}$) for comparison with the oxygen criterion (Fig. 3.3). During the winter period of deep convection, when vertical gradients in temperature and density nearly disappear, even the modified classical criteria overestimated the MLD, whereas the oxygen criterion seems to be a suitable method in MLD determination. At time of stable stratification the modified classical criteria as

well as the oxygen criterion are comparable in determining the MLD (Fig. 3.4).

At a specific time of the year, the oxygen concentration gradient, between surface and depth, is smaller than the O_2 criteria of $5 \mu\text{mol L}^{-1}$, leading to ambiguous MLD. This is due to the strong variability of oxygen in surface waters which during fall causes the surface-to-depth gradient to disappear. These values are replaced by $\Delta\theta$ determined MLD. Mixed layer depths > 400 m were additionally checked by visual inspection.

The onset of convection and the associated deepening of the mixed layer can be identified every year by using oxygen as indicator (Fig. 3.8). The peak of the convection and the renewal of water mass can also be well identified to occur every year approximately in March/April through a deep winter mixed layer with nearly homogeneous cold and salt water from the surface to intermediate depth.

The deepest mixed layer observed by the profiling floats during the three winters (February-April) were 1350 m in 2003/2004, 710 m in 2004/2005, and 900 m in 2005/2006. Mixed layer depth > 600 m were located in the western basin of the Labrador Sea, which is consistent with observations of *Lavender et al.* [2000] and *Våge et al.* [2009].

3 Variability on Seasonal to Interannual Time Scales

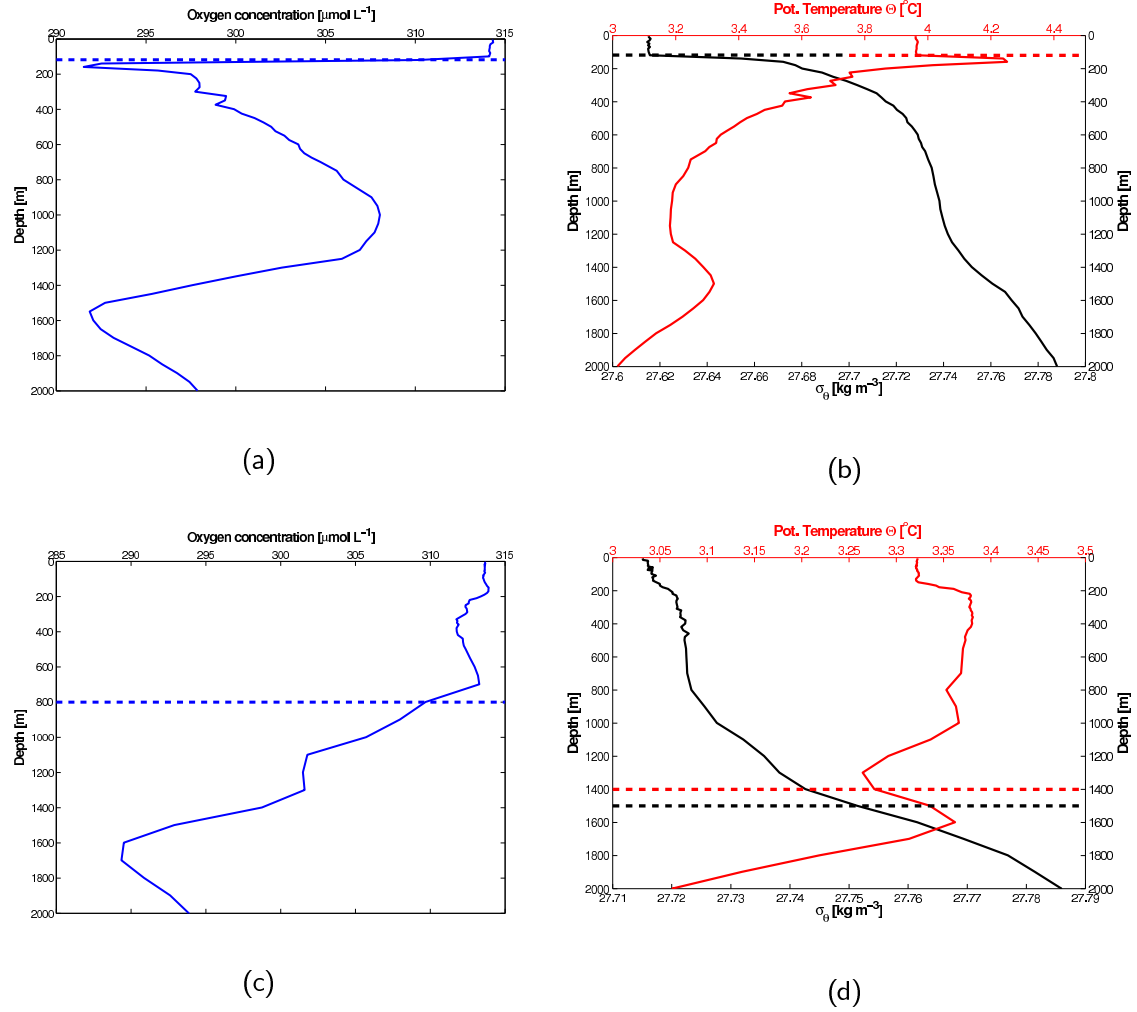


Figure 3.4: Vertical profiles of O_2 concentration (a,c), potential temperature (θ , red) and density (σ_{θ} , black)(b,d). In time of stratification the O_2 criterion (a) as well as the modified classical criteria are comparable in determining the MLD (here 120 m). During convection the O_2 criterion (c) determines a realistic MLD (~ 800 m), whereas the modified classical criteria overestimate the MLD (b) by ~ 600 m (θ) to ~ 700 m (σ_{θ}), due to the weak gradients in θ and σ_{θ} .

3.3 Labrador Sea Salinity and Temperature Cycle

The variability in temperature and salinity during the course of the year is the dominant signal in the upper central Labrador Sea. Interactions of strong meteorological conditions, currents as well as convection in the central Labrador Sea show a strong seasonal cycle. Sea surface temperature (SST) influences the atmosphere through its effect of sensible and latent heat flux across the air-sea interface. Ekman advection also influence the mean SST gradient. A decrease in temperature results in increasing density, so the temperature stratification generally produces a stable density stratification. A decrease in salinity, therefore produces a density decrease, so the salinity stratification would produce an unstable density stratification. The most straight-forward method, analyzing interannual trends, is using the mean for every month deduced from the float data set. The advantage of this method is that the standard deviations for each month can be determined easily.

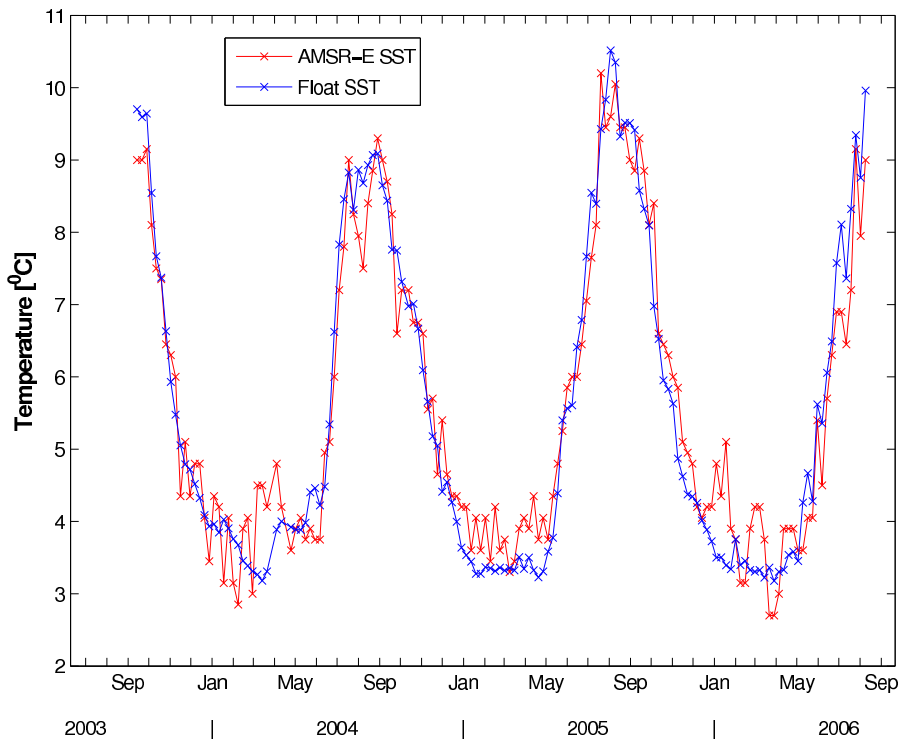


Figure 3.5: Comparison of sea surface temperature measurements by the floats (blue line) and the Advanced Microwave Scanning Radiometer-EOS on the NASA EOS satellite aqua (red line), daily product in $0.25^\circ \times 0.25^\circ$ spatial resolution. (<http://map.nasa.gov/data/amsre/sst/>)

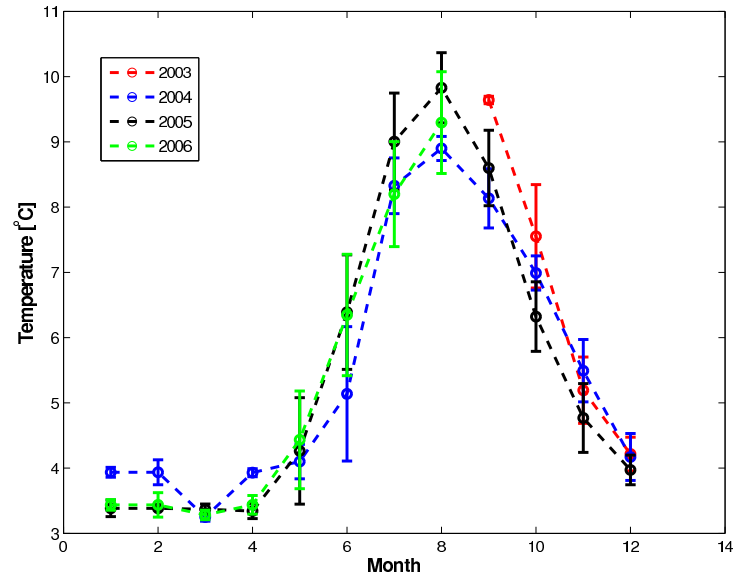
3 Variability on Seasonal to Interannual Time Scales

A disadvantage of this method is that extreme low or extreme high measurements, which can modulate the seasonal cycle, are smoothed. Remotely sensed microwave SST data were compared with in situ sea surface temperatures measured by the profiling floats, which have been shown before to agree rather well. The in situ temperature differed by -0.06°C with a standard deviation of 0.59°C from the SST measured by the satellite (Fig. 3.5).

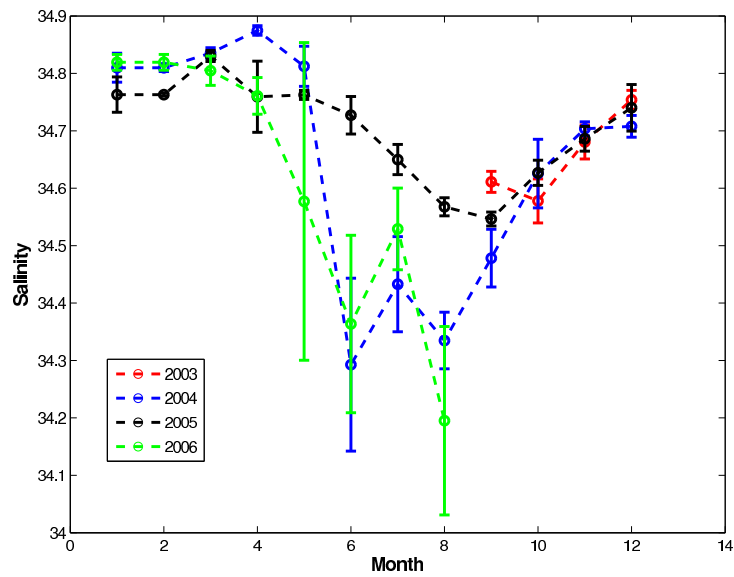
The mean monthly measurements of sea surface temperature (SST) and sea surface salinity (SSS) are shown in Figure 3.6 a+b. Monthly mean SSS varies in general from 34.20 psu to 34.87 psu and SST varies from 3.3°C to 9.8°C . The seasonal cycle can be changed dramatically, during times of pronounced forcing and/or by advection, due to enhanced or stopped convection, mixing, thermal forcing or advection [Schmidt, 2008]. The mean monthly cycle of temperature shows low SST from December to April. The second year of observation (2004) has the smallest seasonal fluctuations, reaching the lowest maximum in August of all years. May to August exhibits a strong increase of temperature with maximum values of 8.9°C to 9.8°C . In the following months until December, temperature as well as salinity decrease. At the beginning of each year the sea surface water is cold and salty.

April to June exhibits a short freshening (Fig. 3.6b) in 2004 and 2006, reaching maximum in June. In July, a salinification of 0.14 psu (2004) and 0.17 psu (2006) interrupt the freshening. A stronger second freshening is observed in both years in August, decreasing 2004 until November. The decrease in 2006 is not presented, due to the fact that the float drifted out of study region. The observed freshening cycles have been discovered and described before by Schmidt and Send [2007] and Schmidt [2008] and the float observations are in a good agreement with it. The timing of the observed end of the first freshening and the onset of the second freshening is nearly one month later than observed by Schmidt [2008]. In 2005, the two freshening pulses cannot be seen, however a less intense but prolonged freshening period from March to September is observed, decreasing until November. The variable freshening cycle in 2005 could result from a combination of heat loss to the atmosphere, lateral mixing and advection of relatively salty and warm recirculated Irminger Sea Water, or vertical mixing with the layer beneath. Another reason could be addressed to the high variability of the first pulse and its absence in years with high eddy kinetic energy (EKE) [Straneo, 2006]. The temperature evolution reveals a warming trend in 2005 and 2006 in surface waters of

3.3 Labrador Sea Salinity and Temperature Cycle



(a)



(b)

Figure 3.6: Central Labrador Sea surface temperatures (a) and sea surface salinity (b) annual cycles, as monthly bins with standard deviation are shown. Red dashed line denotes year 2003, blue dashed line year 2004, black dashed line year 2005 and green dashed line 2006.

0.3 to 0.8°C referred to 2004 (Fig. 3.6a). An increase of about 0.6 °C for 1996 to 2005 of the vertically averaged temperature was found by *Avsic et al.* [2006]. The spring restratification occurs fast and warm and saline waters occupying the upper 200 m (Fig 3.7a,b).

The reasons for the higher standard deviation from May to August could be related to the arrival of eddies or waters from dissipating eddies from the northern central Labrador Sea [*Schmidt, 2008*].

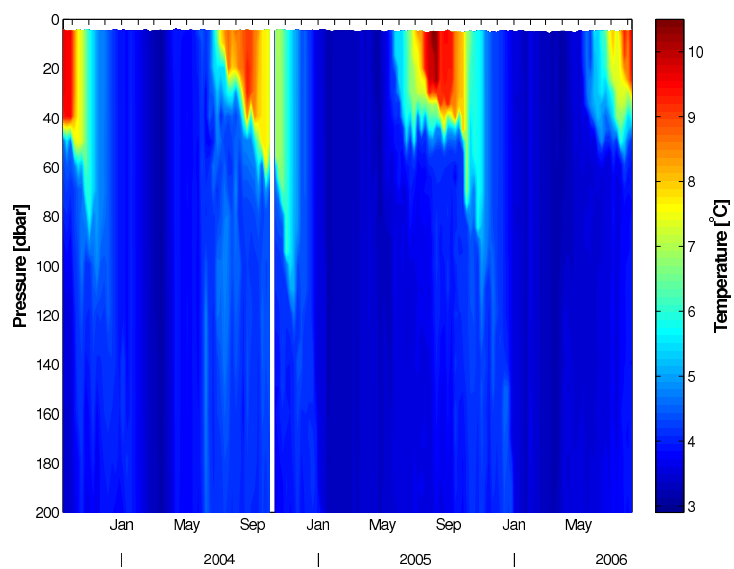
The local salinity maximum, of April 2004, likely due to the temperature minimum occurring of about one month earlier, is associated with deep winter convection of this year. The annual salinity cycles are dominated by strong variations/fluctuations generally in summertime, whereas the annual temperature cycles are more uniform and predictable.

3.4 Oxygen Cycle

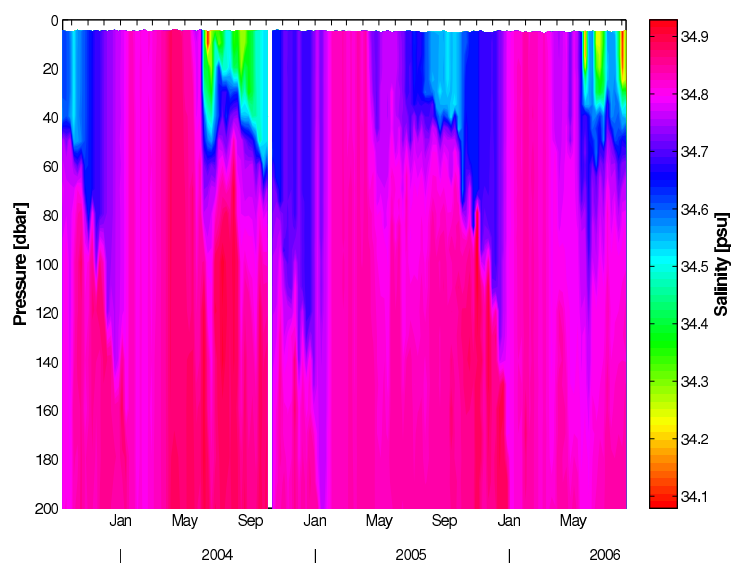
The annual cycle of oxygen varies depending on depth. The biological community in the upper ocean (i.e. photosynthesis in the euphotic zone) is a net source of oxygen. The interior ocean has no internal oxygen source. Below this O₂ production zone, oxygen is consumed by bacterial respiration (O₂ sink). This change in the O₂ concentration is well captured by the profiling floats (Fig. 3.8).

The O₂ concentration in the oceans interior therefore reflects a balance between supply through circulation and loss through respiration. Within the mixed layer, O₂ concentration is often very close to the O₂ saturation. Variation in the saturation result, in part, from net community O₂ production, surface heat fluxes, advection and turbulent diffusion, waves (oxygen injection by bubbles) and by air-sea gas exchange. The ventilation of the upper ocean or oxygen intake is mostly driven by the deepening of the mixed layer in wintertime.

The seasonal O₂ concentration and saturation cycles are shown in Figure 3.9 a+b. During deep convection periods strong uptake of oxygen from the atmosphere occurs which leads to a rapid buildup of the oxygen inventory down to the maximum convection depth. It is of interest to note, however, that due to the short time scale of the rapid



(a)



(b)

Figure 3.7: Time series of the temperature (a) and salinity (b) of the upper 200 m in the convection region of the central Labrador Sea. The white line indicates the separation between the earlier deployed float 4900607 and the later deployed float 4900611.

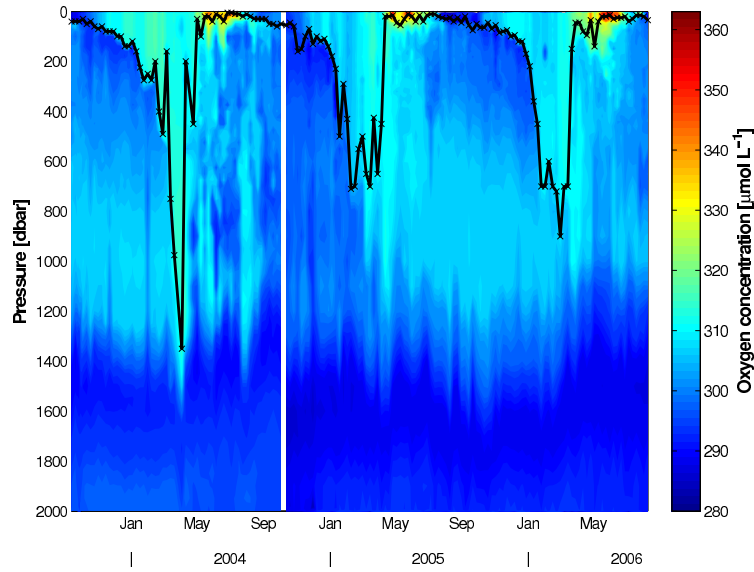
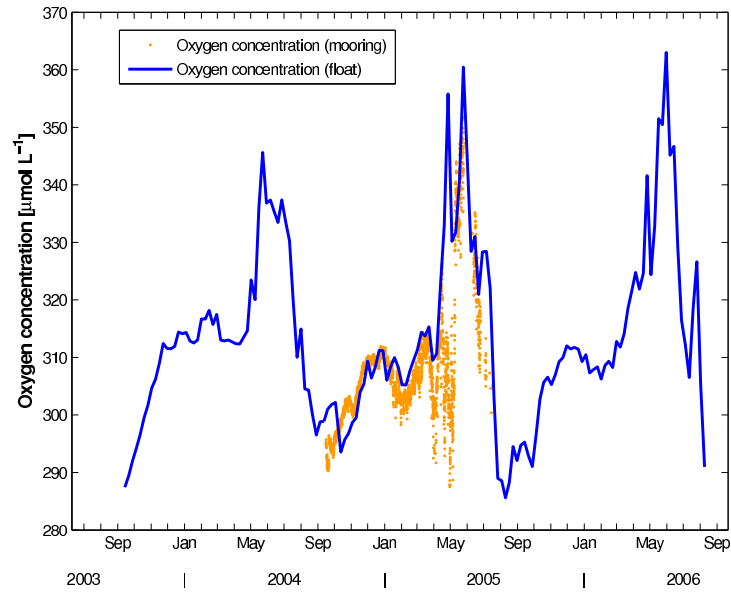


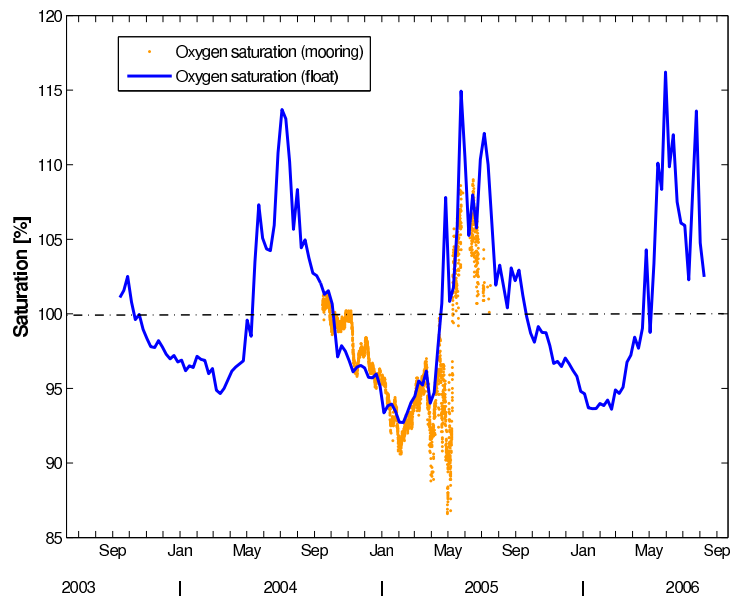
Figure 3.8: Time series of the oxygen concentration (O_2) of the upper 2000 m in the convection region of the central Labrador Sea. Also shown is mixed layer depth (black line) estimated from the float oxygen profiles with an oxygen criterion of $\Delta O_2 = 5 \mu\text{mol L}^{-1}$. The white line indicates the separation between the earlier deployed float 4900607 and the later deployed float 4900611.

deepening convection the mixed layer never reaches equilibrium with the atmosphere but typically stays by 5-7% undersaturated (see also Körtzinger *et al.* [2008]). These waters ventilate the upper thermocline. After the cessation of the convection activity the convectively mixed volume is almost instantly sealed from atmospheric contact by a rapidly forming warm and fresh (sea ice meltwater) surface layer. In this layer the spring bloom soon forms which causes production of oxygen and depletion of winter time nutrient concentration. Therefore, the mixed layer changes from undersaturated to strongly supersaturated by up to 16% for oxygen in late spring. The annual cycle of the oxygen concentration is characterized by a spring maximum (i.e. end of May) and a late summer/early fall minimum, consistent with a ventilation-respiration cycle [Najjar and Keeling., 1997]. The timing of the observed seasonal O_2 maximum of April/May is somewhat earlier than in the climatologies of Najjar and Keeling [1997] and Keeling *et al.* [1998], which points at the smoothing effect of interpolation for a climatological cycle.

The peak-to-peak variation in surface O_2 concentrations ($\sim 58 \mu\text{mol L}^{-1}$ in 2003/2004, $\sim 67 \mu\text{mol L}^{-1}$ in 2004/2005 and $\sim 77 \mu\text{mol L}^{-1}$ in 2005/2006) are slightly larger than



(a)



(b)

Figure 3.9: Time series of oxygen concentration (a) and saturation (b) at sea surface observed by floats (blue) compared with measurements at the K1 mooring (orange). Oxygen saturation was calculated using the oxygen solubility after *García and Gordon* [1992]. During fall/winter the oxygen concentration at the surface is significantly undersaturated by up to 7% and in spring/summertime supersaturated by up to 16%. Float and mooring data are in a good agreement. The K1 mooring data are taken from *Körtzinger et al.* [2008].

3 Variability on Seasonal to Interannual Time Scales

in the climatologies ($\sim 35\text{--}45 \mu\text{mol kg}^{-1}$ again illustrating their smoothed nature). The local maximum in surface O_2 concentrations increases by $\sim 17.4 \mu\text{mol L}^{-1}$, indicating an increase or faster buildup of primary production. In late summer/early fall equilibrium with the atmosphere is nearly reached, at this time the net community O_2 production has become small and the water column is well stratified. The oxygen concentration as well as the saturation are in an excellent agreement with measurements of the long-term oceanographic mooring site K1, located in the central Labrador Sea (56.5°N , 52.6°W). There the O_2 optode sensor (Model 3830, Aanderaa Data Instruments, Bergen, Norway) was deployed at a nominal depth of about 38 m. A two-point laboratory calibration was performed, at 0% and 100% O_2 saturation, to calibrate the oxygen sensor, prior to deployment. The resulting accuracy was estimated at $2 \mu\text{mol kg}^{-1}$ [Körtzinger *et al.*, 2008].

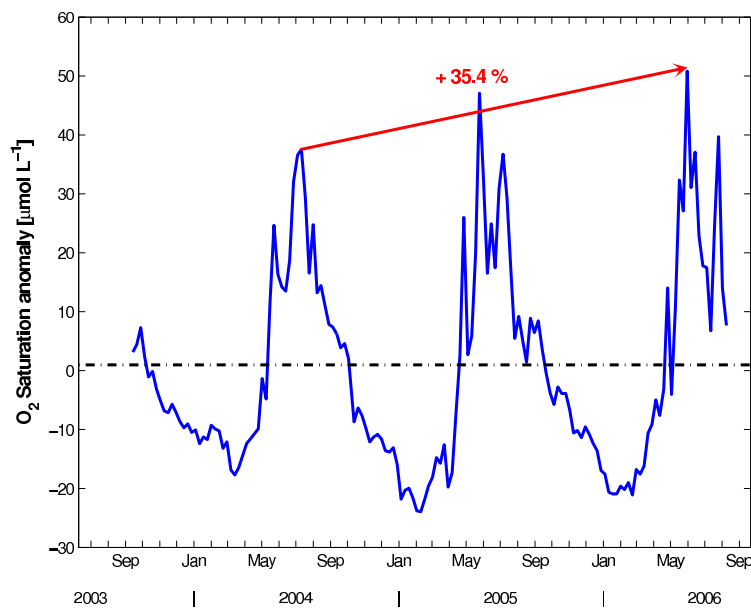


Figure 3.10: Surface O_2 saturation anomaly in the central Labrador Sea. Summer-time saturation increases by $13.3 \mu\text{mol L}^{-1}$ or $+35.4\%$ between 2004 and 2006, indicating higher or more rapid biological activities.

The surface O_2 saturation anomaly ($\text{O}_2^{\text{meas}} - \text{O}_2^{\text{sat}}$) varies during the year (Fig. 3.9). Biological activity as well as temperature (which affect both oxygen concentration and solubility) are the main factors regulating O_2 saturation. During fall/winter respiration and the effect of surface cooling decrease the oxygen saturation anomaly drastically from $\sim +45$ to $\sim -20 \mu\text{mol L}^{-1}$. In spring/summer when restratification occurs and the mixed

layer shoals the water turns from undersaturated to supersaturated, due to spring bloom. The rather constant increase of the maximal saturation anomaly by $13.3 \mu\text{mol L}^{-1}$ or $+35.4\%$ between 2004 and 2006, indicates higher or more rapid biological activities (i.e. primary production).

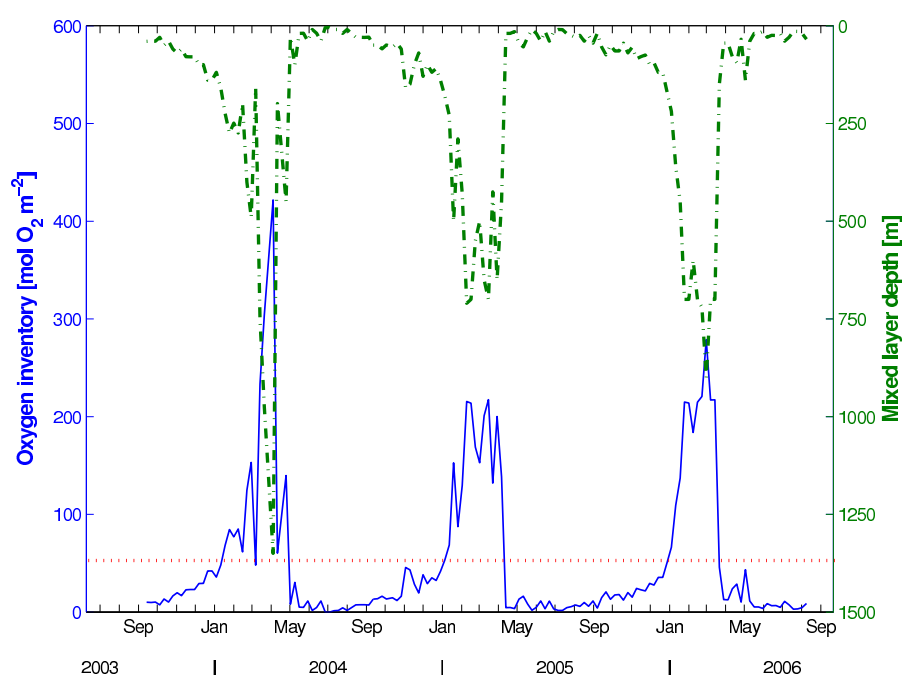
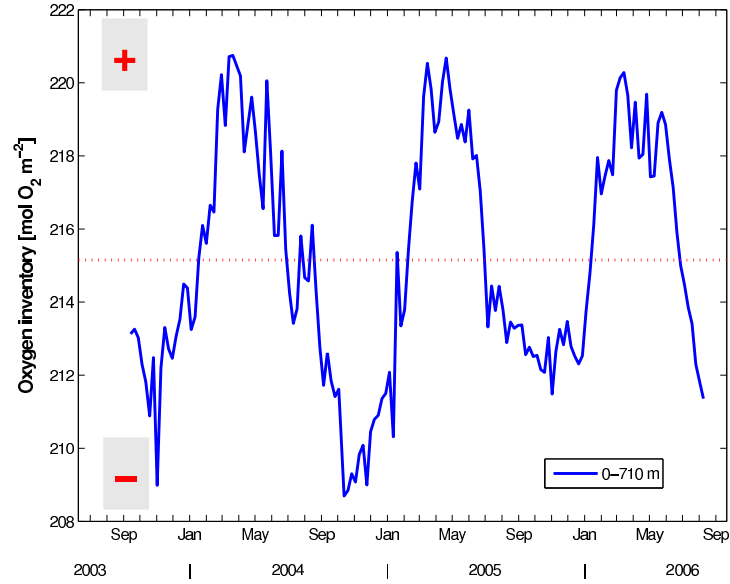


Figure 3.11: Temporal development of the O_2 inventory, calculated between surface and mixed layer depth (blue line), mixed layer depth (dashed green line) and average O_2 inventory (dotted red line) are shown.

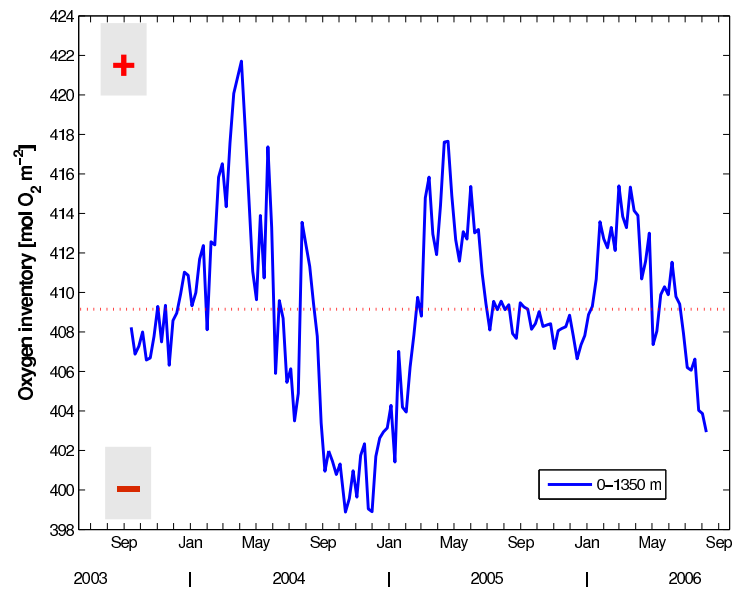
The transition from shallow summer mixed layer into a convectively overturning deep winter mixed layer was associated with an oxygen inventory increase (Fig. 3.11), driven by the rapid deepening of the mixed layer. This deepening was associated with exposing large volumes of undersaturated water to the atmosphere leading to air-sea flux of oxygen into the ocean. The wintertime inventory exhibits a ventilation-respiration cycle. When the mixed layer reaches its maximum in February-April the mixed layer is well ventilated. Oxygen inventory of the mixed layer increase 2004 to $\sim 370 \text{ mol O}_2 \text{ m}^{-2}$, 2005 to $\sim 149 \text{ mol O}_2 \text{ m}^{-2}$ and 2006 to $\sim 227 \text{ mol O}_2 \text{ m}^{-2}$. Integrating the O_2 inventory to the maximum winter mixed layer depth of the respective year, yields an increase of $15.1 \text{ mol O}_2 \text{ m}^{-2}$ in 2003/2004, $11.1 \text{ mol O}_2 \text{ m}^{-2}$ in 2004/2005 and $8.3 \text{ mol O}_2 \text{ m}^{-2}$ in 2005/2006.

After cessation of the convection the inventory increase is stopped and the homoge-

3 Variability on Seasonal to Interannual Time Scales



(a)



(b)

Figure 3.12: Temporal development of the O_2 inventory of the upper 710 m (a) and the upper 1350 m (b) in the convective region. The average O_2 inventory is illustrated by the dotted red line. Positive anomalies are indicated by "+" and negative anomalies by "-".

neously mixed water is capped by a shallow low-salinity and warm surface layer, sealed from the atmosphere (Fig. 3.6b). The extremely rapid decrease of the mixed layer O_2 inventory after the convection is striking and is driven by outgassing in summer. The mixed layer O_2 inventory decreases throughout the summer, through respiration and lateral export of the ventilated water. This "deep breath" in the subpolar north Atlantic Ocean was also observed by *Körtzinger et al.* [2004].

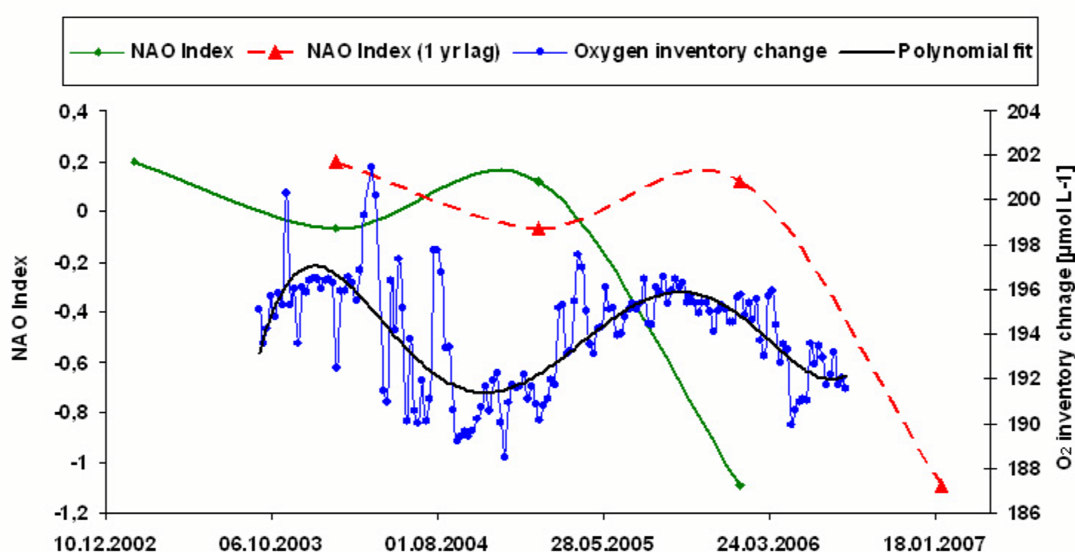


Figure 3.13: Variability of ΔO_2 inventory versus time in the central Labrador Sea during the time periode of September 14, 2003 to August 9, 2006, between maximal winter mixed Layer (1350 m) and shallowest winter mixed layer (710 m), blue line. The polynomial fit of ΔO_2 inventory is indicated by the black line. The green line shows the NAO index during the time periode of 2003-2006 (plotted at January 30 of each year) and lagged by one year (dotted red line).

The oxygen inventory cycles of the upper 710 m, i.e. the shallowest maximal winter MLD, and of the upper 1350 m, i.e. the deepest maximum winter MLD, are shown in Figure 3.12 a+b. The average O_2 inventory is indicated by the dotted red line, that positive O_2 inventory anomalies are indicated by "+" and negative O_2 inventory anomalies by "-". The positive anomalies in Figure 3.12a in wintertime are of nearly in the same magnitude of 5.20 to 5.67 mol O_2 m⁻², indicating a constant annual ventilation of the upper 710 m. Deeper down the situation is slightly different (Fig. 3.12b), the ventilation of the upper 1350 m decreases by 50% from 12.62 mol O_2 m⁻² in 2004 to 6.31 mol O_2 m⁻² in 2006. The local neagive anomaly peak in late fall of

3 Variability on Seasonal to Interannual Time Scales

2004 are observed in both O_2 inventory cycle. This could be explained by mixing of less oxygenated surrounding waters.

The difference between the 1350 m and 710 m of O_2 inventory can be seen in Figure 3.13. Displayed is the interannual cycle of ΔO_2 inventory between 2003 and 2006. The ΔO_2 inventory shows strong fluctuations in 2003 to 2005. This scatter could be explained by the strong variability and modulation in the buildup and the decay of the O_2 inventory in the convection region during this time period. The green line denotes the NAO-index (plotted at January 30, of each year) and lagged by one year (red line). This indicates that the NAO may have some effect on the ventilation and hence buildup of the deep oxygen inventory with a lag period of about 1 year.

It has to be noted, however, that the restricted time of the data in the central Labrador Sea region prohibited a precise determination of ΔO_2 inventory - NAO index connection. Long term observations could be helpful in accurate determination of this phenomenon. It is thus possible that the ΔO_2 inventory is modulated by what is responsible for the interannual variability of the NAO.

Chapter 4

Air-sea gas transfer coefficient for oxygen derived from float data

C.Kihm and A.Körtzinger

Leibniz-Institut für Meereswissenschaften an der Universität Kiel, Düsterbrooker Weg
20, 24105 Kiel, Germany.

Abstract

We estimated the air-sea gas transfer coefficient for oxygen using three consecutive years (Sept. 2003 to Aug. 2006) of high-quality oxygen measurements from profiling floats in the central Labrador Sea. Mixed layer oxygen concentrations exhibit strong seasonality characterized by biologically and thermally driven outgassing during spring/summer and uptake during fall/winter caused by cooling and ventilation of oxygen-deficient subsurface waters. Mixed layer oxygen budgets excluding the spring bloom period are employed to estimate the air-sea transfer coefficient for oxygen. By using co-located wind speed data acquired by scatterometry from the QuikSCAT satellite, wind speed dependent parameterizations for the air-sea transfer coefficient k_{660} (CO_2 at 20°C and salinity 35) are established and compared with prominent parameterizations from the literature. Quadratic, cubic and biquadratic functions are fitted to the data for short-term and long-term wind speed averages separately. In both cases the quadratic functions yield the poorest fit to the observations. The stronger curvature of the cubic functions provides a significantly improved fit that is even slightly superseded by the biquadratic function. Our results generally confirm the stronger wind speed dependencies among the suite of published parameterizations. Also the better fits found for cubic or even biquadratic functions point at the strong importance of very high wind speed for air-sea gas exchange.

4.1 Introduction

For several decades, significant effort has gone into determining the relationship between the air-sea gas transfer coefficient and wind speed. Using such a relationship, gas fluxes can be calculated from measured partial pressure differences, in our case of oxygen, and wind speed over the ocean. In this study we followed a budget approach to determine the air-sea gas transfer coefficient for oxygen in the convection region of the central Labrador Sea. Changes in the vertical mixed layer oxygen inventory between two consecutive oxygen profiles were interpreted to be generally dominated by air-sea exchange of oxygen. We excluded the spring bloom period where this assumption is clearly violated due to high biological productivity and the concurrent production of oxygen. In the remaining data however, small scale spatial variability is inevitably included in the analysis and creates considerable scatter in the obtained results.

4.2 Methods

4.2.1 Oxygen floats

In this study we use dissolved oxygen concentrations measured by two profiling floats in the Labrador Sea (Fig. 4.1). Each float (APEX, Webb Research Inc., Falmouth, USA) was equipped with an oxygen optode sensor (Model 3830, Aanderaa Data Instruments, Bergen, Norway) as well as the SBE-41 CTD instrument (Sea-Bird Electronics Inc., Bellevue/WA, USA). During the float's ascent from its profiling depth (2000 dbar) to the surface, temperature, conductivity (salinity), pressure and oxygen are measured at 72 depth levels. At the surface the float transmits the collected data via the Argos satellite system and then dives to its drift (parking) depth of 800 dbar. This measurement cycle is repeated every 7 days. Float 4900607 was deployed on September 7, 2003 and float 4900611 on September 15, 2004. Following thorough quality control, 150 profiles from the two floats containing 61 to 72 vertical data points each were included in the present analysis.

4.2.2 Mixed Layer Depth

Mixed layer depths (MLD) were estimated from vertical temperature, salinity and oxygen profiles measured by the two ARGO floats 4900607 and 4900611. The classical criteria of *Monterey and Levitus* [1997] for temperature ($\Delta T = 0.5^\circ\text{C}$) as well as for density ($\Delta\sigma = 0.125 \text{ kg m}^{-3}$) are not suitable in subpolar oceans. Using these classical criteria caused significant overestimation of the mixed layer depth particularly during the winter period of deep convection when vertical gradients in T and σ nearly disappear. We applied oxygen as a tracer for the estimation of the ventilated mixed layer depth as proposed by *Körtzinger et al.* [2008]. Where oxygen data were available, an oxygen difference criterion ($\Delta O_2 = 5 \mu\text{mol L}^{-1}$) was applied to estimate mixed layer depth. Mixed layer depths $> 400 \text{ m}$ were additionally checked by visual inspection and ambiguous MLD values were replaced by the visually determined mixed layer depth of the oxygen profile. We also applied a modified classical criterion ($\Delta\theta = 0.15^\circ\text{C}$ and $\Delta\sigma_\theta = 0.03 \text{ kg m}^{-3}$) for comparison with the oxygen criterion. The deepest mixed layer depths observed by the profiling floats during the three winters (February-April) were 1350 m in 2003/2004, 710 m in 2004/2005, and 900 m in 2005/2006.

4.2.3 Wind Data

The Sea winds scatterometer on the QuikSCAT Satellite was launched in 1999 and delivers wind speed data at global coverage. The highest spatial resolution is 25 km gridded onto a geographical grid of about $0.25^\circ \times 0.25^\circ$. In this study we utilize QuickSCAT wind speed level 3 data (http://podaac.jpl.nasa.gov/DATA_PRODUCT/OVW/index.html) from September 2003 to August 2006. The level 3 file contains only the latest measurement for each day with a location accuracy of 10 km (relative). Several studies (e.g. *Boutin et al.* [2009]) demonstrated the good quality of the QuickSCAT wind data ($\text{RMS} \sim 1 \text{ m s}^{-1}$). Wind data were matched with float profiles using the average position between each pair of surfacings. To include information about wind speed variance we also used the 8 neighbor points around this location. The variance of wind speed can have a significant influence on the gas transfer velocity calculated from a non-linear relationship between gas transfer and wind speed. Long-term winds were obtained by averaging

linearly over the 9 grid points at each mean float position as well as over the 7-day interval. Squared (cubed, bisquared) winds were used to calculate quadratic (cubic, biquadratic) long-term wind parametrizations. Quadratic (cubic, biquadratic) short-term wind parametrizations were calculated using winds at the average float position of each pair of surfacings, averaged over a 7-day interval by using the following equation:

$$u_{10} = \sqrt[b]{\sum \left(\frac{u^b}{n} \right)} \quad (4.1)$$

where b is 2 for the quadratic wind, 3 for the cubic wind or 4 for the biquadratic wind, and n is the number of observations.

4.2.4 Calibration of oxygen data

The raw oxygen data from the optodes were corrected for pressure and salinity using the float's pressure and salinity readings (Aanderaa Manual; *Tengberg et al.* [2006]) employing the 3.2 % per 1000 dbar pressure correction of *Uchida et al.* [2008]. As shown by several other authors (e.g. *Körtzinger et al.* [2005]; *Uchida et al.* [2008]) the factory calibration of the oxygen optodes is generally inadequate. For post-calibration the float oxygen data were compared to oxygen concentrations measured on discrete samples by Winkler titration (accuracy $< 1.0 \mu\text{mol L}^{-1}$). The float and Winkler reference data points were matched in depth-space. For float 4900611 the first profile was compared with 7 Winkler samples from R/V Charles Darwin cruise 162 taken 7 days before and in a distance of approx. 17 nm. The oxygen concentrations of float 4900611 were corrected with a linear depth-dependent function yielding corrections ranging from $23.7 \mu\text{mol L}^{-1}$ (shallow) to $32.5 \mu\text{mol L}^{-1}$ (deep) with a standard deviation of $\pm 1.8 \mu\text{mol L}^{-1}$ ($R^2=0.76$). For float 4900607 the first profile was compared with a Winkler-calibrated CTD oxygen profile taken 8 days before and in a distance of approx. 20 nm during R/V Meteor cruise 59/3. Float 4900607 was corrected in the same way, i.e. with a linear depth-dependent function yielding corrections ranging from $11.3 \mu\text{mol L}^{-1}$ to $21.2 \mu\text{mol L}^{-1}$ with a standard deviation of $\pm 1.5 \mu\text{mol L}^{-1}$ ($R^2=0.72$). The observed depth dependence of the initial residuals points at the 3.2% depth correction being too low to fully account for the pressure effect on the oxygen measurement. Matching floats and

reference data points in density-space did not significantly improve the results nor the accuracy of the correction. Oxygen data shallower than 100 dbar were not included in the correction. The remaining residuals between calibrated oxygen float data and the reference data were normally distributed with depth.

4.2.5 Estimation of gas transfer coefficient

To estimate the air-sea gas transfer coefficient we assumed that the change in the mixed layer oxygen inventory between two consecutive oxygen profiles is primarily driven by air-sea exchange with advection playing only a minor role. During the spring bloom period the mixed layer shoals, promoting phytoplankton growth and oxygen production, resulting in increasing surface oxygen concentrations. During this time of the year the above assumption is clearly violated and the period of the spring bloom was therefore excluded from the analysis, more precisely the period of increasing oxygen concentrations. Gas transfer coefficients estimated as described in detail below were also disregarded when the signs of the gas transfer and the change of the oxygen inventory were not consistent indicating a dominance of the advective signals. Finally, we ignored those transfer coefficients where the air-sea oxygen disequilibrium, i.e. the thermodynamic driving force of the net gas flux, was $< 1 \mu\text{mol L}^{-1}$.

The flux of O_2 , F_{O_2} , across the air-sea interface can be determined from the bulk equation:

$$F_{\text{O}_2} = k_{\text{O}_2} \cdot \Delta[\text{O}_2] \quad (4.2)$$

with

$$\Delta[\text{O}_2] = [\text{O}_2^{\text{sat}}] - [\text{O}_2^{\text{sea}}] \quad (4.3)$$

where k_{O_2} is the transfer coefficient for oxygen, O_2^{sea} and O_2^{sat} are the measured and the equilibrium oxygen concentrations of surface seawater. In fact we used $[\overline{\Delta\text{O}_2}]$, the mean oxygen disequilibrium between two float profiles (n =number of profile):

$$[\overline{\Delta\text{O}_2}] = \frac{(\Delta[\text{O}_2]_n + \Delta[\text{O}_2]_{n+1})}{2} \quad (4.4)$$

If we assume that the O_2 column inventory change in the mixed layer (using the deeper one of the two mixed layer depths as lower boundary of integration), ΔO_2^{inv} , between two consecutive profiles represents the net air-sea oxygen flux F_{O_2} into or out of the water column, the transfer coefficient k_{O_2} can be calculated using the measured air-sea disequilibrium, $\Delta[O_2]$. The k_{O_2} obtained this way (eq. 4.5) is valid only for the Schmidt number (Sc) of oxygen at in-situ T and S and needs to be scaled to k_{660} using equation 4.6 and equation 4.7. The coefficients in equation 4.7 are taken from *Wanninkhof* [1992].

$$k_{O_2} = \frac{F_{O_2}}{\Delta[O_2]} = \frac{\Delta O_2^{inv}}{\Delta[O_2]} \quad (4.5)$$

$$k_{660} = k_{O_2} \cdot (Sc/660)^{-1/2} \quad (4.6)$$

$$Sc = 1953.4 - 128 \cdot T + 3.9918 \cdot T^2 - 0.050091 \cdot T^3 \quad (4.7)$$

4.2.6 Wind distribution

For the global wind speed distribution the Rayleigh distribution function is a good approximation. There are, however, regional variances which can influence the relationship between transfer coefficient and long-term wind speed. The use of time-averaged winds leads to an underestimation. The corresponding enhancement factor R , which expresses the effect of the wind speed distribution on the transfer coefficient in a non-linear relationship, is given by:

$$R = \frac{\sum u^b}{n} / \left(\frac{\sum u}{n} \right)^b \quad (4.8)$$

where n is the number of observations and the exponent b is 2 for quadratic dependence, 3 for cubic dependence or 4 for biquadratic dependence. The enhancement factor accounts for the underestimation by a linearly averaged long-term wind in a quadratic, cubic or biquadratic wind speed dependence of the transfer coefficient.

4.3 Results and Discussion

After correction to within $1.8 \mu\text{mol L}^{-1}$ and $1.5 \mu\text{mol L}^{-1}$ resp. of the Winkler-based oxygen reference we obtained a high-quality oxygen time-series of the upper 2000 m in the central Labrador Sea (Fig. 4.2) which shows pronounced seasonality (see also *Körtzinger et al.* [2008]). The most striking feature is deep convection during winter-time which extends down to depths that vary between 1350 m in winter 2003/2004 and 700-900 m in the two following winters. During these convection periods strong uptake of oxygen from the atmosphere occurs which leads to a rapid buildup of the oxygen inventory down to the maximum convection depth (see also *Körtzinger et al.* [2004]). It is of interest to note, however, that due to the short time scale of the rapidly deepening convection the mixed layer never reaches equilibrium with the atmosphere but typically stays at 5-7% undersaturation (Fig. 4.3). After cessation of the convection activity the convectively mixed volume is almost instantly sealed from atmospheric contact by a rapidly forming warm and fresh (sea ice meltwater) surface layer. In this layer the spring bloom soon forms which causes production of oxygen (and depletion of winter time nutrient concentrations). As a consequence the mixed layer changes from undersaturated to strongly supersaturated by up to 16 % for oxygen. This period of strong in-situ oxygen formation was excluded entirely from our analysis as air-sea exchange is not the dominant effect anymore for changes in the mixed layer oxygen inventory. After depletion of surface nutrients the spring bloom decays and the oxygen supersaturation is gradually reduced by air-sea exchange and the effect of surface cooling. The mixed layer again turns back to undersaturated when it starts deepening towards the end of the year (Fig. 4.3). The sub-surface waters underneath the shallow summer mixed layer show clear sign of a strong respiration signal which mirrors the remineralization of a major fraction of the summer export production in the overlying waters. This evolving seasonal oxygen deficit is a major driver for the strong oxygen fluxes into the ocean in the following deep convection period.

Following the approach and selection criteria outlined in section 4.2 we yielded a total of 69 estimates of the oxygen flux for time periods (typically 7 days) bracketed by two consecutive oxygen profiles. By calculating the average air-sea oxygen disequilibrium of these pairs of profiles we were able to calculate the apparent transfer coefficients for oxygen. Using the temperature-dependent Schmidt number for oxygen and a square-

root Schmidt number dependence of k , these transfer coefficients were scaled to the transfer coefficient of CO_2 in seawater at 20°C and a salinity of 35 (k_{660}). These estimates of the transfer coefficient were then matched with the wind speed data for the respective locations and time periods to investigate their wind speed dependence. This dependence was explored in two different ways representing different types of wind speed data.

For long-term winds, i.e. wind speed averaged linearly over periods of weeks to months, all wind speed data points ($9 \text{ pixels} \times 7 \text{ days} = 63 \text{ data points}$) were averaged into a single arithmetic mean wind speed. However, as shown in Figure 4.4, the daily wind speed was highly variable and varied between 0.24 and 28.6 m s^{-1} with an average wind speed of $9.0 \pm 4.6 \text{ m s}^{-1}$. For high wind speed ($> 10 \text{ m s}^{-1}$), *Wanninkhof* [1992] and *Wanninkhof and McGillis* [1999] yield higher transfer coefficients which are in a good agreement with our results and in contrast to the other three parametrizations. For short-term winds, the entire wind speed distribution (shown in Fig. 4.4 for the entire data set) of the respective period was retained by an average wind speed calculated using a quadratic, cubic or biquadratic dependence (eq. 4.1).

The estimated air-sea gas transfer coefficient k_{660} , separated into four seasons, and the quadratic, cubic and biquadratic relationships for long-term winds are shown in Figure 4.5. At the end of spring the central Labrador Sea is characterized by low wind speed, shallow mixed layers, small changes in surface oxygen concentrations and in mixed layer oxygen inventory resulting in low gas transfer velocities and outgassing. The quadratic, cubic and biquadratic parametrizations of k_{660} are compared with the prominent quadratic and cubic parametrizations of *Liss and Merlivat* [1986], *Wanninkhof* [1992], *Wanninkhof and McGillis* [1999], *Nightingale et al.* [2000] and *Sweeney et al.* [2007] (hereafter referred to as LM86, W92, WM99, N00 and S07). Both the quadratic parameterizations for short-term and long-term winds (Fig. 4.6) overestimate estimated k_{660} at low and intermediate wind speed and tend to underestimate at wind speed $> 8 \text{ m s}^{-1}$. The stronger curvature of the cubic and biquadratic function generally fit estimated k_{660} values better. The biquadratic function also shows little overestimation at low winds and smaller underestimation at high winds. For short-term winds, the quadratic function shows much stronger wind speed dependence than W92, N00, and S07 which is partly an effect of the overestimation at low/intermediate wind speed. The cubic function falls almost exactly on top of the WM99 parameterization. The

biquadratic function yields rather similar k_{660} values with a smaller tendency though to underestimation at lower wind speed. For long-term winds, the quadratic fit also shows stronger wind speed dependence of k_{660} than W92 whereas the cubic fit yields k_{660} values that fall below WM99. Again the biquadratic function is similar to the cubic but slightly reduces overestimation at low wind speed. All fits are forced through the origin. The enhancement factors obtained here (Table 4.1) are very similar to the ones calculated by Wanninkhof *et al.* [2002] using a Rayleigh wind speed distribution and 6-hourly wind speed data. Our wind speed data (Fig. 4.4) can indeed be approximated well by a Rayleigh function, i.e. a special form of the Weibull function where the shape parameter $k = 2$.

In summary, we were able to constrain the wind speed dependent transfer coefficient for air-sea gas exchange of O_2 by oxygen time-series measured from profiling floats in the Labrador Sea. In general, our results show wind speed dependencies that lie in the upper band of prominent parametrizations. Also, the stronger curvature of cubic (or even biquadratic) dependencies fits the observations better pointing at the importance of high wind speed for air-sea gas exchange.

Acknowledgments. This study was supported by the Deutsche Forschungsgemeinschaft (DFG) through SFB 460. It was also funded through the integrated project CarboOcean under the 6th framework programme of the European Commission.

Table 4.1: Compilation of the coefficient a in $k = a u_{10}^b$ as estimated in this study (standard errors in parentheses). Also given is the enhancement factor R .

Parameter	quadratic approx.	cubic approx.	biquadratic approx.
long-term wind	0.52 (± 0.04)	0.042 (± 0.003)	0.0031 (± 0.0003)
short-term wind	0.44 (± 0.03)	0.029 (± 0.002)	0.0016 (± 0.0001)
enhancement factor R	1.16	1.48	1.94

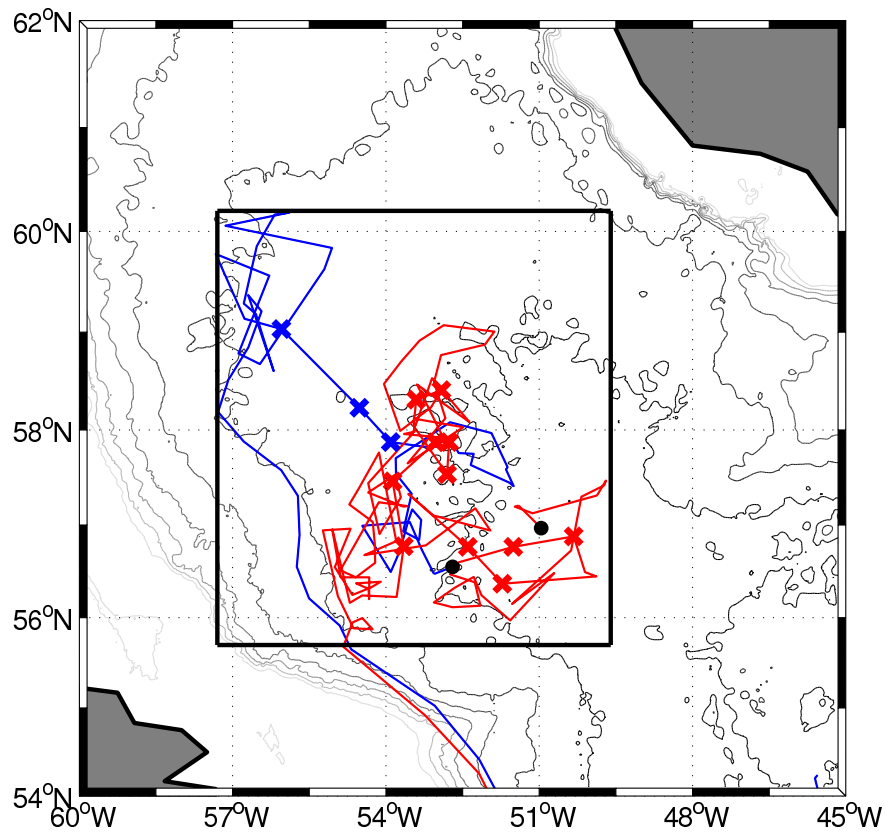


Figure 4.1: Trajectories of two APEX floats equipped with an Aanderaa oxygen optode (Model 3830, Aanderaa Data Instruments, Bergen, Norway) in the central Labrador Sea during the period September 2003 to August 2006. The blue line shows the track of float 4900607 (September 14, 2003 to October 3, 2004) and the red line that of float 4900611 (October 13, 2004 to August 9, 2006); the black dots denote the deployment positions. The drift depth of both floats was 800 dbar and the profiling depth was 2000 dbar. This study only includes profiles taken within the rectangular box which marks the approximate location of the area of deep winter convection. The crosses indicate where mixed layer depths > 600 m were found. The bathymetry contour interval is 500 dbar.

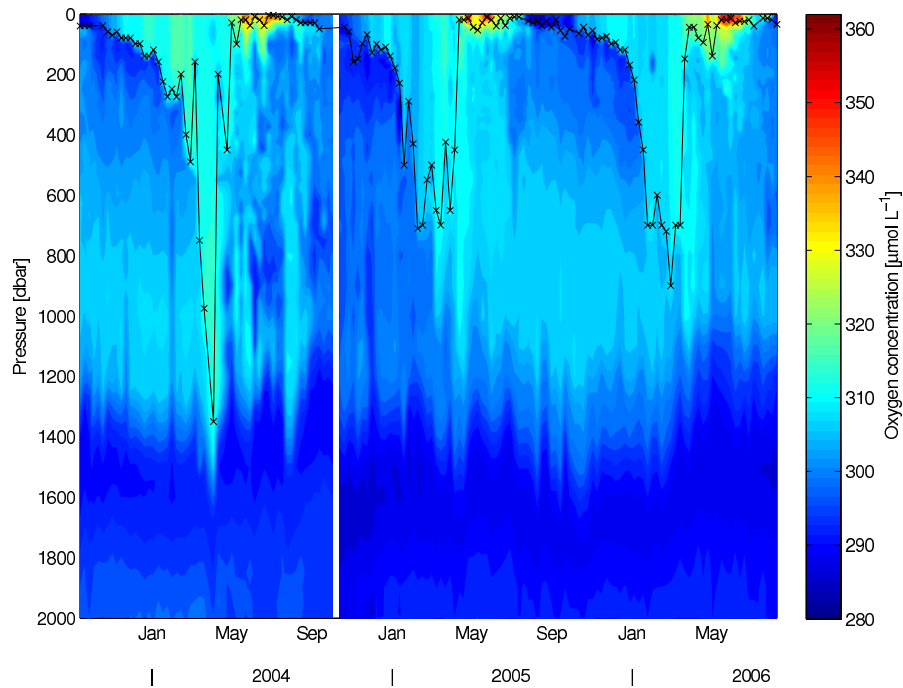


Figure 4.2: Time serie of the oxygen concentration (O_2) of the upper 2000 m in the convection region of the central Labrador Sea (Fig. 4.1). Also shown is mixed layer depth (black crosses) estimated from the float oxygen profiles with an oxygen criterion of $\Delta O_2 = 5 \mu\text{mol L}^{-1}$. The white line indicates the separation between the earlier deployed float 4900607 and the later deployed float 4900611.

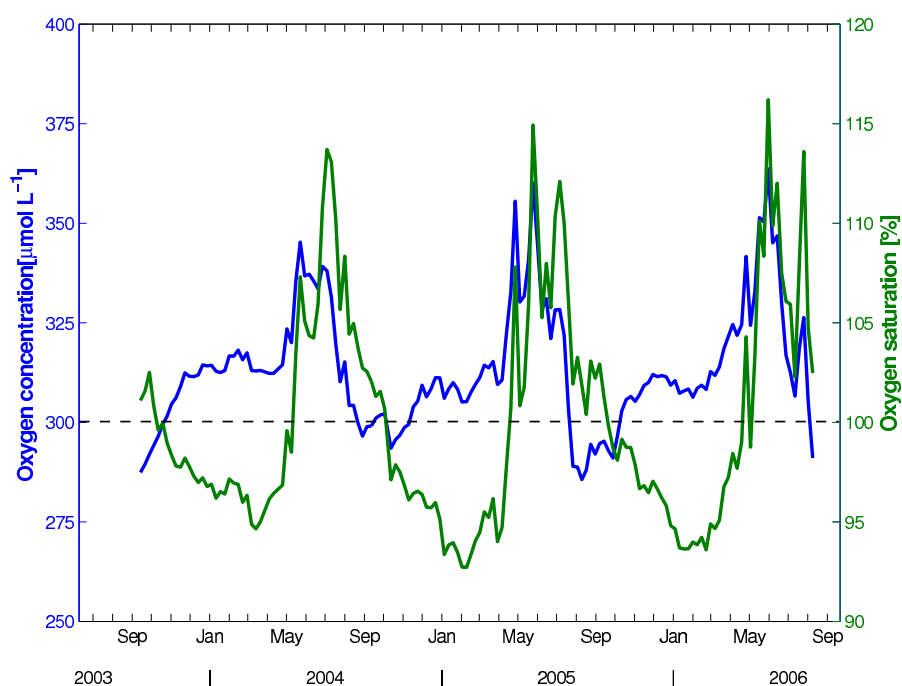


Figure 4.3: Time series of oxygen concentration (blue line) and saturation (green line) at the sea surface (6 m) in the central Labrador Sea. Oxygen saturation was calculated using oxygen solubility after *Garcia and Gordon* [1992]. During wintertime the oxygen concentration at the surface is significantly undersaturated by up to 7% and in spring/summertime supersaturated by up to 16%.

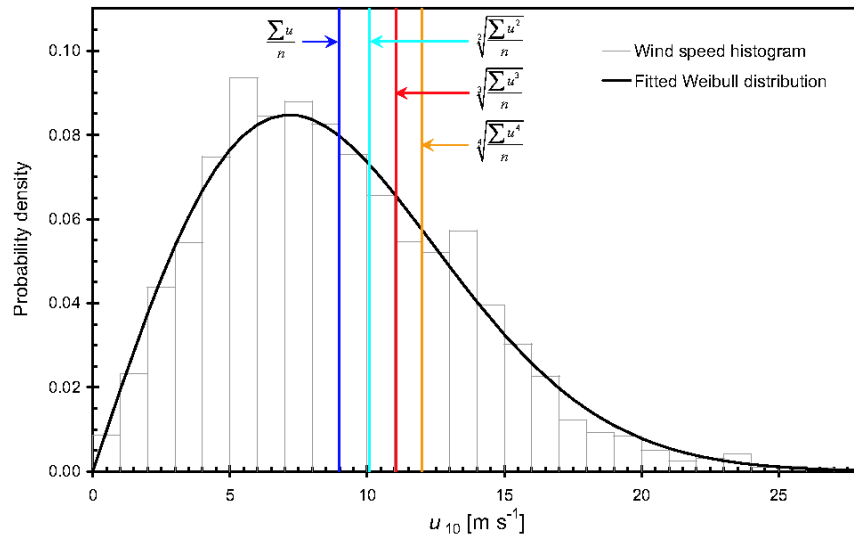


Figure 4.4: Distribution of QuickScat winds over the central Labrador Sea during the period September 2003 to August 2006 as well as the probability density according to a Weibull function with shape parameter $k = 2$ (Rayleigh function). Also shown are wind averages for a linear, quadratic, cubic and biquadratic dependence.

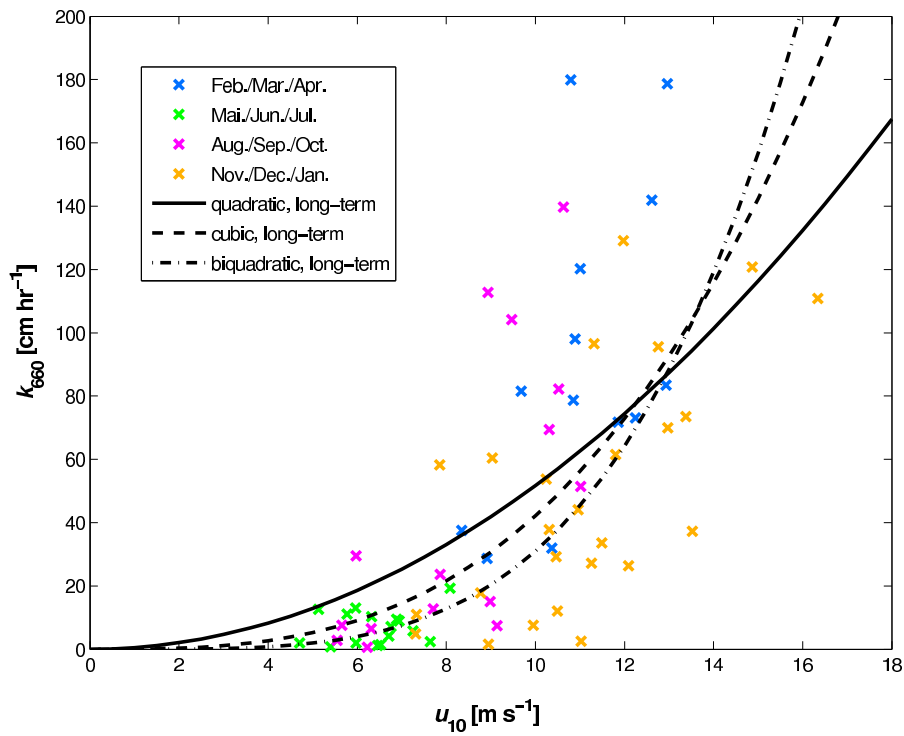


Figure 4.5: Estimated gas transfer coefficient k_{660} vs. long-term wind speed separated into four seasons FMA, MJJ, ASO and NDJ. The lines represent quadratic (solid) , cubic (dashed) or biquadratic (dash-dotted) functions fitted to the data. Wind speed is averaged linearly over the respective time increment of 7 days (long-term winds).

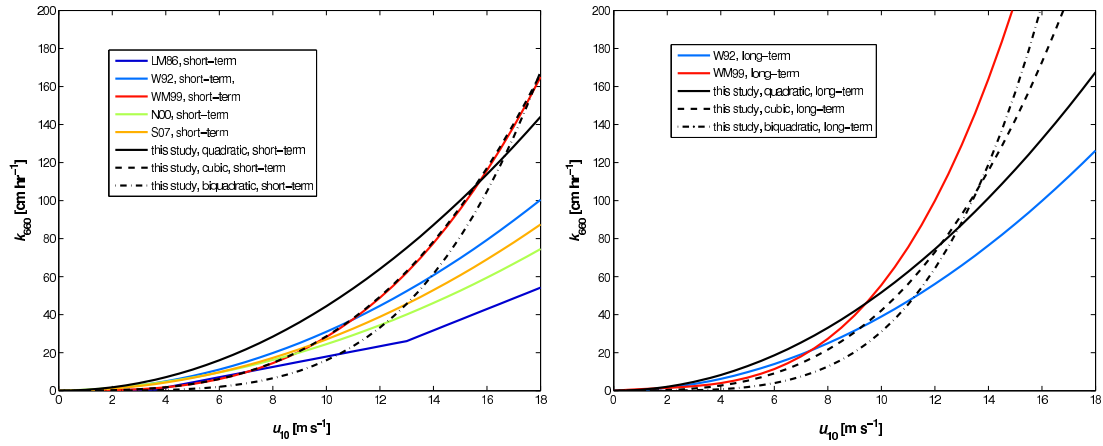


Figure 4.6: Comparison of fits (a) for short-term winds and (b) for long-term winds with prominent parametrizations from the literature. The latter include the relationships of (a) *Liss and Merlivat* [1986], *Wanninkhof* [1992], *Wanninkhof and McGillis* [1999], *Nightingale et al.* [2000] and *Sweeney et al.* [2007] (hereafter referred to as LM86, W92, WM99, N00 and S07) and (b) *Wanninkhof* [1992] and *Wanninkhof and McGillis* [1999]. In (a) are the obtained short-term relationships where the solid black line ($k = 0.44 u_{10}^2$) is the quadratic relationship, the dashed black line ($k = 0.029 u_{10}^3$) is the cubic relationship and the dash-dotted black line ($k = 0.0016 u_{10}^4$) is the biquadratic relationship. In (b) the solid black line ($k = 0.52 u_{10}^2$) is the quadratic relationship, the dashed black line ($k = 0.042 u_{10}^3$) the cubic relationship and the dash-dotted line ($k = 0.0031 u_{10}^4$) the biquadratic relationship for long-term winds. All data were normalized to $Sc = 660$.

Chapter 5

Particulate organic carbon flux deduced from profiling oxygen float data in the Labrador Sea

C.Kihm and A.Körtzinger

Leibniz-Institut für Meereswissenschaften an der Universität Kiel, Düsternbrooker Weg
20, 24105 Kiel, Germany.

Abstract

The vertical export of organic carbon from the surface ocean contributes to the uptake of CO₂ from the atmosphere. The magnitude of the biological pump strongly varies regionally, as well as on seasonal and interannual time scales. The gravitational flux of particulate organic carbon (POC) drives longterm biological carbon sequestration and is the central part of the biological pump. We estimated the POC flux on isopycnal surfaces in the mesopelagic layer of the central Labrador Sea and adjacent slope region by vertical integration of carbon remineralization rates in the time between Apr. 2005 and Nov. 2006. The carbon remineralization rates were obtained by converting oxygen utilization rates (OUR) derived from float observations, using a Redfield stoichiometric ratio of -O₂:C_{org} of 1.34 ± 0.06 . By integration of these rates we obtain an estimate for the remineralization of organic carbon of $\sim 62.4 \text{ g C m}^{-2} \text{ yr}^{-1}$ (OUR based on apparent oxygen utilization) and $\sim 81.6 \text{ g C m}^{-2} \text{ yr}^{-1}$ (OUR based on oxygen concentrations) for the central Labrador Sea and $\sim 154.8 \text{ g C m}^{-2} \text{ yr}^{-1}$ (OUR based on apparent oxygen utilization) and $\sim 118.8 \text{ g C m}^{-2} \text{ yr}^{-1}$ (OUR based on oxygen concentrations) for the shelf current. Commonly the relationship between particulate organic flux and depth is described by a power law function, which requires the knowledge of POC flux at 100 (F_{100}). The remineralization of the POC flux in the upper ocean (100 m to 150 m) appears to occur faster and more efficient near the shelf than in the central Labrador Sea.

5.1 Introduction

The biological and physical processes in the ocean that control the air-sea CO₂ balance play an important role in our climate system. Phytoplankton contributes the major part of the total annual primary production. The amount of available nutrients as well as light in the photic zone are responsible for phytoplankton growth. Most of the phytoplankton biomass is transferred to higher trophic levels but some fraction finds the way into the ocean's interior through gravitational settling. Most of the organic carbon which sinks to depth is remineralized by bacteria, or consumed by zooplankton and thus converted back into inorganic forms. All these processes are commonly referred to as the biological pump [Volk and Hoffert, 1985]. The biological pump removes CO₂ from the surface ocean and hence the atmosphere resulting in sequestration (storage) of carbon for periods of decades to centuries, depending on the depth of remineralization. The temperature dependence (Q_{10} factor) of respiration gives rise to the expectation that remineralization depth might change under a changing climate [Riebesell *et al.*, 2009]. The remineralization of POC and DOC is mirrored in the utilization of oxygen beneath the ventilated mixed layer. Providing DOC respiration is negligible, the local oxygen utilization rate (OUR) at a given depth should thus equal the second depth derivative of the POC flux ($d^2 F/dz^2$). The subpolar North Atlantic ocean is an important region of atmospheric CO₂ uptake and characterized by high primary productivity and an efficient biological pump. In this study we estimated the vertical flux of (POC) by vertical integration of carbon remineralization rates (CRR), in the region of the central Labrador Sea and the boundary current (slope current). Carbon remineralization was be estimated from oxygen utilization rates derived from oxygen float data using the Redfield stoichiometric ratio of $-O_2:C_{org} = 1.34 \pm 0.06$ by Körtzinger *et al.* [2001] for conversion to carbon.

5.2 Methods

5.2.1 Oxygen floats

Oxygen measurements were made with an oxygen optode sensor (Model 3830, Aanderaa Data Instruments, Bergen, Norway) mounted on the end cap of a profiling float (APEX, Webb Research Inc., Falmouth, USA) also equipped with the SBE-41 CTD instrument (Sea-Bird Electronics Inc., Bellevue/WA, USA). The float was deployed in the central Labrador Sea where it remained for 665 days and eventually entered into the boundary current (Fig. 5.1). Every seven days, a measurement sequence begins with a descent to 2000 dbar from a 800 dbar parking depth. Temperature, conductivity (salinity), pressure and oxygen are measured continuously at 72 depth levels during the ascent from the profiling depth to the surface. At the surface the float transmits the collected data via the Argos satellite system and then dives back to its drift (parking) depth. Float 4900611 was deployed on September 15, 2004. In the present analysis only quality controlled profiles were included.

5.2.2 Calibration of oxygen data

The raw oxygen data from the optodes were corrected for pressure and salinity using the floats pressure and salinity readings (Aanderaa Manual; *Tengberg et al.* [2006]) and the 3.2% per 1000 dbar pressure correction proposed by *Uchida et al.* [2008]. Several authors (e.g. *Körtzinger et al.* [2005]; *Uchida et al.* [2008]) showed that the factory calibration of the oxygen optodes is generally insufficient. For post-calibration, the float oxygen data were compared to oxygen concentrations measured on discrete samples by Winkler titration (accuracy $< 1.0 \mu\text{mol L}^{-1}$). The float and Winkler reference data points were matched in depth-space. Matching float and reference data points in density-space did not significantly improve the results or the accuracy of the calibration. For float 4900611, the first profile was compared with Winkler samples from R/V Charles Darwin cruise taken 7 days before and in a distance of approx 17 nm. The oxygen concentrations of float 4900611 were corrected with a linear depth-dependent function yielding corrections ranging from $23.7 \mu\text{mol L}^{-1}$ (shallow) to $32.5 \mu\text{mol L}^{-1}$ (deep) with a standard deviation of $\pm 1.8 \mu\text{mol L}^{-1}$ ($R^2=0.76$). Oxygen data shallower than 100

dbar were not included in the correction. The residuals between final calibrated oxygen float data and the reference data were normally distributed with depth.

5.2.3 Oxygen Utilization Rate

The oxygen utilization rate (OUR) was estimated via the temporal change of the apparent oxygen utilization (oxygen concentration) on reference isopycnal surfaces, below the spring/summer mixed layer (< 100 m) [see also *Martz et al.*, 2008]. The analysis was restricted to the time period of April to December 2005 in the central Labrador Sea and August to November 2006 in the boundary current, i.e. the period after the cessation of deep convection which is characterized by rather shallow mixed layer depths and the spring phytoplankton bloom. This approach assumes advective signals to be absent or at least negligible during this period. In reality, this assumption will not be always correct. Since a formal correction of advective signals is not possible this caveat has to be accepted. It can be assumed, however, that advection will largely cause enhanced scatter rather than a systematic bias. We use an oxygen difference criterion ($\Delta O_2 = 5 \mu\text{mol L}^{-1}$) as proposed by *Körtzinger et al.* [2008] to estimate the mixed layer depth. We also applied a modified classical criterion ($\Delta\theta = 0.15^\circ\text{C}$ and $\Delta\sigma_\theta = 0.03 \text{ kg m}^{-3}$) for comparison with the oxygen criterion. The average reference isopycnal surfaces at reference depths were calculated by using the following equation:

$$\sigma_{\theta,ref.} = \sum_{i=1}^n \frac{\sigma_\theta(z)}{n} \quad (5.1)$$

where n is the number of profiles and z is the reference depth (100, 150, 200, 300, 400, 500, 600 and 700 m) (Fig 5.2a). The oxygen utilization rate at each average reference isopycnal surface is then given by the slope of a linear regression of apparent oxygen utilization (oxygen concentration) on time.

5.2.4 Estimation of particulate organic carbon flux

The equation of *Martin et al.* [1987] describes the POC flux as a function of depth in a normalized power law of the form:

$$F(z) = F_{100} \cdot (z/100)^{-b} \quad (5.2)$$

where $F(z)$ is the POC flux at a given depth z (positive downward), F_{100} is the POC flux at 100 m, and b is a unitless fitting parameter. This equation requires knowledge of the POC flux at 100 m. We assume that the POC flux at 100 m can be estimated by vertical integration of the carbon remineralization rate between 100 m and infinity. A simple approach to estimate the amount of carbon remineralization driving the oxygen consumption was made by *Jenkins* [1982] using a log-linear consumption rate-depth dependence, converted to CRR, of the form:

$$\ln(CRR) = m \cdot z + c \quad (5.3)$$

where CRR is the carbon remineralization rate (in $\mu\text{mol L}^{-1} \text{ yr}^{-1}$), m is the slope, z is the depth in m and c is the intercept (Fig. 5.3a). Vertical integration of equation 5.4 between 100 m and infinity (or an upper depth boundary) yields an estimate of F_{100} :

$$F_{100} = \int_{100}^a \ln(CRR) \, dz = \int_{100}^a e^{(m \cdot z + c)} \, dz \quad (5.4)$$

where a is the max. depth of integration, here chosen as 3000 m. The unitless scaling factor b of the prominent representation by *Martin et al.* [1987] can be estimated as the slope of the linear regression of $\ln CRR$ on the natural logarithm of depth.

5.3 Results and Discussion

The data presented here, were separated into two regions, the central Labrador Sea and the adjacent Labrador slope region (Fig. 5.1). Carbon remineralization rates are based on the conversion between oxygen and carbon rates of production and remineralization with the Redfield stoichiometric ratio for $-O_2:C_{org}=1.34 \pm 0.06$ by *Körtzinger et al.* [2001]. Remineralization rates were calculated on isopycnal surfaces in the depth range of 100 m to 700 m. The 100 m upper limit is safely below the maximum mixed layer depth of the spring/summer period.

The sub-surface layer below the mixed layer, also often referred to as mesopelagic zone, shows a clear sign of respiration which must be driven by export production from the photic zone. The OUR decrease with increasing depth as expected from the fact that organic matter is produced in the upper ocean and remineralized on its way to depth (Fig. 5.2a). Within the upper ocean (100 m - 150 m), the remineralization of organic matter at the boundary current (bc) is by a factor of 3 higher than in the central Labrador Sea (cLS), showing the higher export production in the boundary current (Fig. 5.2b). The decrease of the POC flux is also more rapid in the bc region. This may be indicative of a more labile or less ballasted material. At depth, the POC decrease slows consistently.

The use of a log-linear consumption rate-depth dependence as proposed by *Jenkins* [1982] provides an estimate of the net oxygen consumed below the euphotic zone (~ 100 m). Integrating from the lower bound of the euphotic zone to infinity one obtains an oxygen consumption of $7.0 \text{ mol O}_2 \text{ m}^{-2} \text{ yr}^{-1}$ ($9.1 \text{ mol O}_2 \text{ m}^{-2} \text{ yr}^{-1}$) in the cLS compared to $17.3 \text{ mol O}_2 \text{ m}^{-2} \text{ yr}^{-1}$ ($13.3 \text{ mol O}_2 \text{ m}^{-2} \text{ yr}^{-1}$) in the bc. This corresponds to a net carbon flux out of the euphotic zone of $5.2 \text{ mol C m}^{-2} \text{ yr}^{-1}$ ($6.8 \text{ mol C m}^{-2} \text{ yr}^{-1}$) for the cLS and $12.9 \text{ mol C m}^{-2} \text{ yr}^{-1}$ ($9.9 \text{ mol C m}^{-2} \text{ yr}^{-1}$) for the bc.

The equation of *Martin et al.* [1987] (Eq. 5.2) describes the flux of particulate organic matter as a function of depth below a reference horizon (i.e. 100 m) and requires the knowledge of the POC flux at that reference depth ($F_{ref.}$). We assumed that the POC flux at 100 m can be estimated by vertical integration of the carbon remineralization rate from 100 m to infinity (Section 5.2.4). As proposed by *Martin et al.* [1987] the unitless fitting parameter b can be estimated as the slope of the linear regression of

$\ln(\text{CRR})$ on $\ln(z)$ (Fig. 5.3a,b).

In the central Labrador Sea the estimated exponent $b=1.22 (\pm 0.12)$ ($b=1.28 (\pm 0.12)$) for the time period of April - December 2005. We found a value of $b=1.40 (\pm 0.30)$ ($b=1.75 (\pm 0.49)$) for the boundary current for the time period of August - November 2006 (Fig. 5.4). A smaller value of b represents a faster transfer of organic matter to depth or a slower respiration rate. This can be interpreted as different lability or mineral ballasting of the POC. A more labile composition of the organic matter, leading to faster remineralization and a shorter remineralization length could thus influence the POC flux profile and result in a higher b value. The estimated b values in this study are significantly larger than the determined mean value of the sediment trap studies from the Joint Global Ocean Flux Study (JGOFS) in the late 1980s with values of $0.82 (\pm 0.16)$ [Berelson *et al.*, 2001] and 0.946 for the North Atlantic Bloom Experiment (NABE) from 1989 to 1991 site at 48°N , 21°W [Martin *et al.*, 1993]. However, the cLS value of b is in an excellent agreement with the value of $1.28 (\pm 0.06)$ found by Berelson *et al.* [2001] for the NABE study. The discrepancy between the two b values of the NABE study could be explained by the different methods in determining the export flux at 100 m [Berelson *et al.*, 2001]. The scaling factor b varied considerably from region to region due to the variations in the remineralization kinetic, where regions with higher flux generally tend to show higher b values. Similar variations in the scaling factor b were found by Schlitzer *et al.* [2002] analyzing data from the Southern Ocean.

Lutz *et al.* [2002] noted the inability to fit the sediment trap data using a single parameter b . Due to vertical changes in lability of organic matter, sinking rate and mineral ballast effect, they therefore suggest to use a double exponential curve, one representing the labile organic matter with a relatively short remineralization length scale and one representing the more refractive resistance organic matter with a longer remineralization length scale. There is some indication that double exponential curve might also fit our observation slightly better. It is noteworthy that several authors (e.g., Lutz *et al.* [2002]) pointed out that the Martin *et al.* [1987] relationship in region with strong variable exponent b overestimate the estimated POC flux ($< 2000\text{ m}$).

As reported by Jenkins *et al.* [1985]; Feely *et al.* [2004]; Martz *et al.* [2008] there is a discrepancy between sediment trap-derived and OUR-derived b values. Further exists great uncertainty how to best quantify the F_{100} flux. A detailed discussion of errors in

the exponent b has been given by *Primeau* [2006].

In summary, we were able to present POC flux profiles for the central Labrador Sea and the adjacent slope region by vertical integration of carbon remineralization rates deduced from profiling oxygen float. The estimated b values appears to be somewhat on the high end of the range of values derived from sediment trap data. The remineralization of organic matter appears to be faster in the slope region. Compared to the modeled DOC/POC export flux ratios with depth for the global ocean of *Hansell et al.* [2009] we can assume an overestimation of POC export in the upper 500 m of about 10-20%. It has to be noted, however, that the scatter of the data in the bc region prohibited a precise determination of the b values. The difference to the CLS region is therefore statistically not significant.

Acknowledgments. This study was supported by the Deutsche Forschungsgemeinschaft (DFG) through SFB 460. It was also funded through the integrated project CarboOcean under the 6th framework programme of the European Commission.

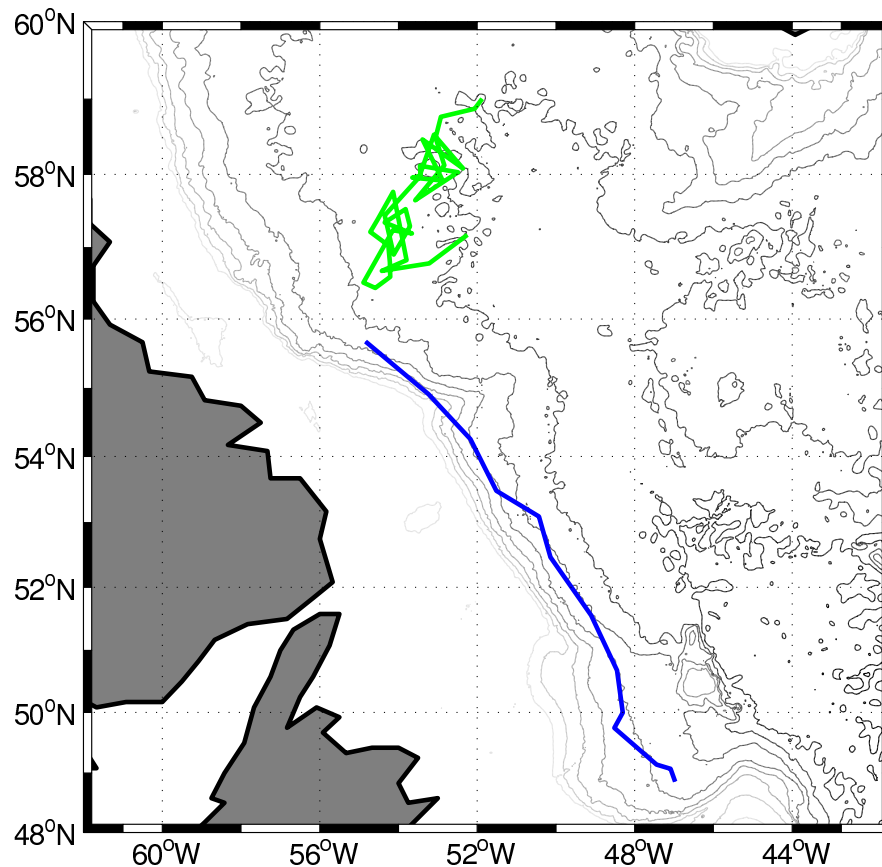


Figure 5.1: Trajectories of float 4900611 equipped with a CTD and an Aanderaa oxygen optode (Model 3830, Aanderaa Data Instruments, Bergen, Norway) in the Labrador Sea. The green line shows the track of float 4900611 in the central Labrador Sea during the time period April 13, 2005 to December 7, 2005 and the blue line indicates the track in the boundary current during the time period August 16, 2006 to November 22, 2006. The drift depth of the float was 800 dbar and the profiling depth was 2000 dbar. The bathymetry contour interval is 500 dbar.

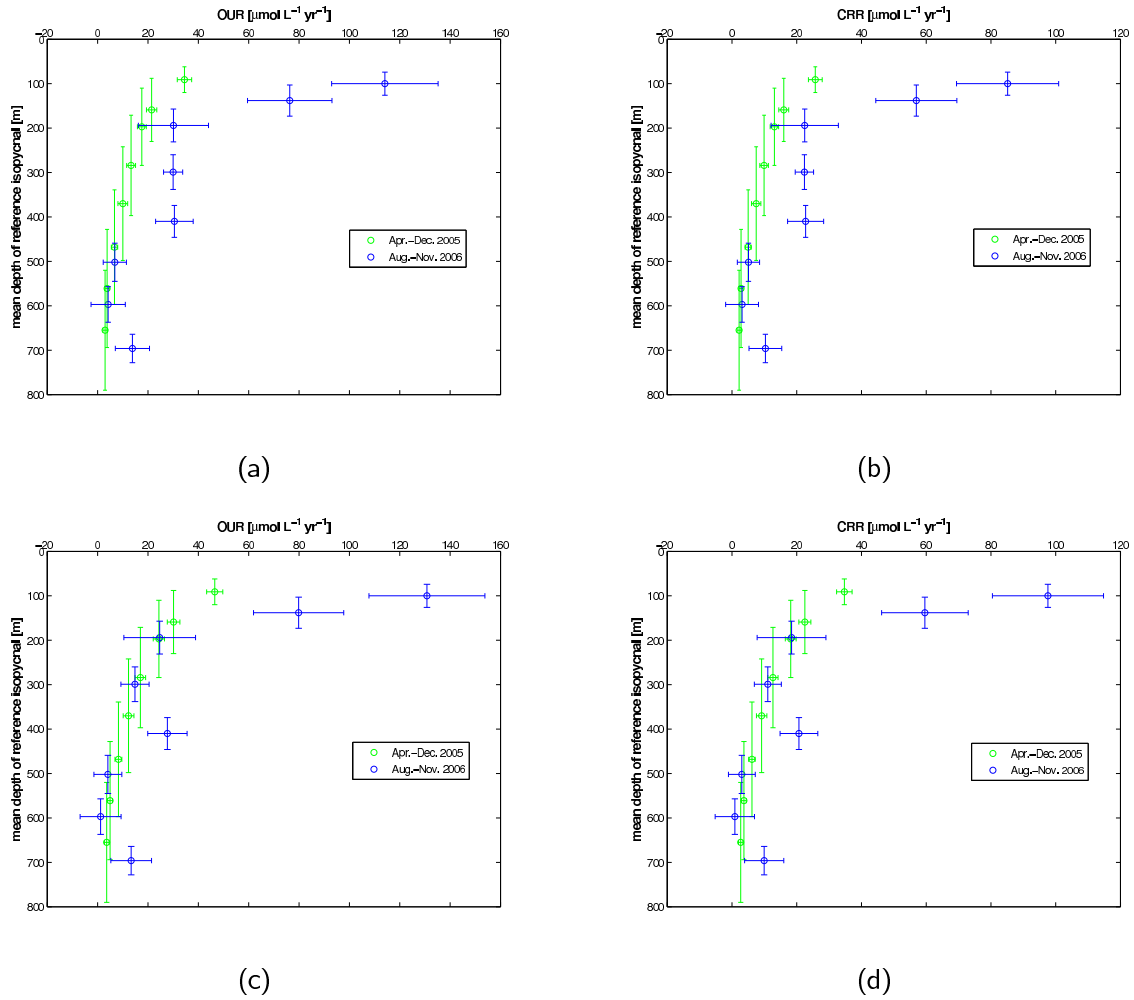


Figure 5.2: Oxygen utilization rate (OUR, a) AOU derived and c) O_2 derived) and carbon remineralization rate (CRR, b) AOU derived and d) O_2 derived) for float 4900611 in the central Labrador Sea (green) and in the boundary current (blue). The rates are calculated from April 2005 to December 2005 (central Labrador Sea) and from August 2006 to November 2006 (boundary current). The remineralization of organic material of the upper ocean of ~ 100 to 150 m (center to the lower bound of the epipelagic zone) is in the boundary current by a factor of ~ 3 higher than in the central Labrador Sea. All rates are computed on mean isopycnal surfaces.

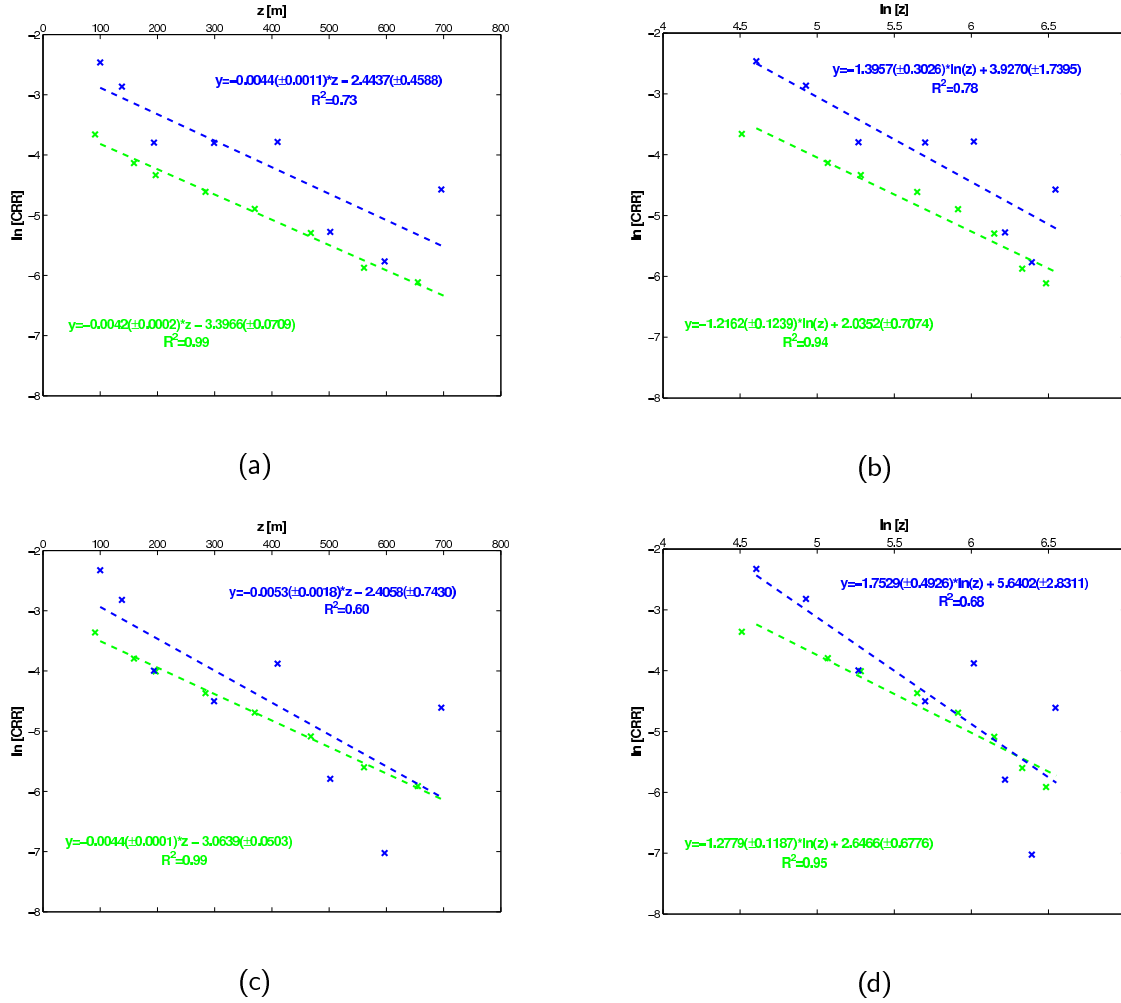


Figure 5.3: a+c) Plot of $\ln \text{CRR}$ versus depth (z) for the central Labrador Sea (green line) and the boundary current (blue line). Integration between 100 m and 3000 m, yields an estimate of the POC flux at 100 m (F_{100}). b+d) The slope of the linear regression of $\ln \text{CRR}$ on $\ln z$ equals the unitless scale factor b of the normalized power function of *Martin et al.* [1987] (Equation 5.2). Note the significantly better fit obtained for the cLS region (green equation).

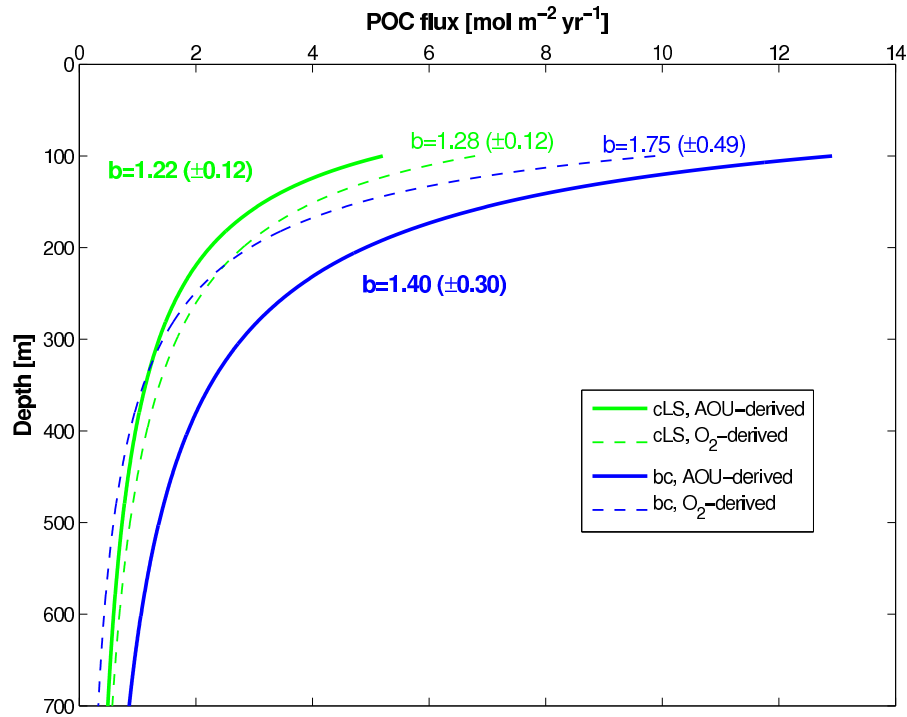


Figure 5.4: Argo float derived particulate organic carbon flux as a function of depth for the central Labrador Sea (green line, $F=5.2(z/100)^{-1.22\pm0.12}$; green dotted line, $F=6.8(z/100)^{-1.28\pm0.12}$) and the boundary current (blue line, $F=12.9(z/100)^{-1.40\pm0.30}$; blue dotted line, $F=9.9(z/100)^{-1.75\pm0.49}$) as described by *Martin et al.* [1987]. The scaling factor b is slightly larger in the boundary current as in the central Labrador Sea, indicating a faster transfer of organic matter to depth. Note, however, the comparatively high error of the b value estimated for the bc region.

Chapter 6

Conclusions and Outlook

6.1 Conclusions

Profiling floats equipped with oxygen optode sensors are helpful to improve our understanding how and why oceanic O_2 is changing [Keeling *et al.*, 2009; Johnson *et al.*, 2009]. The advantage of this oxygen sensor is its long-term stability and high precision [Tengberg *et al.*, 2006]. Nevertheless, very often the factory-calibration does not provide adequate accuracy [Körtzinger *et al.*, 2005] and post-calibration is necessary. For post-calibration the float oxygen data were compared to oxygen concentrations measured on discrete samples by Winkler titration (accuracy $< 1.0 \mu\text{mol L}^{-1}$). There exist also the possibility to use air measurements for drift control of the sensor which was not employed here.

1. A new Δ -criterion, using the oxygen, concentration is established to estimate the mixed layer depth [Körtzinger *et al.*, 2008]. In this study, the depth at which the O_2 concentration differs from the surface O_2 concentration by $5 \mu\text{mol L}^{-1}$ was determined as lower bound of the mixed layer. The main advantage of this method is that oxygen gradients are generally more distinctive, particularly during convection, than temperature or density gradients. ΔO_2 -criterion is comparable with $\Delta\theta = 0.15^\circ\text{C}$ and $\Delta\sigma_\theta = 0.03 \text{ kg m}^{-3}$ criteria during summertime.
2. The separation of the freshening in two freshening periods for the central Labrador

Sea as described by *Schmidt and Send* [2007] was observed/confirmed by the profiling floats. The timing of the onset of the freshening is nearly one month earlier as described by *Schmidt and Send* [2007].

3. The observed central Labrador Sea temperature and salinity cycle has high similarities with previous works [*Avsic et al.*, 2006; *Yashayaev et al.*, 2009]. A slightly sea surface temperature warming between 2005 and 2006 of 0.3°C to 0.8°C, referred to 2004, was identified.
4. The observed seasonal cycle of O₂ agree well with the climatology of *Najjar and Keeling* [1997, 2000] and *Keeling et al.* [1998]. The observed seasonal O₂ maximum in May is somewhat earlier than in the climatologies of *Najjar and Keeling* [1997] and shows an overall increase of about 17.4 μmol L⁻¹. This could be indicating an increase or more rapid biological activities (primary production), which is reflected by an increase of the maximum supersaturation during the spring bloom periode.
5. "Deep breathing" in the convectively region of the Labrador Sea was observed by the profiling floats. This oxygen intake was mostly driven by fast deepening of the mixed layer, exposing undersaturated water to the atmosphere. The O₂ inventory increases by 15.1 mol O₂ m⁻² in 2003/2004, by 11.1 mol O₂ m⁻² in 2004/2005 and by 8.3 mol O₂ m⁻² in 2005/2006, when integrated to the maximum winter mixed depth of the respective year.
6. Time evolution of the deep ΔO₂-inventory (710-1350 m) appears to be connected with the one year lagged NAO index, however. There is no clear understanding of the connection between ΔO₂-inventory and NAO index.
7. Our estimates of air-sea gas transfer coefficient k_{660} for oxygen show wind speed dependencies that lie near upper bound of prominent parametrizations. Our results generally confirm the stronger wind speed dependencies among the suite of published parametrizations. Also the better fits found for cubic or even biquadratic functions point at the strong importance of very high wind speed for air-sea gas exchange.
8. We present POC flux profiles for the central Labrador Sea and the adjacent slope region by vertical integration of carbon remineralization rates deduced from profiling oxygen float. Despite being somewhat on the high end of the range of b

values derived from sediment trap data, our estimates of b for the central Labrador Sea is in an excellent agreement with estimated b value of the NABE experiment [Berelson *et al.*, 2001]. It has to be noted, however, that the scatter of the data in the slope region prohibited a precise determination of the b values.

6.2 Outlook

Two aspects of recent works:

The development of new oxygen sensor calibration methods, with regards to simplified handling and procedure, cheap and high accuracy, is still going on. Calibration with an electrochemical oxygen generator could be a solution. Well-defined oxygen standard solution can be obtained, if the oxygen is produced continuously by the electrolysis of an alkaline carrier solution in a flow through the system. The produced oxygen concentration depends on the electrolysis current and on the flow rate, which is regulated in a constant flow by a flow rate controller, of the solution. The choice of the calibration matrix can therefore be adjusted with as many concentration pairs as on likes. For accuracy, a threshold of about $1 \mu\text{mol L}^{-1}$, in the magnitude of Winkler titration, is desirable. A coherent understanding of production mechanisms, their controlling features and interdependence is needed in laboratory development and field testing.

A new prototype based on the autonomous drifting profiler NEMO (Navigating European Marine Observer) has been developed. NEMO has been further developed on the basis of the SOLO (Sounding Oceanographic Lagrangian Observer) Float. This prototype NEMO float is equipped with an oxygen optode sensor (Model 3835, Aanderaa Data Instruments, Bergen, Norway) mounted on the upper endcap of the float, as well as the SBE-41 CTD sensor (Sea-Bird Electronics Inc., Bellevue/WA, USA). Additionally a PSI CO₂-Pro sensor (Pro Oceanus, Halifax, Canada) is mounted on a new developed external interface. The field of application of the new NEMO prototype float is northern of Cape Verde. The ascent/descent as well as the park/profile cycle can be individually adapted (e.g., to the sensor characteristic). .

The NEMO prototype float has been further improved in:

- external interface to integrate new sensors (e.g. pCO₂, nitrate)
- autonomous external energy supply for the additional sensors
- optional Iridium telemetry combined with GPS (e.g., recovery of the float)
- bidirectional communication in real-time (e.g., changing park/profile depth)
- internal memory chip to save technical and scientific parameters
- user-friendly software interface

Consequently the fields of application is enormous. The first results of the prototype NEMO float provided helpful technical and scientific informations for the manufacturer and for the customer. The development and improvement is still going on and will motivate for future work.

Danksagung

Zuerst möchte ich mich bei Herrn Prof. Dr. Arne Körtzinger für die Möglichkeit zur Verfassung dieser Dissertation sowie für die hervorragende Unterstützung und exzellente Betreuung herzlich bedanken. Arne hatte stets ein offenes Ohr bei Fragen, Anregungen sowie bei Problemen und versprühte fortwährend motivierende Energie, die sehr zum Gelingen dieser Arbeit beigetragen hat.

Ein Dankeschön auch an die Abteilungsmitarbeiter und Kollegen aus den unterschiedlichen Fachbereichen und der C(O₂)-Arbeitsgruppe, die mir sowohl bei technischen als auch bei wissenschaftlichen Fragen mit Rat und Tat zur Seite standen.

Bedanken möchte ich mich auch bei allen Freunden, Kommilitonen, Kollegen und Wissenschaftlern, die mich seit dem ersten Tag des Studiums begleitet haben.

Ein Dankeschön auch an alle diejenigen, die nicht namentlich genannt sind, aber wissen, dass sie gemeint sind.

Mein besonderer Dank gilt meiner Mama, Mami, Rebekka, Jonas und Lilly, die durch ihr Vertrauen, ihre Unterstützung und ihre Liebe, zum Gelingen meines Studium und meiner Dissertation entscheidend beigetragen haben.

Bibliography

- Avsic, T., J. Karstensen, U. Send, and J. Fischer, Interannual variability of newly formed Labrador Sea Water from 1994 to 2005, *Geophys. Res. Lett.*, *33*, L21S02, doi:10.1029/2006GL026913, 2006.
- Barnett, T. P., D. W. Pierce, K. M. AchutaRao, P. J. Gleckler, B. D. Santer, J. M. Gregory, and W. M. Washington, Penetration of human-induced warming into the world's oceans, *Science*, *309*(5732), 284–287, doi:10.1126/science.1112418, 2005.
- Bates, N. R., Interannual variability of the oceanic CO₂ sink in the subtropical gyre of the North Atlantic Ocean over the last 2 decades, *J. Geophys. Res.-Oceans*, *112*(C9), doi:10.1029/2006JC003759, 2007.
- Benson, B. B., and D. Krause, The concentration and isotopic fractionation of oxygen dissolved in fresh-water and seawater in equilibrium with the Atmosphere, *Limnol. Oceanogr.*, *29*(3), 620–632, 1984.
- Berelson, W. M., The flux of particulate organic carbon into the ocean interior: A comparison of four U.S. JGOFS regional studies, *Oceanography*, *13*, 59–67., 2001.
- Bopp, L., C. Le Quere, M. Heimann, A. C. Manning, and P. Monfray, Climate-induced oceanic oxygen fluxes: Implications for the contemporary carbon budget, *Glob. Biogeochem. Cycle*, *16*(2), doi:10.1029/2001GB001445, 2002.
- Boutin, J., J. Etcheto, L. Merlivat, and Y. Rangama, Influence of gas exchange coefficient parameterisation on seasonal and regional variability of CO₂ air-sea fluxes, *Geophys. Res. Lett.*, *29*(8), doi:10.1029/2001GL013872, 2002.
- Boutin, J., Y. Quilfen, L. Merlivat, and J. F. Piolle, Global average of air-sea CO₂ trans-

BIBLIOGRAPHY

- fer velocity from QuikSCAT scatterometer wind speeds, *J. Geophys. Res.-Oceans*, **114**, doi:10.1029/2007JC004168, 2009.
- Carpenter, J. H., The Chesapeake Bay Institute technique for the Winkler dissolved oxygen method, *Limnol. Oceanogr.*, **10**, 141–143, 1965.
- Clarke, R. A., and J. C. Gascard, The formation of Labrador Sea Water, Part I, large-scale processes, *J. Phys. Oceanogr.*, **13**(10), 1764–1778, 1983.
- Demas, J. N., B. A. DeGraff, and P. B. Coleman, Oxygen sensors based on luminescence quenching, *Anal. Chem.*, **71**(23), 793A–800A, 1999.
- Dickson, B., I. Yashayaev, J. Meincke, B. Turrell, S. Dye, and J. Holfort, Rapid freshening of the deep North Atlantic Ocean over the past four decades, *Nature*, **416**(6883), 832–837, 2002.
- Dickson, R., J. Lazier, J. Meincke, P. Rhines, and J. Swift, Long-term coordinated changes in the convective activity of the North Atlantic, *Prog. Oceanogr.*, **38**(3), 241–295, 1996.
- Dore, J. E., R. Lukas, D. W. Sadler, M. J. Church, and D. M. Karl, Physical and biogeochemical modulation of ocean acidification in the central North Pacific, *Proc. Natl. Acad. Sci. U. S. A.*, **106**(30), 12,235–12,240, doi:10.1073/pnas.0906044106, 2009.
- Ducklow, H. W., D. K. Steinberg, and K. O. Buesseler, Upper ocean carbon export and the biological pump, *Oceanography*, **14**(4), 50–58, 2001.
- Fairwall, C. W., J. E. Hare, J. B. Edson, and W. R. McGillis, Parametrization and micrometeorological measurement of air-sea gas transfer, *Bound. Layer Meteor.*, **96**, 63–105, 2000.
- Frölicher, T. L., F. Joos, G. K. Plattner, M. Steinacher, and S. C. Doney, Natural variability and anthropogenic trends in oceanic oxygen in a coupled carbon cycle-climate model ensemble, *Glob. Biogeochem. Cycle*, **23**, doi:10.1029/2008GB003316, 2009.
- Garcia, H., A. Cruzado, L. Gordon, and J. Escanez, Decadal-scale chemical variability in the subtropical North Atlantic deduced from nutrient and oxygen data, *J. Geophys. Res.-Oceans*, **103**(C2), 2817–2830, 1998.

- Garcia, H. E., and R. F. Keeling, On the global oxygen anomaly and air-sea flux, *J. Geophys. Res.*, *106*, 31,155–31,166, 2001.
- Gordon, H. R., and H. Garcia, Oxygen solubility in seawater: better fitting equations, *Limnol. Oceanogr.*, *37*, 1307–1312, 1992.
- Gray, K. S., U. A. Leuenberger, D. Brubaker, S. Quraishi, C. S. Hogeman, and V. A. Imadojemu, Effects of intermittent hypoxia on sympathetic activity and blood pressure in humans, *Auton. Neurosci-Basic Clin.*, *121*(1-2), 87–93, doi:10.1016/j.autneu.2005.06.003, 2005.
- Group, L. S., The Labrador Sea deep convection experiment, *Bull. Amer. Meteor. Soc.*, *79*, 2033–2058, 1998.
- Gruber, N., et al., "Adding oxygen to Argo: Developing a global in-situ observatory for ocean deoxygenation and biogeochemistry" in Proceedings of OceanObs'09: Sustained Ocean Observations and Information for Society (Vol. 2), Venice, Italy, 21-25 September 2009, Hall, J., Harrison D.E. & Stammer, D., Eds., ESA Publication WPP-306, *submitted*, 2010.
- Hansell, D. A., C. A. Carlson, D. J. Repeta, and R. Schlitzer, Dissolved organic matter in the ocean a controversy stimulates new insights, *Oceanography*, *22*(4, Sp. Iss. SI), 202–211, 2009.
- Hansen, H. P., Determination of oxygen. In: Grasshoff, K., Kremling, K., Ehrhardt, M. (Eds.), *Methods of Seawater Analysis*. Verlag Chemie, Weinheim, pp. 75–89, 1999.
- Hurrell, J. W., Y. Kushnir, G. Ottersen, and V. Visbeck, An Overview of the North Atlantic Oscillation, in The "The North Atlantic Oscillation" edited by J.W. Hurrell, Y. Kushnir, G. Ottersen and M. Visbeck (EDS), *Geophysical Monograph Series*, *134*, 1–36, 2003.
- IPCC, Climate Change 2007: Synthesis Report, *Intergovernmental Panel on Climate Change, Fourth Assessment Report, Valencia, Spain*, 2007.
- Ito, T., M. J. Follows, and E. A. Boyle, Is AOU a good measure for respiration in the oceans?, *Geophys. Res. Lett.*, *31*, L17,305, doi:10.1029/2004GL020900, 2004.
- Jenkins, W., Studying subtropical thermocline ventilation and circulation using tritium and He-3, *J. Geophys. Res.-Oceans*, *103*(C8), 15,817–15,831, 1998.

BIBLIOGRAPHY

- Jenkins, W., and J. Goldman, Seasonal oxygen cycling and primary production in the Sargasso Sea, *J. Mar. Res.*, 43(2), 465–491, 1985.
- Jenkins, W. J., Oxygen utilization rates in the North Atlantic subtropical gyre and primary production in oligotrophic systems, *Nature*, 300(5889), 246–248, 1982.
- Jenkins, W. J., and S. C. Doney, The subtropical nutrient spiral, *Glob. Biogeochem. Cycle*, 17(4), doi:10.1029/2003GB002085, 2003.
- Johnson, G., J. Bullister, and N. Gruber, Labrador Sea Water property variations in the northeastern Atlantic Ocean, *Geophys. Res. Lett.*, 32(7), doi:10.1029/2005GL022404, 2005.
- Johnson, K. S., et al., Observing Biogeochemical cycle at global scales with profiling floats and gliders prospects for a global array, *Oceanography*, 22(3, Sp. Iss. SI), 216–225, 2009.
- Kara, A. B., P. A. Rochford, and H. E. Hurlburt, An optimal definition for ocean mixed layer depth, *J. Geophys. Res.-Oceans*, 105(C7), 16,803–16,821, 2000.
- Keeling, R., B. Stephens, R. Najjar, S. Doney, D. Archer, and M. Heimann, Seasonal variations in the atmospheric O₂/N₂ ratio in relation to the kinetics of air-sea gas exchange, *Glob. Biogeochem. Cycle*, 12(1), 141–163, 1998.
- Keeling, R., A. Körtzinger, and N. Gruber, Ocean deoxygenation in a warming world, *Annual Review of Marine Science*, 2, 463–493, 2010.
- Klimant, I., M. Kuhl, R. N. Glud, and G. Holst, Optical measurement of oxygen and temperature in microscale: strategies and biological applications, *Sens. Actuator B-Chem.*, 38(1-3), 29–37, 1997.
- Körtzinger, A., J. I. Hedges, and P. D. Quay, Redfield ratios revisited: Removing the biasing effect of anthropogenic CO₂, *Limnol. Oceanogr.*, 46(4), 964–970, 2001.
- Körtzinger, A., J. Schimanski, U. Send, and D. Wallace, The ocean takes a deep breath, *Science*, 306(5700), 1337, 2004.
- Körtzinger, A., J. Schimanski, and U. Send, High quality oxygen measurements from profiling floats: A promising new technique, *J. Atmos. Ocean. Technol.*, 22(3), 302–308, 2005.

- Körtzinger, A., U. Send, D. W. R. Wallace, J. Karstensen, and M. DeGrandpre, Seasonal cycle of O₂ and pCO₂ in the central Labrador Sea: Atmospheric, biological, and physical implications, *Glob. Biogeochem. Cycle*, 22(1), doi:10.1029/2007GB003029, 2008.
- Lavender, K., R. Davis, and W. Owens, Observations of open-ocean deep convection in the Labrador Sea from subsurface floats, *J. Phys. Oceanogr.*, 32(2), 511–526, 2002.
- Lavender, K. L., R. E. Davis, and W. B. Owens, Mid-depth recirculation observed in the interior Labrador and Irminger seas by direct velocity measurements, *Nature*, 407(6800), 66–69, 2000.
- Lazier, J., R. Hendry, A. Clarke, I. Yashayaev, and P. Rhines, Convection and restratification in the Labrador Sea, 1990–2000, *Deep-Sea Res. Part I-Oceanogr. Res. Pap.*, 49(10), 1819–1835, 2002.
- Lazier, J. R. N., Renewal of Labrador Sea Water, *Deep-Sea Research*, 20(4), 341–353, 1973.
- Levitus, S., J. Antonov, and T. Boyer, Warming of the world ocean, 1955–2003, *Geophys. Res. Lett.*, 32(2), doi:10.1029/2004GL021592, 2005.
- Lilly, J., M. Rhines, M. Visbeck, R. Davis, J. Lazier, F. Schott, and D. Farmer, Observing deep convection in the Labrador Sea during winter 1994–1995, *J. Phys. Oceanogr.*, 29, 2065–208, 1999.
- Lilly, J., P. Rhines, F. Schott, K. Lavender, J. Lazier, U. Send, and E. D’Asaro, Observations of the Labrador Sea eddy field, *Prog. Oceanogr.*, 59(1), 75–176, doi:10.1016/j.pocean.2003.08.013, 2003.
- Liss, P. S., and L. Merlivat, Air-sea gas exchange rates: Introduction and synthesis, in the Role of Air-Sea Exchange, *Geochemical Cycling*, 23, 113–127, 1986.
- Lorbacher, K., D. Dommenges, P. P. Niiler, and A. Koehl, Ocean mixed layer depth: A subsurface proxy of ocean-atmosphere variability, *J. Geophys. Res.-Oceans*, 111(C7), doi:10.1029/2003JC002157, 2006.
- Lutz, M., R. Dunbar, and K. Caldeira, Regional variability in the vertical flux of particulate organic carbon in the ocean interior, *Glob. Biogeochem. Cycle*, 16(3), doi:10.1029/2000GB001383, 2002.

BIBLIOGRAPHY

- Martin, J., G. Knauer, D. Karl, and W. Broenkow, VERTEX: carbon cycling in the northeast Pacific, *Deep Sea Research*, 34(2), 267–285, 1987.
- Martin, J., S. Fitzwater, R. Gordon, C. Hunter, and S. Tanner, Iron, primary production and carbon-nitrogen flux studies during the JGOFS North Atlantic Bloom Experiment, *Deep Sea Research Part II*, 40(1-2), 115–134, 1993.
- Martz, T. R., K. S. Johnson, and S. C. Riser, Ocean metabolism observed with oxygen sensors on profiling floats in the South Pacific, *Limnol. Oceanogr.*, 53(5, Part 2), 2094–2111, 2008.
- McGillis, W. R., J. B. Edson, J. E. Hare, and C. W. Fairall, Direct covariance air-sea CO₂ fluxes, *J. Geophys. Res.-Oceans*, 106(C8), 16,729–16,745, 2001.
- Montégut, C. D., G. Madec, A. S. Fischer, A. Lazar, and D. Iudicone, Mixed layer depth over the global ocean: An examination of profile data and a profile-based climatology, *J. Geophys. Res.-Oceans*, 109(C12), doi:10.1029/2004JC002378, 2004.
- Monterey, G., and S. Levitus, Seasonal variability of mixed layer depth for the World Ocean, NOAA NESDIS Atlas, *Natl. Oceanic and Atmos. c Admin*, 14, 100pp, 1997.
- Naegler, T., P. Ciais, K. Rodgers, and I. Levin, Excess radiocarbon constraints on air-sea gas exchange and the uptake of CO₂ by the oceans, *Geophys. Res. Lett.*, 33(11), doi:10.1029/2005GL025408, 2006.
- Najjar, R., and R. Keeling, Analysis of the mean annual cycle of the dissolved oxygen anomaly in the World Ocean, *J. Mar. Res.*, 55(1), 117–151, 1997.
- Najjar, R., and R. Keeling, Mean annual cycle of the air-sea oxygen flux: A global view, *Glob. Biogeochem. Cycle*, 14(2), 573–584, 2000.
- Nightingale, P. D., G. Malin, C. S. Law, A. J. Watson, P. S. Liss, M. I. Liddiocat, J. Boutin, and R. C. Upstill-Goddard, In situ evaluation of air-sea gas exchange parametrizations using novel conservative and volatile tracers, *Glob. Biogeochem. Cycle*, 14, 373–387, 2000.
- Pahlow, M., and U. Riebesell, Temporal trends in deep ocean Redfield ratios, *Science*, 287(5454), 831–833, 2000.

- Pickard, G. L., and W. J. Emery, Descriptive Physical Oceanography - An Introduction, *Pergamon Press*, 5th edition, 283 pp., 1990.
- Pickart, R. S., D. J. Torres, and R. A. Clarke, Hydrography of the Labrador Sea during active convection, *J. Phys. Oceanogr.*, 32(2), 428–457, 2002.
- Plattner, G. K., F. Joos, T. F. Stocker, and O. Marchal, Feedback mechanisms and sensitivities of ocean carbon uptake under global warming, *Tellus Ser. B-Chem. Phys. Meteorol.*, 53(5), 564–592, 2001.
- Primeau, F., On the variability of the exponent in the power law depth dependence of POC flux estimated from sediment traps, *Deep-Sea Res. Part I-Oceanogr. Res. Pap.*, 53(8), 1335–1343, doi:10.1016/j.dsr.2006.06.003, 2006.
- Redfield, A. C., B. H. Ketchum, and F. A. Richards, The influence of organisms in the composition of sea water, In: *The Sea, Vol. 2, edited by M. N. Hill*, pp. 26–77, Interscience, New York, 1963.
- Reid, J. L., On the use of dissolved oxygen as an indicator of winter convection, *Naval Res. Rev.*, 35, 28–39, 1982.
- Riebesell, U., A. Körtzinger, and A. Oschlies, Sensitivities of marine carbon fluxes to ocean change, *Proceedings of the National Academy of Sciences of the United States of America*, 106(49), 20,602–20,609, doi:10.1073/pnas.0813291106, 2009.
- Riser, S. C., and K. S. Johnson, Net production of oxygen in the subtropical ocean, *Nature*, 451, 323–325, doi:10.1038/nature06441, 2008.
- Roemmich, D., S. Riser, R. Davis, and Y. Desaubies, Autonomous profiling floats: Workhorse for broad-scale ocean observations, *Mar. Technol. Soc. J.*, 38(2), 21–29, 2004.
- Roemmich, D., G. C. Johnson, S. Riser, R. Davis, J. Gilson, W. B. Owens, S. L. Garzoli, C. Schmid, and M. Ignaszewski, The Argo Program Observing the Global Ocean with Profiling Floats, *Oceanography*, 22(2, Sp. Iss. SI), 34–43, 2009.
- Rudnick, D. L., R. E. Davis, C. C. Eriksen, D. M. Fratantoni, and M. J. Perry, Underwater gliders for ocean research, *Marine Technology Society Journal*, 38, 73–84, 2004.

BIBLIOGRAPHY

- Sabine, C., et al., The oceanic sink for anthropogenic CO₂, *Science*, 305(5682), 367–371, 2004.
- Santana-Casiano, J. M., M. Gonzalez-Davila, M.-J. Rueda, O. Llinas, and E.-F. Gonzalez-Davila, The interannual variability of oceanic CO₂ parameters in the north-east Atlantic subtropical gyre at the ESTOC site, *Glob. Biogeochem. Cycle*, 21(1), doi:10.1029/2006GB002788, 2007.
- Sarmiento, J. L., G. Thiele, R. M. Key, and W. S. Moore, Oxygen and nitrate new production and remineralization in the North Atlantic subtropical gyre, *J. Geophys. Res.-Oceans*, 95(C10), 18,303–18,315, 1990.
- Sarmiento, J. L., N. Gruber, M. A. Brzezinski, and J. P. Dunne, High-latitude controls of thermocline nutrients and low latitude biological productivity, *Nature*, 427(6969), 56–60, doi:10.1038/nature02127, 2004.
- Schlitzer, R., Carbon export fluxes in the Southern Ocean: results from inverse modeling and comparison with satellite-based estimates, *Deep-Sea Res. Part II-Top. Stud. Oceanogr.*, 49(9-10), 1623–1644, 2002.
- Schmidt, S., Upper Labrador Sea freshwater : seasonal to decadal variability, *Dissertation, Leibniz Institut für Meereswissenschaften, IFM-GEOMAR*, 133 pp., 2008.
- Schmidt, S., and U. Send, Origin and composition of seasonal Labrador sea freshwater, *J. Phys. Oceanogr.*, 37(6), 1445–1454, doi:10.1175/JPO3065.1, 2007.
- Simo, R., Production of atmospheric sulfur by oceanic plankton: biogeochemical, ecological and evolutionary links, *Trends Ecol. Evol.*, 16(6), 287–294, 2001.
- Smith, W. H. F., and D. T. Sandwell, Global seafloor topography from satellite altimetry and ship depth sounding, *Science*, 277, 1956–1962, 1997.
- Sprintall, J., and D. Roemmich, Characterizing the structure of the surface layer in the Pacific Ocean, *J. Geophys. Res.-Oceans*, 104(C10), 23,297–23,311, 1999.
- Stramma, L., G. C. Johnson, J. Sprintall, and V. Mohrholz, Expanding oxygen-minimum zones in the tropical oceans, *Science*, 320(5876), 655–658, doi:10.1126/science.1153847, 2008.

- Straneo, F., Heat and freshwater transport through the central Labrador Sea, *J. Phys. Oceanogr.*, 36(4), 606–628, 2006.
- Sweeney, C., E. Gloor, A. R. Jacobson, R. M. Key, G. McKinley, J. L. Sarmiento, and R. Wanninkhof, Constraining global air-sea gas exchange for CO₂ with recent bomb ¹⁴C measurements, *Glob. Biogeochem. Cycle*, 21(2), doi:10.1029/2006GB002784, 2007.
- Tengberg, A., et al., Evaluation of a lifetime-based optode to measure oxygen in aquatic systems, *Limnol. Oceanogr. Meth.*, 4, 7–17, 2006.
- Tengberg, A., J. Hovdenes, D. Barranger, O. Brocandel, R. Diaz, J. Sarkkula, C. Huber, and A. Stangelmayer, Optodes to measure oxygen in the aquatic environment, *Sea Technology*, 44(2), 10–15, 2003.
- Uchida, H., T. Kawano, I. Kaneko, and M. Fukasawa, In Situ Calibration of Optode-Based Oxygen Sensors, *J. Atmos. Ocean. Technol.*, 25(12), 2271–2281, doi:10.1175/2008JTECHO549.1, 2008.
- Våge, K., R. S. Pickart, V. Thierry, G. Reverdin, C. M. Lee, B. Petrie, T. A. Agnew, A. Wong, and M. H. Ribergaard, Surprising return of deep convection to the subpolar North Atlantic Ocean in winter 2007-2008, *Nat. Geosci.*, 2(1), 67–72, doi:10.1038/NGEO382, 2009.
- Volk, T., and M. I. Hoffert, Ocean carbon pumps: Analysis of relative strengths and efficiencies in ocean-driven atmospheric CO₂ changes. In: E.T. Sundquist and W.S. Broecker (eds) *The Carbon Cycle and Atmospheric CO₂: Natural Variations Archean to Present.*, *Geophys. Monogr. Ser.*, 32, pp. 99–110., AGU, Washington, D.C., 1985.
- Wanninkhof, R., Relationship between wind-speed and gas-exchange over the ocean, *J. Geophys. Res.-Oceans*, 97(C5), 7373–7382, 1992.
- Wanninkhof, R., and W. R. McGillis, A cubic relationship between air-sea CO₂ exchange and wind speed, *Geophys. Res. Lett.*, 26(13), 1889–1892, 1999.
- Wanninkhof, R., R. C. Doney, T. Takahashi, and W. R. McGilles, The Effect of Using Time-Averaged Winds on Regional Air-Sea CO₂ Fluxes, *Geophysical monograph*, 127, 351–356, 2002.

BIBLIOGRAPHY

- Wanninkhof, R., W. E. Asher, D. T. Ho, C. Sweeney, and W. R. McGillis, Advances in Quantifying Air-Sea Gas Exchange and Environmental Forcing, *Annu. Rev. Mar. Sci.*, *1*, 213–244, doi:10.1146/annurev.marine.010908.163742, 2009.
- Watson, A. J., et al., Tracking the Variable North Atlantic Sink for Atmospheric CO₂, *Science*, *326*(5958), 1391–1393, doi:10.1126/science.1177394, 2009.
- Winkler, L. W., The determination of dissolved oxygen, *Ber. Dtsch. Chem. Ges.*, *21*, 2843–2846, 1888.
- Yashayaev, I., Hydrographic changes in the Labrador Sea, 1960-2005 (vol 73, pg242, 2007), *Prog. Oceanogr.*, *75*(4), 857–859, doi:10.1016/j.pocean.2007.09.001, 2007.
- Yashayaev, I., and J. W. Loder, Enhanced production of Labrador Sea Water in 2008, *Geophys. Res. Lett.*, *36*, doi:10.1029/2008GL036162, 2009.

Eidesstattliche Versicherung

Hiermit erkläre ich an Eides statt, dass ich die vorliegende Dissertation selbständig verfasst und keine anderen als die angegebenen Quellen und Hilfsmittel verwendet habe.

Die Arbeit wurde bisher weder in gleicher noch in ähnlicher Form einer anderen Prüfungsbehörde vorgelegt und auch noch nicht veröffentlicht.

Kiel, Februar 8, 2010

(Christoph Kihm)

curriculum vitæ

Name	Christoph Kihm
Date of Birth	March 16 st 1978
Place of Birth	Völklingen (Saarland)
Marriage Status	unmarried, 2 childs
Nationality	German
Address	Wiker Str. 58 24106 Kiel
Telephone:	+49 431/3207818(private) +49 431 600-4116 (office)
E-Mail:	ckihm@ifm-geomar.de (office)

Languages	German French English
------------------	-----------------------------

Employment

since 03/2006	Scientific assistant in the Marine Biogeochemistry devison at IFM-GEOMAR
04/2005 - 12/2005	Scientific assistant in the SFB 460 project at IFM-GEOMAR
09/2004 - 03/2005	Scientific assistant in the NOCES (Nothern Ocean Carbon Exchange Study) project at IFM-GEMOAR
05/2001 - 08/2004	Student assistant in physical Oceanography and Theory and Modelling Devisions at IFM-GEOMAR

Education

since 03/2006	PhD student in the group of Prof. Dr. Arne Körtzinger at the Leibniz Institute of Marine Sciences at University Kiel (IFM-GEOMAR)
08/2004	Final degree (Diplom Ozeanograph) Thesis title: Auswirkung der bio-physikalischen Kopplung im äquatorialen Tropischen Pazifik während eines Westerly-Wind Events (Advisor Prof. Dr. A. Timmermann)
09/1998 - 08/2004	Study of physical oceanography at the he Leibniz Institute of Marine Sciences at University Kiel (IFM-GEOMAR)

1997	university-entrance diploma
1994 - 1997	Wirtschaftswissenschaftliches Gymnasium Saarbrücken (economy grammar school)
1988 - 1994	Integrierte Gesamtschule Rastbachtal (comprehensive school)
1984 - 1988	Grundschule Aschbachtal Gersweiler (elementary school)

Research

02/2008 *Atalante Leg 3 cruise*, Tropical Atlantic

Publications

- 2010 Kihm, C. and A. Körtzinger, Air-sea gas transfer coefficient for oxygen derived from float data *submitted to Journal of Geophysical Research Oceans*
- 2010 Kihm, C. and A. Körtzinger, Particulate organic carbon flux deduced from profiling oxygen float data in the Labrador Sea, *prepared to be submitted to Journal of Marine Systems*

May 28, 2010